Master's Thesis

Annelot Schuring

Moiré patterns in graphene on hexagonal substrates

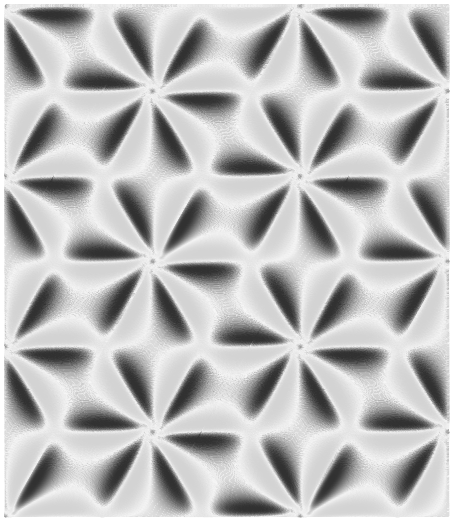

Supervisors:
Prof. dr. A. Fasolino
M. M. van Wijk MSc.

External advisor:
Dr. U. Zeitler

August 2014

Theory of Condensed Matter
Institute for Molecules and Materials
Radboud University Nijmegen

Short summary

We present a theoretical/computational study of moiré patterns in graphene on hexagonal substrates, in particular graphene on graphene and graphene on hexagonal boron nitride (h-BN). We first consider rotated graphene on graphene systems. By varying the angle of rotation between the two layers, one can create beautiful super periodicity: moiré patterns. One period of this hexagonal pattern is called a moiron. Our ambition is to answer this main question: How does minimization of the energy affect the moiré patterns? Starting our simulations, we keep the substrate fixed and let the top layer relax by minimizing the energy given by an empirical but accurate potential. The first thing we observe is that the atoms in the top layer move to an energetically more favourable position, which results in smaller areas of the unfavourable AA stacking and larger areas of the favourable AB stacking. By investigating the interatomic distance and the distortion of the lattice, we find that these smaller AA and larger AB stacked areas are achieved through uniform compression and stretching respectively. A final representation of the system we consider is the displacement of the atoms due to relaxation. Our results show that the atoms move in a vortex around the center of a moiron, which is locally AA stacked.

Next, we investigate the difference in behaviour for varying rotation angles. Inspired by recent experiments on graphene on h-BN, we are searching for a commensurate-incommensurate transition that would occur at some critical angle for graphene on graphene. After considering various samples with different rotation angles and investigating various representations of the system, we conclude that we do not find evidence for such a transition. However, we do find a different type of transition around a critical angle $\theta_c \approx 1.4^\circ$. This transition is most clearly visible in the bond lengths and displacement of the atoms. We examine the average bond length for atoms along the bisector of the sample and we find that the continuous sine like behaviour for angles larger than θ_c becomes discontinuous for angles smaller than θ_c. Furthermore, when we look at the displacement of the atoms due to minimization of energy, we can distinguish a ring of atoms that perform maximal displacement. We find that for large angles this ring is positioned further from the center of the moiron than for small rotation angles. For very small rotation angles the ring of maximal displacement is approaching the center of the moiron. We suggest the following explanation: the center of a moiron is AA stacked. For rotation angles larger than θ_c, this AA stacked area before relaxation is only very small. Most of the displacement then takes place in another part of the moiron. For angles smaller than θ_c the AA stacked area in the center of the moiron becomes significantly large, so that during minimization these areas become most important in energy minimization. Hence, for small rotation angles, the ring of maximal displacement approaches the center of the moiron, namely the AA stacked area.

Moving on to our second system, we study an unrotated layer of graphene on a h-BN substrate. Our ambition is to create an appropriate model for this system. We start modeling the h-BN substrate by simply using graphene with a 1.8% larger lattice constant. We let the top layer relax and investigate the interatomic distance after relaxation. Comparing our results to the experimentally observed patterns, we see that regions of local stretching or compression in our results correspond to local compression or stretching respectively in the experiment. Therefore, we need to make our model more realistic. We take into account that carbon-nitrogen interaction is much stronger than carbon-boron interaction. Furthermore, we slightly stretch the graphene layer prior to relaxation. With this approach, we obtain moiré patterns just like in the experiment. We conclude that graphene stretches globally to adapt to the h-BN substrate, and that including the difference in interaction between CN and CB is crucial for simulating graphene on h-BN. The next step will be to simulate rotated samples and hopefully confirm the commensurate-incommensurate transition that was seen experimentally. Altogether, both our results for graphene on graphene and for graphene on h-BN show that relaxing the top layer affects the moiré patterns and helps us in understanding the system.

Contents

1 Introduction

In 2010, Andre Geim and Konstantin Novoselov received the Nobel Prize in Physics for their experiments on graphene; a single layer of carbon atoms, arranged in hexagons like a chicken wire. They performed experiments which showed some remarkable properties of this two dimensional material. Not only is graphene the thinnest material possible, it is also remarkably strong, transparent and a good conductor.[1] Furthermore, the existence of graphene was surprising, since mathematically the Mermin-Wagner theorem had shown that two dimensional crystalline materials cannot be stable within the harmonic approximation.[2] Many experiments are being done to gain more insight in this fascinating new material. Research on graphene and other two-dimensional materials has even led to a whole new class of materials: van der Waals heterostructures which consist of several layers of 2-D crystals.[3] Graphene promises to be useful in future high-tech applications. Recently, technology giant Samsung showed their first flexible graphene-based phone prototype.[4]

The stacking of two or more not identical layers of material results in so called moiré patterns. These patterns can be used to measure strain. They create a modulation of interatomic distances that can affect the electronic and transport properties of multiple layer systems.[5] In this thesis, we first focus on moiré patterns in double layer graphene as a function of the orientation of the layers with respect to each other. Even though a rotation of 60° between the layers is the most energetically favourable configuration, other angles can be interesting to explore. For example, while sliding a layer of graphene over another layer, a rotation of 60° exhibits high friction compared to some other angles.[6] Second, we want to move towards discussing a system where a layer of graphene sits on top of a layer of hexagonal Boron Nitride (h-BN). h-BN has the same crystal structure as graphene, except that the lattice does not have equivalent sublattices and the interatomic distance is 1.44 Å, while the interatomic distance for graphene is 1.42 Å. Since h-BN is a large bandgap semiconductor, graphene placed on top of h-BN would have interesting electronic properties. For example, using h-BN as a substrate significantly increases the mobility of graphene.[7]

In this study we will consider several configurations of two (rotated) layers of graphene. Our main question is: how do the atoms in the top layer adapt to the rigid bottom layer? In our simulations we let the atoms in the top layer relax under the potential of the substrate. During this minimization of energy we first allow only atomic displacement within the plane, keeping a fixed interlayer distance. At the end of this work we will show that this restriction does not qualitatively change the properties of the system. We start by considering the energies related to such systems after relaxation and first consider AB stacking, which is the lowest energy configuration. Then we consider configurations with other rotation angles and compare their energies to the energy corresponding to AB stacking. Next, we look at four different properties of our graphene on graphene samples after relaxation as a function of the rotation angle. We consider substrate overlay, interatomic distance, distortion of the lattice and displacement of the atoms due to minimization. In these properties we are searching for a phase transition at a critical angle of rotation, between a commensurate and an incommensurate phase. In recent work on graphene on h-BN, such a phase transition was found experimentally.[8] Furthermore, we try to identify a two-dimensional equivalent of the Aubry transition in the framework of the Frenkel-Kontorova model. Finally, we aim to create an appropriate model for graphene on h-BN. This model can be used in future research projects to reproduce the experimental results found for graphene on h-BN.[8]

2 Graphene

2.1 Crystal structure of graphene

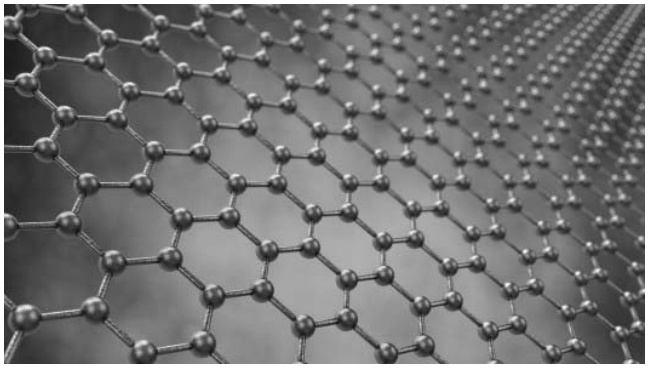

Figure 1: A representation of single layer graphene. The carbon atoms form the honeycomb lattice.

Graphene is a layer of carbon atoms which is one atom thick. The atoms form the honeycomb lattice as shown in Figure 1. Let us first look at some properties of the crystal. As shown in Figure 2, a possible choice of the lattice vectors is:

$$\vec{a}_1 = \frac{a}{2}(3, \sqrt{3}), \qquad \vec{a}_2 = \frac{a}{2}(3, -\sqrt{3}) \tag{1}$$

where a≈1.42 Å the interatomic distance or lattice constant. These vectors build the unit cell of graphene, which contains two carbon atoms at (0,0) and (2a,0). The honeycomb lattice is bipartite and consists of two sublattices, A and B. Each atom from one sublattice is surrounded only by atoms from the other sublattice (see Figure 2).

The nearest neighbours of an atom in sublattice A are reached through the nearest neighbour vectors:

$$\vec{\delta}_{A,1} = -\frac{a}{2}(1, \sqrt{3}), \qquad \vec{\delta}_{A,2} = \frac{a}{2}(-1, \sqrt{3}), \qquad \vec{\delta}_{A,3} = a(1, 0) \tag{2}$$

and the nearest neighbours vectors for an atom in sublattice B are:

$$\vec{\delta}_{B,1} = \frac{a}{2}(1, \sqrt{3}), \qquad \vec{\delta}_{B,2} = \frac{a}{2}(1, -\sqrt{3}), \qquad \vec{\delta}_{B,3} = a(-1, 0) \tag{3}$$

The reciprocal lattice vectors are:

$$\vec{b}_1 = \frac{2\pi}{3a}(1, \sqrt{3}), \qquad \vec{b}_2 = \frac{2\pi}{3a}(1, -\sqrt{3}) \tag{4}$$

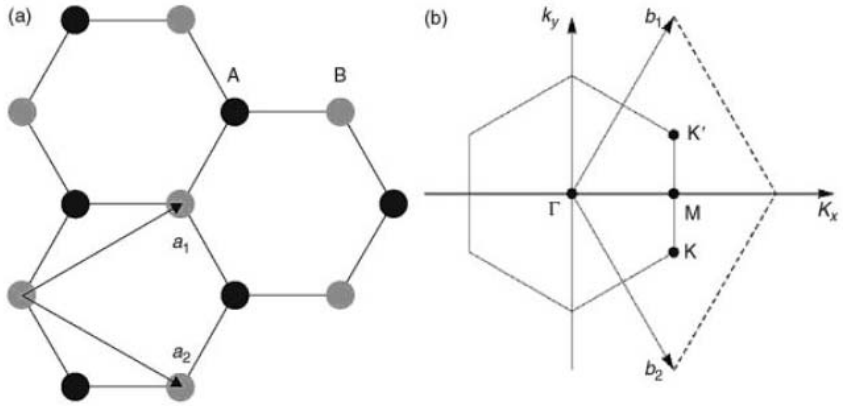

Figure 2: (a) Honeycomb lattice with lattice vectors $\vec{a}_1$ and $\vec{a}_2$ and sublattices A and B indicated as black and grey respectively. (b) Reciprocal lattice vectors $\vec{b}_1$ and $\vec{b}_2$ and some special points in the Brillouin Zone: K=($\frac{2\pi}{3a}$, $\frac{2\pi}{3\sqrt{3}a}$), K′=($\frac{2\pi}{3a}$, $-\frac{2\pi}{3\sqrt{3}a}$) and M=($\frac{2\pi}{3a}$,0).[9]

2.2 Electronic structure of ideal graphene

To help understand why graphene has been such a hot topic in the past few years, we will briefly discuss some of its electronic properties and touch upon an interesting feature: the massless Dirac fermions in graphene.

The carbon atom has six electrons. Two of them completely fill the 1s shell. In graphene, 2s and 2p electrons form covalent bonds in the so called sp^2 hybridization, while the fourth electron is a p electron that is free to move through the crystal. The orbits that lie in the plane form σ bonds, and the electron with the p orbital perpendicular to the plane forms a π bond. The σ states form occupied and empty bands with a direct band gap of approximately 8 eV at the center of the Brillouin Zone (G point in Figure 3), which is a sign of how strong these bonds are. The σ states are not interesting for low-energy physics. However, the π states form a single band with a conical self-crossing point at K and by symmetry also at K′(see figure 2b and 3). This point is characteristic of graphene, and is part of the reason graphene has some fascinating electronic properties.[9] The existence of the self-crossing point means graphene is classified as a gapless semiconductor.

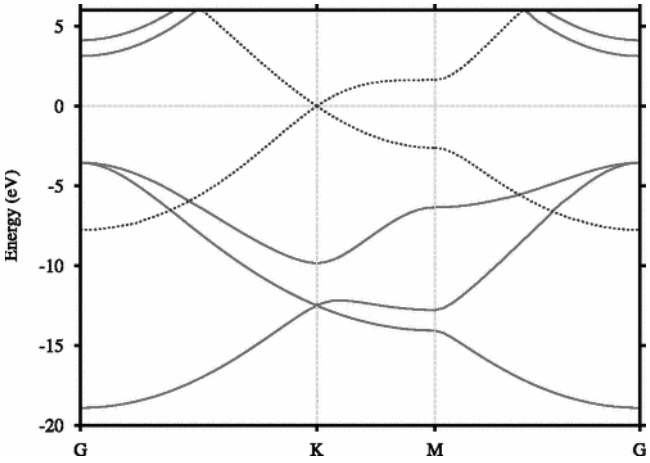

Figure 3: Band structure of a single graphene layer. Solid red lines are σ bands and dotted blue lines are π bands that have a self-crossing point in K.[10]

2.2.1 Massless Dirac fermions

An interesting feature of graphene is that electrons near the conical point behave like massless Dirac fermions.[9] Let us consider the tight-binding approximation and nearest-neighbour approximation with hopping parameter t. The effective Hamiltonian near the conical points for the π states can be written as:

$$\hat{H} = -i\hbar v \vec{\sigma} \nabla \tag{5}$$

where $v = \frac{3a|t|}{2} \approx c/300$ is the electron velocity at the conical points and σ_x and σ_y are two of the Pauli matrices:

$$\sigma_0 = \begin{pmatrix} 1 & 0 \\ 0 & 1 \end{pmatrix} \qquad \sigma_x = \begin{pmatrix} 0 & 1 \\ 1 & 0 \end{pmatrix} \qquad \sigma_y = \begin{pmatrix} 0 & -i \\ i & 0 \end{pmatrix} \qquad \sigma_z = \begin{pmatrix} 1 & 0 \\ 0 & -1 \end{pmatrix} \tag{6}$$

This Hamiltonian is a 2×2 matrix because in the nearest-neighbour approximation there are no hopping processes within the two sublattices, only hopping between them. We then compare it to the Dirac equation:

$$\hat{H} = -i\hbar c \vec{\sigma} \nabla + mc^2 \sigma_z \tag{7}$$

For m=0 this Hamiltonian has the same form as in equation 5. We thus conclude that electrons in graphene behave like massless Dirac fermions with velocity $v \approx c/300$.

2.3 Moiré patterns in bilayer graphene

The most energetically favourable way to stack two layers of graphene is to rotate one layer by 60° with respect to the other. In graphite, this kind of configuration is repeated. This is called Bernal stacking. Here, the atoms from sublattice A in the bottom layer, are directly below the atoms from sublattice B in the top layer. When we look at these two layers from above, a nice periodicity is visible (see Figure 4).

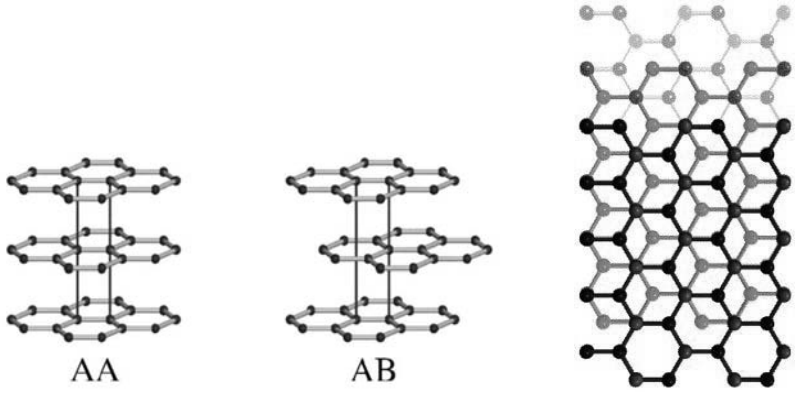

(a) (b)

Figure 4: (a) The least optimal stacking (AA) where the layers are completely aligned and the most optimal stacking (AB) where a layer is rotated 60° with respect to the bottom layer. This is also called Bernal stacking. (b) A top view of Bernal stacked layers of graphene.

Rotating one layer by 60° is not the only way to create some super periodicity. We can create a rhomboid-shaped supercell with basis vector (n,m) that is commensurate with a second layer for a specific rotation angle, θ. This angle can be expressed in terms of n and m:

$$\theta = \cos^{-1}\left(\frac{2n^2 + 2nm - m^2}{2(n^2 + nm + m^2)}\right) \tag{8}$$

Here, n and m are integers and n > m.
This expression, which we will now derive, is also used by Savini et al.[11]

For every pair of n and m, we can construct the corresponding supercell with vectors $\vec{t}_1$ and $\vec{t}_2$. These vectors are of equal length and have an angle of 60° between them, such that they end at equivalent lattice sites. Therefore, information about one vector is sufficient to build the supercell. For convenience, let us choose the lattice vectors (see Figure 5):

$$\vec{a}_1 = a(\sqrt{3}, 0), \qquad \vec{a}_1 = \frac{a}{2}(\sqrt{3}, 3) \tag{9}$$

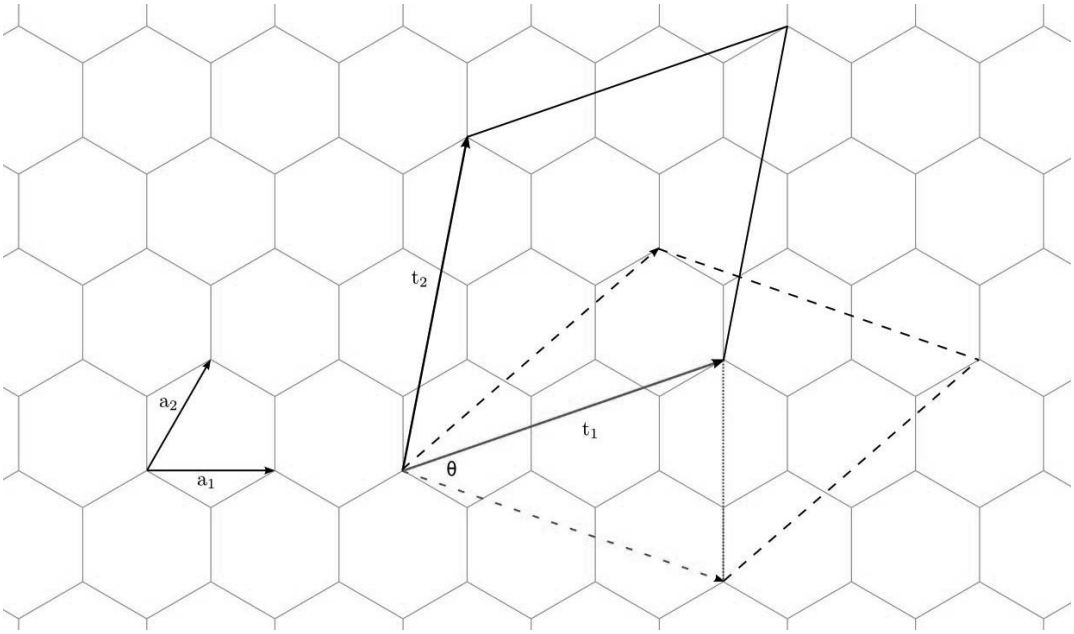

Figure 5: A supercell constructed with $\vec{t_1}$ and $\vec{t_2}$ is rotated by its corresponding commensurate angle θ. For this specific case, (n,m)=(2,1) and θ=38.21°

We then define the supercell vector $\vec{t_1}$:

$$\vec{t_1} \equiv n\vec{a_1} + m\vec{a_2} = \frac{a}{2}\begin{pmatrix} 2\sqrt{3}n + \sqrt{3}m \\ 3m \end{pmatrix} \tag{10}$$

To obtain commensurability, we rotate $\vec{t_1}$ until it ends at an equivalent lattice site. Now we apply the cosine rule to the red coloured triangle in Figure 5 to find an expression for θ:

$$4{t_{1,y}}^2 = 2|\vec{t_1}|^2 - 2|\vec{t_1}|^2\cos\theta = 2|\vec{t_1}|^2(1-\cos\theta) \tag{11}$$

where $t_{1,y}$ is the vertical component of vector $\vec{t_1}$. Rewriting and using Equation 10, we can derive Equation 8:

$$\cos\theta = \frac{|\vec{t_1}|^2 - 2{t_{1,y}}^2}{|\vec{t_1}|^2} = \frac{2n^2 + 2mn - m^2}{2(n^2 + mn + m^2)} \tag{12}$$

The super periodic structure we see when we stack two supercells rotated by their commensurate angle θ with respect to each other are so called moiré patterns. An example is given in Figure 6

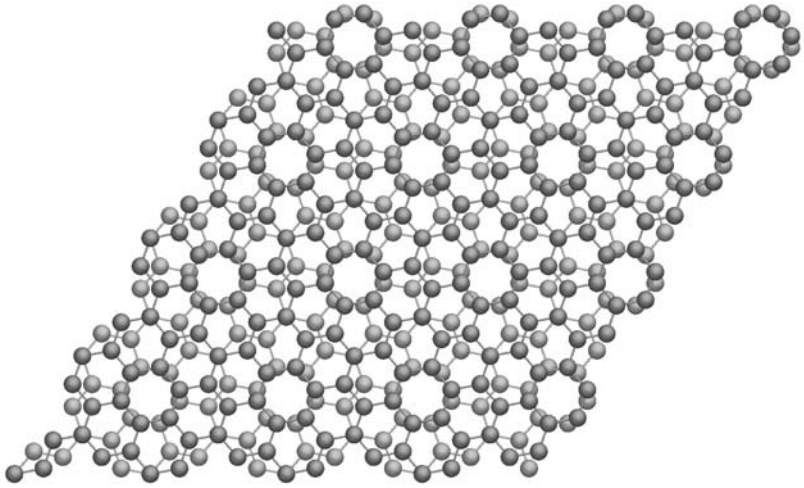

Figure 6: Moiré patterns can appear when stacking two layers of ideal graphene. The top layer (blue) is rotated by θ with respect to the bottom layer of graphene (pink). The bonds between the atoms in one layer are drawn to emphasize the hexagonal lattice structure. This specific sample is a repetition of the supercell belonging to (n,m)=2,1 and θ=38.21°. This sample shows 16 periods of the moiré pattern in total.

For each supercell corresponding to a certain n and m, we consider the number of atoms it contains as a measure of its size. This value, which we will call N, can be derived by dividing the surface of the supercell (V_s) by the surface of the unit cell (V_u). Finally, we should multiply by two, since there are two atoms within one unit cell of graphene. Figure 7 shows all possible N against θ for n≤100.

$$V_s = |\vec{t_1}|^2 \sin 60 = \frac{3\sqrt{3}a^2}{2}(n^2 + nm + m^2), \qquad V_u = |\vec{a}_1|^2 \sin 60 = \frac{3\sqrt{3}a^2}{2}$$

$$N = 2\frac{V_s}{V_u} = 2(n^2 + nm + m^2) \tag{13}$$

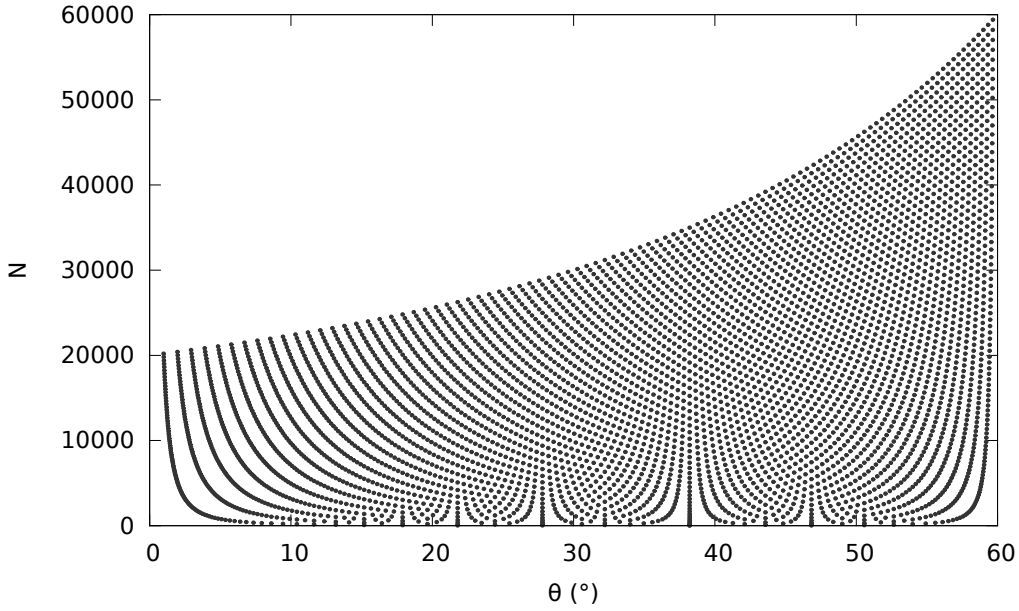

Figure 7: All values of N and their commensurate angle θ for n$\leq$100, derived using Equation 13.

Note that (in Figure 7) more than one value of N belong to the same θ, because multiples of a set (n,m) correspond to the same commensurate angle. For example, the samples (2,1), (4,2), (6,3) etc. all correspond to a rotation angle of θ=38.21°. Next, in Figure 8 we only plot the smallest possible number of atoms within the supercell for each θ and thereby disregard multiples of a sample. When zooming in to the smaller cells by considering only N$\leq$500, we obtain Figure 9. The values of N_{min} and their corresponding angle θ are given in Appendix A.

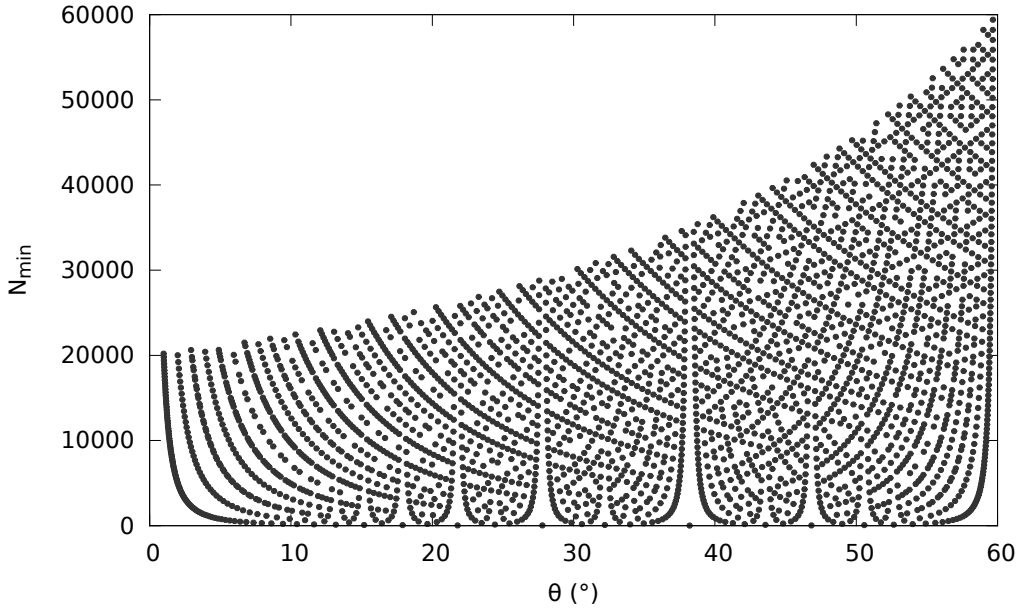

Figure 8: All minimum values of N and their commensurate angle θ for n$\leq$100.

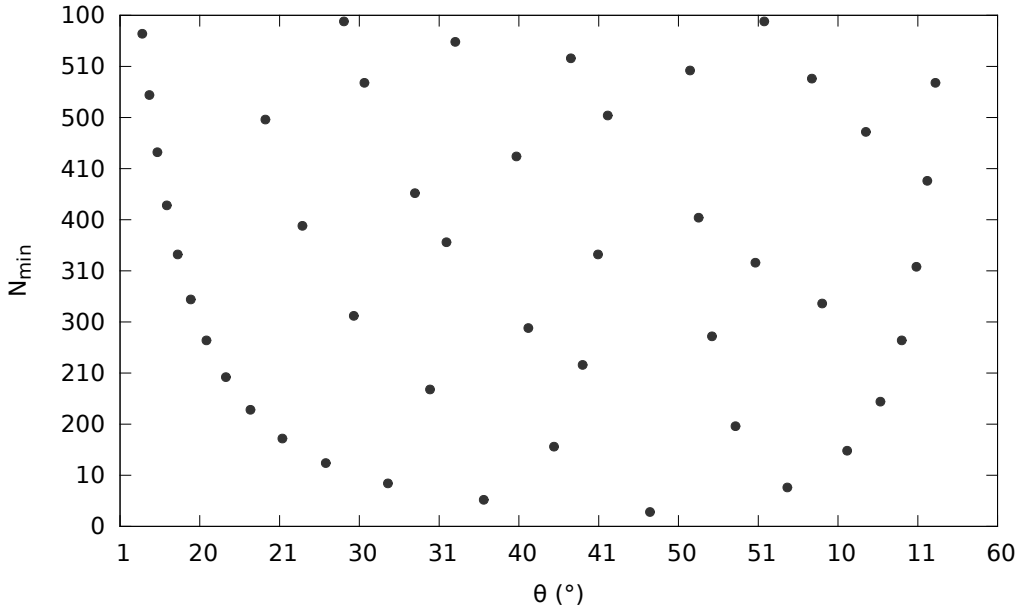

Figure 9: All minimum values of N and their commensurate angle θ for n$\leq$100 and N$\leq$500.

The size of moiré patterns in bilayer graphene can be determined from the supercell vectors. The following derivation is given by Klaus Hermann.[12] We start with general expressions and will continue to make these explicit for graphene. The 2-dimensional lattice vectors of a substrate ($\vec{a}_{o1,2}$) and top layer ($\vec{a'}_{o1,2}$) are connected through a linear transformation:

$$\begin{pmatrix} \vec{a'}_{o1} \\ \vec{a'}_{o2} \end{pmatrix} = M \begin{pmatrix} \vec{a}_{o1} \\ \vec{a}_{o2} \end{pmatrix} \tag{14}$$

For two layers of graphene, calculation of the rotational matrix M leads to:

$$\begin{pmatrix} \vec{a'}_{o1} \\ \vec{a'}_{o2} \end{pmatrix} = \frac{1}{\sin\omega} \begin{pmatrix} \sin(\omega-\theta)\mathbb{1} & \sin\theta\mathbb{1} \\ -\sin\theta\mathbb{1} & \sin(\omega+\theta)\mathbb{1} \end{pmatrix} \begin{pmatrix} \vec{a}_{o1} \\ \vec{a}_{o2} \end{pmatrix} \tag{15}$$

where ω=60° is the angle between $\vec{a}_{o1}$ and $\vec{a}_{o2}$ and $\mathbb{1}$ is the 2-dimensional identity matrix. When filling in θ=0, indeed we find that $\vec{a'}_{o1}$=$\vec{a}_{o1}$ and $\vec{a'}_{o2}$=$\vec{a}_{o2}$. One single period in the moiré pattern, called a *moiron*, can be described in terms of its moiré lattice vectors $\vec{R}_{M1}$ and $\vec{R}_{M2}$. They can be calculated from the substrate lattice vectors:

$$\begin{pmatrix} \vec{R}_{M1} \\ \vec{R}_{M2} \end{pmatrix} = \chi \begin{pmatrix} (\sin(\omega-\theta)-\sin\omega)\mathbb{1} & \sin\theta\mathbb{1} \\ -\sin\theta\mathbb{1} & (\sin(\omega+\theta)-\sin\omega)\mathbb{1} \end{pmatrix} \begin{pmatrix} \vec{a}_{o1} \\ \vec{a}_{o2} \end{pmatrix} \tag{16}$$

where χ=$\frac{1}{2\sin\omega(1-\cos\theta)}$. After some algebra we then find the length of the moiron R_M=$|\vec{R}_{M1}|$=$|\vec{R}_{M2}|$ as a function of θ:

$$R_M = \sqrt{R_{Mi,x}^2 + R_{Mi,y}^2} = a\sqrt{3}\left(2|\sin\frac{\theta}{2}|\right)^{-1} \tag{17}$$

2.4 Effects of minimization on moiré patterns

In this study we place a layer of graphene on a rigid substrate with a certain angle of rotation between them. First, the substrate will be a fixed layer of graphene, but later on we will also consider a fixed graphene-like layer with larger lattice constants to represent a h-BN substrate. While the bottom layer (the substrate) is fixed, the top layer is free to move in accordance with the chosen potential describing the interatomic interaction. Unless stated otherwise, the relaxed layer is *only allowed to move in the xy-plane*, so the atoms within the relaxed layer are fixed in the direction perpendicular to the plane of the sample. Although this setup is not the most realistic, it may be useful because effects of energy minimization will be enhanced when ripples are not allowed. Furthermore, we set the interlayer distance for values much smaller than the equilibrium distance, thereby increasing the interatomic interactions. More details about this potential will follow in section 4. The optical moiré patterns that appear when rotating two

layers of graphene (like the one in Figure 6), are patterns where the minimization is not taken into account yet. We will refer to these as rigid moiré patterns. It is important to know if relaxing the top layer has any effect on the moiré pattern. We can distinguish two possible effects:

- Change in the size of the patterns
- Change of the atomic positions within the pattern

The first effect is impossible, since in our computations the size of the supercell is fixed. Indeed, in Figure 10 we see that the size of the patterns after minimization is identical to the size of the rigid moiré patterns that were predicted in section 2.3.[12] Three points deviate slightly from this line, but this is because the moiré patterns for larger angles become smaller and less well defined.

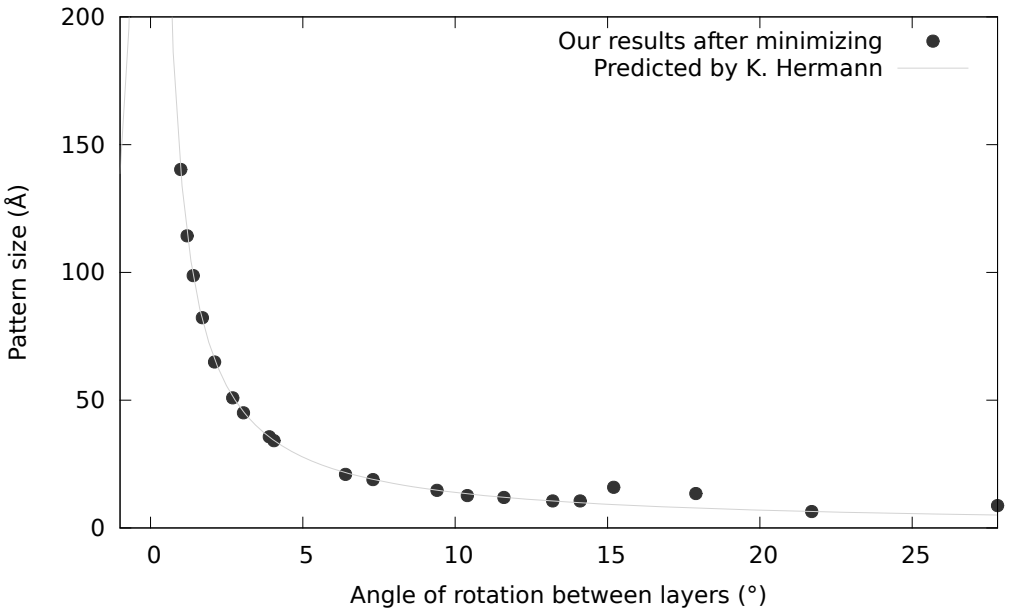

Figure 10: Size of moiré patterns depending on the angle of rotation. The green line is the pattern size predicted by Klaus Hermann and the blue dots indicate the size of our patterns after relaxing the system. The pattern size is proportional to $\sqrt{N}$ (for N see Figure 9).

We will investigate the second possible effect and ask ourselves: How does energy minimization affect the properties of atoms within a moiron in the top layer? We will try several representations of the system to visualize the effects of relaxation:

- The distance in the plane between atoms in the top layer and their nearest neighbour in the bottom layer, which we will call substrate overlay
- The average interatomic distance per atom
- Distortion of the hexagons in the graphene lattice, shown through a gauge field[9]
- Total displacement of atoms in the xy-plane due to minimization of energy

Summarizing, we will examine the effects of relaxing the top layer. Furthermore, we will investigate if there is a difference in behaviour between several configurations of the two layers. Our parameter is the angle between the two layers. In particular, we are looking for a commensurate-incommensurate transition at some critical angle as mentioned by Woods et al.[8]

3 Commensurate-incommensurate transition

3.1 Frenkel-Kontorova model & Aubry transition

The one-dimensional Frenkel-Kontorova (FK) model describes the motion of atoms in a classical harmonic chain subject to an external periodic potential. In making a connection between this model and graphene on a substrate, the springs that connect the atoms may be thought to represent the elastic forces between atoms in the plane, whereas the periodic potential represents the interplanar van der Waals forces with the substrate. The atoms are only allowed to move in the x-direction and only nearest neighbour interaction is taken into account. The energy of a static configuration of the system is given by:

$$E = \sum_{i=1}^{N-1} \frac{\kappa}{2}(x_{i+1} - x_i - a)^2 + \sum_{i=1}^{N} V(x_i) \tag{18}$$

where x_i is the position of atom i and N is the total number of atoms in the chain. The equilibrium spacing of the chain (when $V(x_i)$=0) is a, and the force constant is κ.

A usual choice for the periodic potential is:

$$V(x_i) = \frac{W}{2}\left[1 - \cos\left(\frac{2\pi x_i}{b}\right)\right] \tag{19}$$

where W is a measure for the amplitude and b is the period of the potential. A schematic view of the FK model can be seen in Figure 11. Once a and b are chosen, the model depends only on one parameter, $\lambda = W/\kappa$.

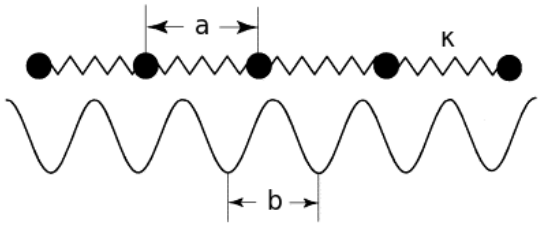

Figure 11: The one-dimensional Frenkel Kontorova model describes the energy of atoms in a classical harmonic chain with force constant κ subjected to an external periodic potential. The equilibrium distance between the atoms in absence of the external potential is denoted by a, and b is the period of the potential.[13]

Let us now introduce the mean interatomic distance l:

$$l = \lim_{N-N' \to \infty} \frac{x_N - x_{N'}}{N - N'} \tag{20}$$

If l/b is a rational number, this leads to a ground state in a so-called commensurate structure. The interesting case however, is where l/b is an irrational number, so that the periods of the chain and the substrate are in competition. This is called an incommensurate structure. When λ is larger than a critical value λ_c, this incommensurate structure undergoes a phase transition to a commensurate structure. This phase transition is called the *transition by breaking of analyticity* or the *Aubry transition*.[14,15] It is illustrated in Figure 12.

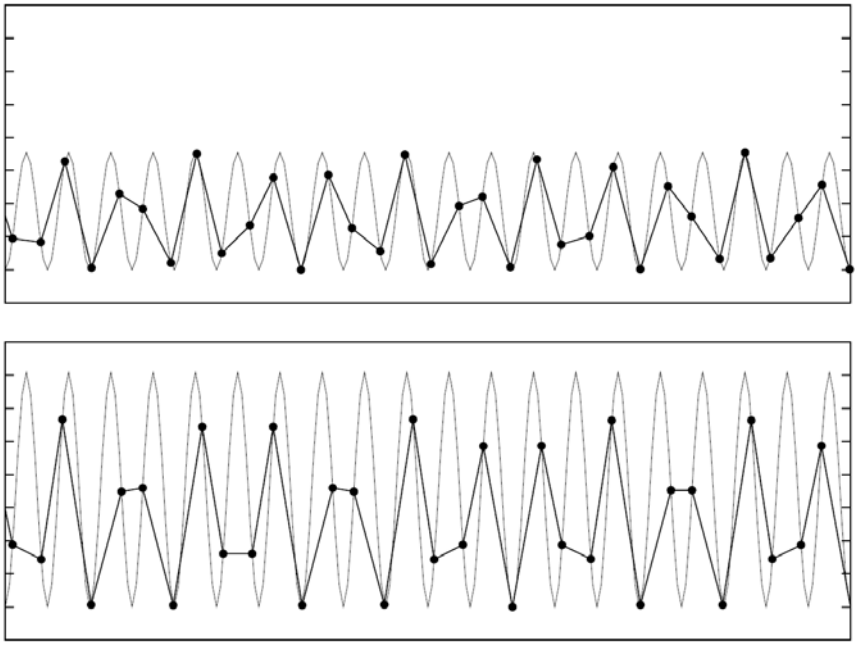

Figure 12: Figures and caption from T. van Erp.[16] Positions of particles in the chain in their ground state configuration for $\lambda < \lambda_c$ (top) and $\lambda > \lambda_c$ (bottom). For $\lambda < \lambda_c$ the particles are distributed at all positions in the periodic potential, while for $\lambda > \lambda_c$ the regions around the tops have become forbidden regions.

Figure 13 shows the depinning force. This is the force needed to slide the layer over the potential and push it out of its equilibrium position. When $\lambda < \lambda_c$, the atoms are distributed equally over the potential, so the depinning force vanishes. When $\lambda > \lambda_c$, there are no more atoms on the maxima of the potential. Therefore, to get the atoms out of their equilibrium position, some atoms have to be pushed over the maxima of the potential. But now there are no atoms coming down from these maxima. Thus, the depinning force becomes finite and depends on the amplitude of the potential and the force constant.

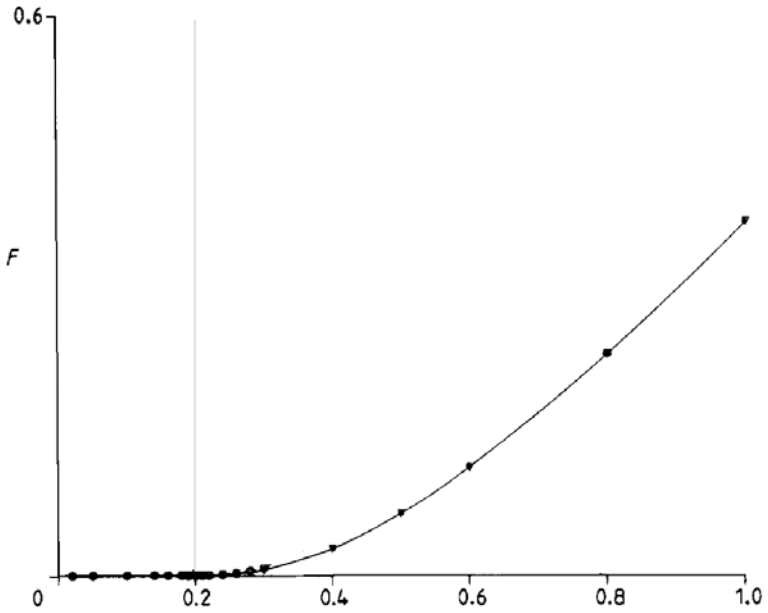

Figure 13: Variation of the depinning force as a function of λ.[15]

Now let us consider this transition in the light of our research. We consider two stacked layers of graphene, rotated by some angle θ with respect to each other. The bottom layer is fixed so it works as a periodic substrate. This substrate works as a periodic potential, analogous to Equation 19. The top layer plays the part of the classical harmonic chain. We will try to find a two-dimensional analogue of such a transition in our samples. By decreasing the interlayer distance we effectively increase the amplitude of our substrate potential, while κ remains constant. We will examine the displacement of the atoms in one specific sample while searching for discontinuous behaviour for some critical value of the interlayer distance.

3.2 Experimentally measured transition

A recent experiment stirred our interest in moiré patterns in graphene, namely the work by Woods et al, *Commensurate-incommensurate transition in graphene on hexagonal boron nitride*.[8] The lattice constant of h-BN is approximately 1.8% larger than the lattice constant for graphene. This paper suggests that graphene adjusts to a slightly different h-BN periodicity either by forming domain walls or by small continuous deformations, depending on the angle of rotation between the two layers. The former is identified as the commensurate state, found for small rotational angles ($\theta \approx 0°$), and the latter as the incommensurate state, for larger rotational angles (above $\theta \approx 1.5°$). Their results are shown below in Figure 14 and 15. Note that the use of the words commensurate and incommensurate within this section are not exactly identical to the definition of commensurate and incommensurate as introduced within the framework of the Frenkel-Kontorova model.

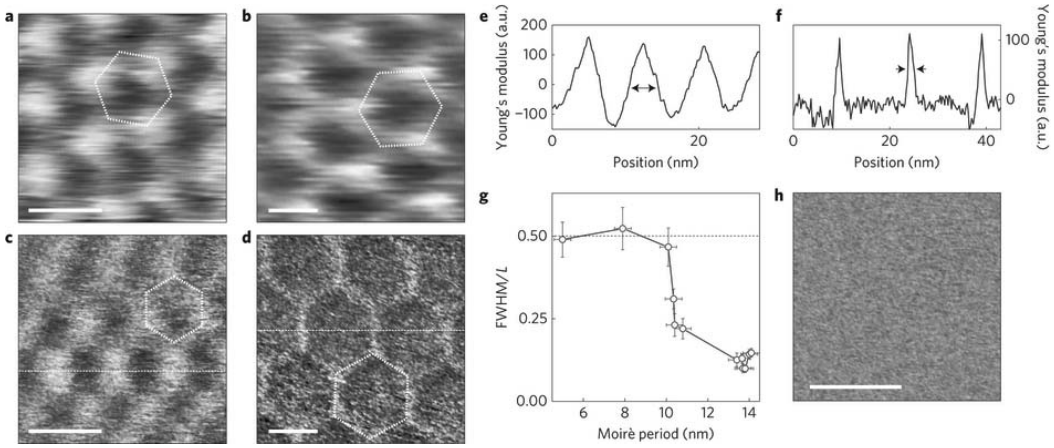

Figure 14: Figures and caption from Woods et al.[8] Experimental observation of moiré patterns for graphene-on-h-BN samples with different relative orientation angles. a) Local resistance measured by conductive Atomic Force Microscopy (AFM) for a graphene-on-hBN sample with an 8 nm moiré pattern, which corresponds to $\theta = 1.5°$. Colour scale: from white to black is from 105 to 120 kΩ. b) Same as in panel a for a sample with a 14 nm moiré periodicity. The crystallographic axes of graphene and hBN are practically aligned, i.e. $\theta \approx 0°$. Colour scale: from 135 to 170 kΩ. c), d) Youngs modulus distribution, for structures with 8 and 14 nm moiré patterns, respectively. e), f) Cross-sections of the Young's modulus distribution taken along the dashed lines in panels c and d, respectively, and averaged over ten scanning lines (approximately 2.5 nm). g) Ratio between full width at half maximum (FWHM) of the peak in the Young's modulus distribution (as marked by arrows in panels e and f) and the period of the moiré structure L, as a function of the period of the moiré structure for several samples. The error bars are determined by the distribution of the sizes of the domains and domain walls measured over an area of 0.5 μm$\times$ 0.5 μm. h) Young's modulus distribution across an unaligned sample (angle between graphene and hBN $\approx 15°$). Scale bars for panels a, b, c, d and h are 10 nm.

In Figure 14e and f the commensurate-incommensurate transition is clearly visible. For rotational angle $\theta = 1.5°$ (e) the Young's modulus along the line has a sine like continuous behaviour, while for $\theta \approx 0$ (f) there are some sharp peaks. The first case is the incommensurate case and the latter the commensurate. We will try to find such a transition in graphene-on-graphene systems.

Figure 15 shows in more detail the moiré pattern for unrotated graphene on h-BN. The position of the atoms within a moiron shows a peculiar behaviour: atomic bonds around the center of the moiron are longer than those between atoms near the sides of the moiron (see Figure 15b and d). We will investigate if this phenomenon also occurs for graphene-on-graphene, before addressing the case of graphene-on-h-BN. Note that the experiment cannot determine the absolute value of the bond length. It would be interesting to know whether or not the interatomic distance of graphene in the center of the moiron matches the larger interatomic distance of the h-BN structure.

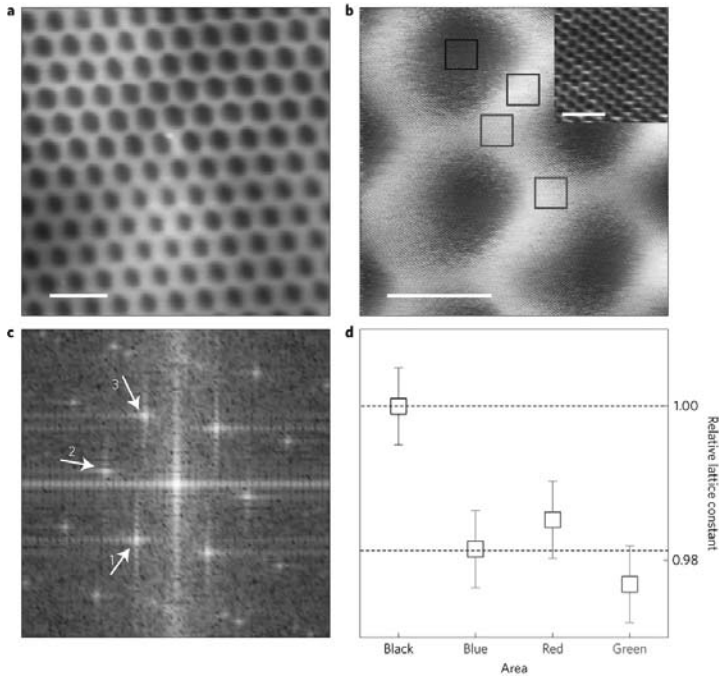

Figure 15: Figures and caption from Woods et al.[8] STM measurements on one of our fully aligned graphene-on-h-BN samples. a) Scanning Tunneling Microscopy (STM) image of one of our aligned samples. A moiré pattern is clearly visible. Scale bar, 30 nm. The sample bias is -0.1 V and the tunnelling current is 300 pA. b) Same as in panel a, but at a higher magnification. Both the moiré pattern and the atomic structure are resolved. Scale bar, 10 nm. The sample bias is -0.1 V and the tunnelling current is 800 pA. Coloured squares (3 nm in size) indicate the fragments used for Fourier transformation to determine the interatomic distance. Inset: a blow up of the area marked by the black square, with the atomic structure clearly visible. Scale bar, 1 nm. c) Example of the Fourier transform of the atomically resolved structure. In this case, as the starting image we used the 3 nm $\times$ 3 nm square image at the vertex of the hexagonal pattern (red square in panel b). The width of the panel is 19 nm^{-1}. d) Relative lattice constants (with respect to those measured for the area marked by the black square in panel b) for different areas within the moiré pattern (colours corresponds to those in panel b, obtained from the positions of the first-order peaks in panel c and averaged over the three directions. The error bars are determined by the width of the peaks in the Fourier transform the atomically resolved structures in panel c and by the spread across the three directions as marked in panel c.

4 Computational methods

All our simulations are done by means of the LAMMPS Molecular Dynamics Simulator,[17] a classical molecular dynamics code. An example of an input script for graphene on graphene sample (n,m)=(15,1) for fixed interlayer distance at 3 Å can be found in Appendix B. We always keep the substrate fixed and let the top layer relax under a potential that combines the REBO potential[18] for intralayer interactions with Kolmogorov Crespi potential[19] for interlayer interactions. Below we will elaborate on these contributions to the potential.

4.1 Intralayer REBO Potential

The intralayer potential we use is the Reactive Empirical Bond-Order (REBO)[18] potential as implemented in LAMMPS. This potential is exclusively short-ranged: two atoms (labeled i and j) only interact if their spacing is less than the cut-off distance $r_{ij}^{max} = 2.0$ Å. Every pair of two covalently-bonded atoms interacts through a potential with two parts:

$$E_{ij}^{REBO} = V_{ij}^{R}(r_{ij}) + b_{ij}V_{ij}^{A}(r_{ij}), \tag{21}$$

where V_{ij}^{R} and V_{ij}^{A} are repulsive and attractive pairwise potentials that depend only on the distance between the two atoms. b_{ij} is the bond-order term between atoms i and j. This term determines the ratio of the attractive contribution to the repulsive contribution. It takes into account many chemical properties of the system that affect the strength of the covalent bonding interaction, such as: coordination numbers, bond angles and conjugation effects. For example, the bond-order term between triply coordinated carbon atoms (sp^2) is much larger than between quadruply coordinated carbon atoms (sp^3). Therefore, the attraction term in graphene is stronger than in diamond for example.[20]

The repulsive term has the following form:

$$V_{ij}^{R} = w_{ij}(r_{ij})\Big[1 + \frac{Q_{ij}}{r_{ij}}\Big]A_{ij}e^{-\alpha_{ij}r_{ij}}, \tag{22}$$

where parameters Q_{ij}, A_{ij} and α_{ij} depend on the atom types i and j. w_{ij} is a bond-weighting factor that switches off the interaction when the distance between two atoms exceeds the typical bonding distance. This factor is a number between zero and one: w_{ij}=0 means an atom pair is nonbonded, w_{ij}=1 means bonded, and 0< w_{ij} <1 means partially bonded. w_{ij} is a switching function that varies smoothly from one to zero over the bonding region:

$$w_{ij} = S'(t_c(r_{ij})), \tag{23}$$

where S' is the switching function and $t_c(r_{ij}) = \frac{r_{ij} - r_{ij}^{min}}{r_{ij}^{max} - r_{ij}^{min}}$.

The attractive pair interaction has the following form:

$$V_{ij}^{A} = -w_{ij}(r_{ij}) \sum_{n=1}^{3} B_{ij}^{(n)} e^{-\beta_{ij}^{(n)} r_{ij}} \tag{24}$$

Here, w_{ij} makes sure that the attractive interaction is switched off smoothly for non-short range interactions. The values for the parameters in equation 22 and 24 for CC bonds are given in Table 1.

Table 1: Parameters for the REBO potential CC bonds

Parameter	Value
Q_{ij} (Å)	0.313 460
α_{ij} (Å^{-1})	4.746 5391
A_{ij} (eV)	10 953.544
$B_{ij}^{(1)}$ (eV)	12 388.792
$B_{ij}^{(2)}$ (eV)	17.567 065
$B_{ij}^{(3)}$ (eV)	30.714 932
$\beta_{ij}^{(1)}$ (Å^{-1})	4.720 4523
$\beta_{ij}^{(2)}$ (Å^{-1})	1.433 2132
$\beta_{ij}^{(3)}$ (Å^{-1})	1.382 6913

In the bottom plot in Figure 16 we see the REBO potential for three types of carbon bonds. The REBO potential for graphene as implemented in LAMMPS is slightly shifted and has an equilibrium bond length of 1.3978 Å, which is slightly smaller than the experimental value of 1.42 Å.

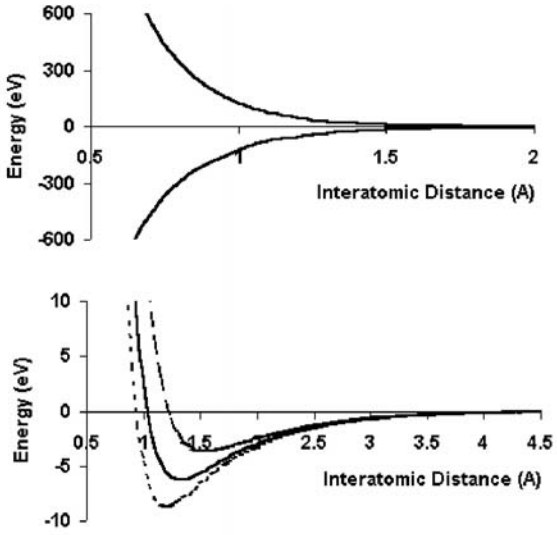

Figure 16: Plots of the REBO potential using the parameters in table 1 from Brenner et al.[18] Top: the attractive and repulsive pair terms from equation 21 as a function of interatomic distance. Bottom: Combined pair terms for triple bonds (dotted curve), double bonds (solid curve), and single bonds (dashed curve) obtained by multiplying the attractive pair term by the corresponding bond-order term b_{ij} and adding it to the repulsive pair term.

4.2 Interlayer Kolmogorov Crespi Potential

A pairwise Lennard-Jones potential is widely used to describe the interaction between two atoms in different layers of graphene. It can describe the overall cohesion between graphene layers quite well, but it is much too smooth to describe variations in the relative alignment of adjacent layers. In other words, it cannot successfully distinguish different configurations. In fact, the Lennard-Jones potential gives too small energy differences between the optimal stacking (AB) and the least optimal stacking (AA).

The variations in relative alignment of two stacked layers is called registry dependence or corrugation. Kolmogorov and Crespi developed a registry-dependent graphitic potential.[19] It has an r^{-6} two-body long ranged van der Waals attraction, an exponential atomic-core repulsion, and a short-ranged term describing the exponentially decaying repulsion due to the interlayer π orbital overlap:

$$V(r_{ij}) = -\left(\frac{r_{ij}}{d}\right)^{-6} + e^{-\lambda_1(r_{ij}-r_0)} + e^{-\lambda_2(z_{ij}-z_0)}e^{-(\rho_{ij}/\delta)^2}\sum C_{2n}(\rho_{ij}/\delta)^{2n} \qquad (25)$$

The units of energy are meV and the fitting parameters are: d, r_0, λ_1, λ_2, z_0, δ and C_{2n}. These parameters are fixed experimentally for an interatomic distance of a=1.42 Å (see Table

2). However, as mentioned above, our intralayer REBO potential favours an equilibrium bond length of 1.3978 Å. Therefore, we need to rescale all distance-dependent parameters accordingly. Furthermore, we also need to rescale the potential when we consider a graphene on an h-BN substrate, which has a bond length that is 1.818 % percent larger than the bond length of graphene: 0.01818×1.3978 Å=1.423 Å.

Table 2: Fitting parameters for registry-dependent graphitic interlayer potential for varying bond lengths. The values for a bond length of 1.42 Å are given by Kolmogorov and Crespi[19] and the values for bond lengths 1.3978 and 1.423 Å are derived from these.

Fitting parameter	Bond length=1.42Å	Bond length=1.3978Å	Bond length=1.423 Å
r_0	4.00 Å	3.937 Å	4.009 Å
z_0	3.44 Å	3.386 Å	3.448 Å
d	4.68 Å	4.6068 Å	4.690 Å
C_0	11.964	11.964	11.964
C_2	6.728	6.728	6.728
C_4	-18.418	-18.418	-18.418
C_6	9.836	9.836	9.836
C_8	-1.8938	-1.8938	-1.8938
C_{10}	-0.6391	-0.6391	-0.6391
C_{12}	0.08652	0.08652	0.08652
δ	0.568 Å	0.55912 Å	0.569 Å
λ_1	4.19 $Å^{-1}$	4.257 $Å^{-1}$	4.180 $Å^{-1}$
λ_2	3.444 $Å^{-1}$	3.499 $Å^{-1}$	3.436 $Å^{-1}$

After adopting the appropriate parameters, one can find the energy profile of the interlayer potential (see Figure 17). The carbon atoms of the substrate (black dots) are at the corners of the hexagons (red). The energetically most *unfavourable* position is directly above such an atom. The energetically most *favourable* position is above the center of a hexagon (green). For two stacked layers of graphene, the most energetically favourable stacking is AB stacking, where half of the atoms in the top layer are at the most favourable position (green) and half of the atoms in the top layer are at the least favourable position (red).

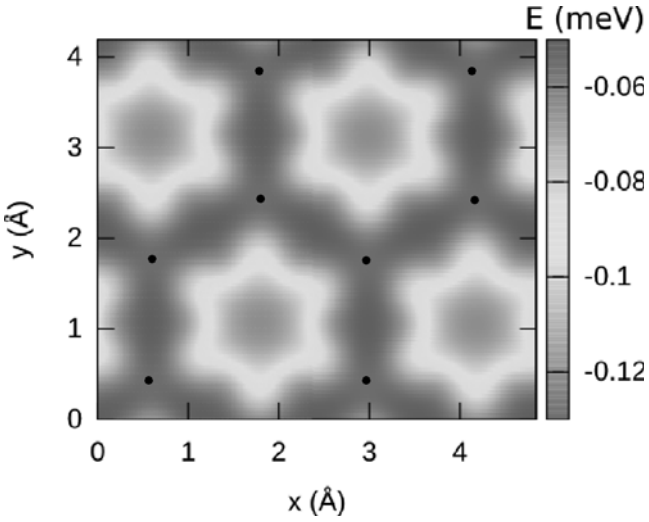

Figure 17: Plot of the interlayer potential by Kolmogorov and Crespi for graphene. The energetically most favourable positions are coloured green, while the least least favourable positions are red. Black dots represent the atoms in the substrate. Courtesy of Merel van Wijk

5 Results: Minimal energy

5.1 Minimal energy AB stacked graphene

After creating an initial configuration for a given rotation angle of the graphene-on-graphene system, we let the top layer relax under the before mentioned potential while keeping the bottom layer fixed. The atoms in the top layer are only allowed to move *within* the plane, maintaining a fixed interlayer distance. In section 6.5 we will show that this restriction does not qualitatively change the properties of the system. We use an energy minimizing algorithm that relies on inertia called FIRE, which stands for *fast inertial relaxation engine*.[21] It finds the position for each atom such that the net force working on it approaches zero.

We want to look at the energies belonging to a two-layer system with different rotation angles between them. To give meaning to these energies, we need some reference point, namely the optimal case: minimal energy for AB stacked graphene. As mentioned in Section 2.3, in AB stacked graphene the top layer is rotated by 60° with respect to the bottom layer. We obtain this minimal energy by calculating the energy per atom for AB stacked graphene for varying interlayer distance. Figure 18 shows that the minimal energy for AB stacked graphene $E_{AB} = -7.82984326406$ eV for an interlayer distance of 3.36999 Å.

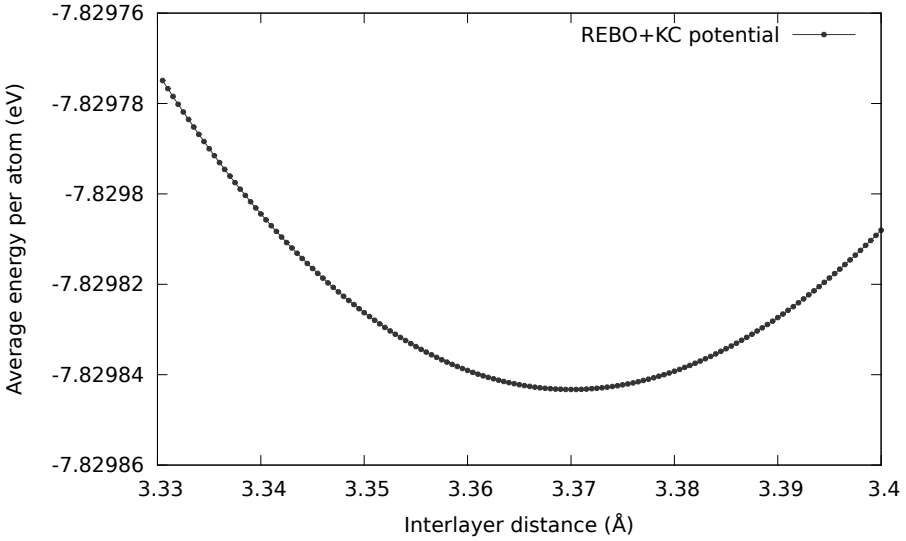

Figure 18: Minimizing the energy of AB stacked graphene by varying the interlayer distance, using our combined REBO and KC potential. The lowest energy point corresponds to -7.82984326406 eV for interlayer distance 3.36999 Å.

5.2 Varying angles

Now we are ready to perform minimization of the average energy per atom for graphene-on-graphene systems where the top layer is rotated by some angle θ as mentioned in Section 2.3. To get an idea of the typical energies, we look at combinations of n and m for which $100 < N < 500$, that is for small moiré patterns (see Figure 9 and 10). We will study three situations for the interlayer distance, z: 3 Å, 3.36999 Å and non-fixed. Here, 3.36999 Å is the optimal interlayer distance for AB stacked graphene in our potential (see Figure 18). The resulting minimal energies are shown in Figure 19, 20 and 21 respectively. We expect the results to be mirror symmetric in the point of 30° and to reach the minimal energy for 0 and 60°. Our results are not exactly symmetric, because samples with small rotation angle contain many atoms, which results in less precise minimization. For the case where z is free to move during minimization, we also looked at the values of z for varying θ, as shown in Figure 22. Here we see that there is a relatively large increase of interplanar distance with θ. Figure 23 shows the calculated minimal energies in comparison to E_{AB}.

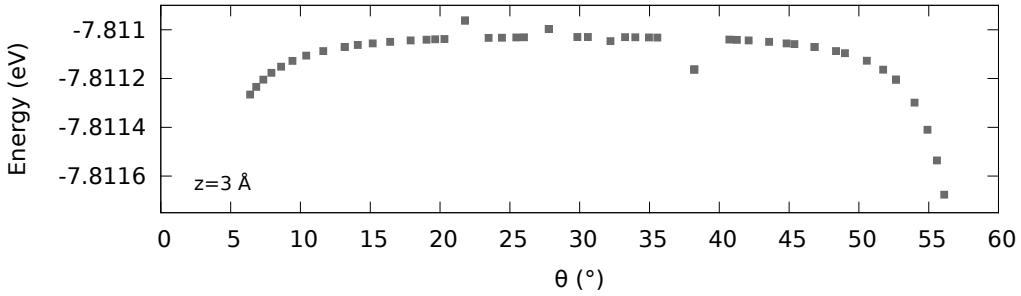

Figure 19: Minimal average energy per atom for bilayer graphene systems for varying rotation angles. The interlayer distance z is fixed at 3 Å.

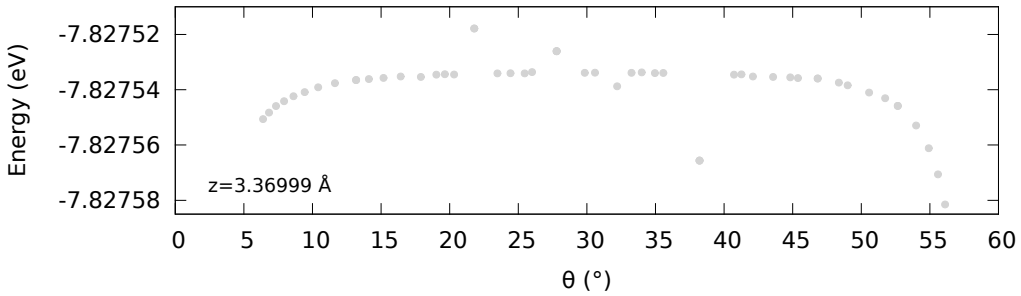

Figure 20: Minimal average energy per atom for bilayer graphene systems for varying rotation angles. The interlayer distance z is fixed at 3.36999 Å.

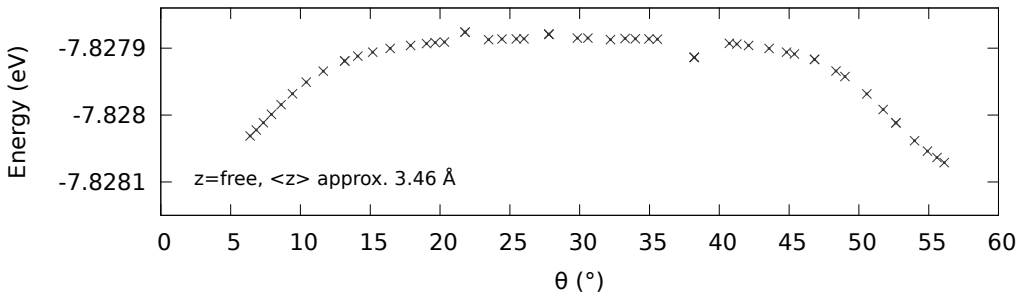

Figure 21: Minimal average energy per atom for bilayer graphene systems for varying rotation angles. The interlayer distance z is free to move. The average interlayer distance is 3.46 Å (see Figure 22).

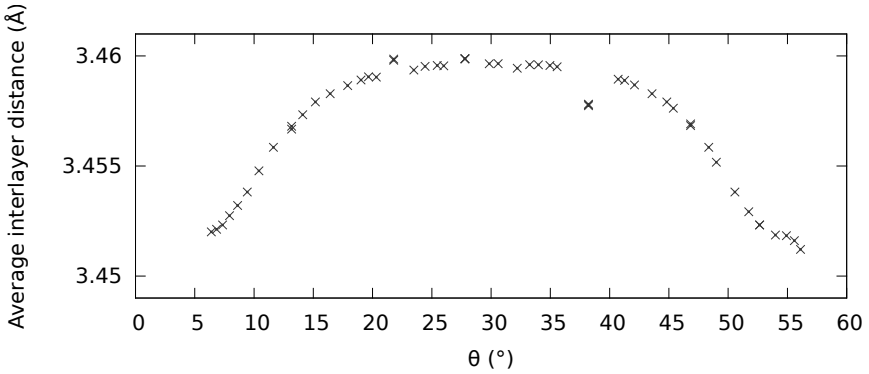

Figure 22: Samples that were also free to move in the z-direction showed the above behaviour for the interlayer distance after minimization. Note that the equilibrium interlayer distance for AB stacked graphene is 3.36999 Å.

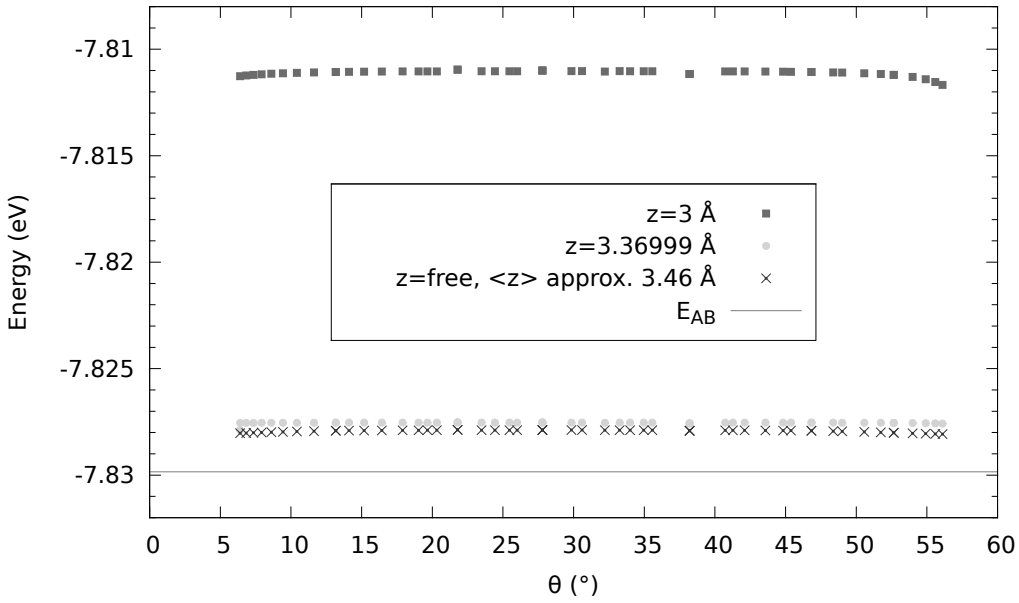

Figure 23: Minimization of all three cases together in one picture. E_{AB} (horizontal solid line) is given as a reference value.

Looking at these results, we see that there is a clear trend for the minimal energy as a function of θ. The least optimal angle is approximately 30°, and the energy decreases while getting further away from this angle. Furthermore, we see that for a fixed interlayer distance much smaller than the equilibrium distance for AB stacked graphene, the difference in energy between the samples is magnified (especially for z= 3Å). This means that any transition phenomena between samples will be enhanced and thus easier to observe. This is expected on the basis of the FK model, because decreasing the interlayer distance increases the interatomic potential while keeping the same values of the intralayer bonding energies. Therefore, in the following simulations when z is fixed we will consider z= 3Å.

6 Results: Effects of minimization on moiré patterns

We will look at four different properties of our samples after relaxation. We first consider the orientation of the top layer with respect to the bottom layer, which we will refer to as the substrate overlay. Next we consider the distortion of the hexagonal lattice by means of a gauge field, the average interatomic distance and finally the displacement of the atoms with respect to their initial unrelaxed configuration. In this final part we will also research the possible existence of an Aubry-like transition as mentioned in section 3.1. For these properties we select and show six of our samples with different rotation angles, all at fixed interlayer distance z= 3Å. Their rigid configuration before relaxation is shown in Appendix C. For every property we consider, we start our results with the largest rotation angle ($\theta = 13.2°$) and end with the smallest ($\theta = 0.46°$). At the very end of this section we will consider the situation where the atoms are free to move out of the plane as well, to make sure keeping the atoms at a fixed interlayer distance did not disturb our findings qualitatively.

6.1 Substrate overlay

To see how the top layer adapts to the substrate, it is interesting to look at the overlay of the two layers *before* and *after* minimization. The results for our selected samples are shown in Figures 24 to 29. We plot only the top layer of each sample. The colour of each atom indicates the distance in the plane to its nearest neighbour in the bottom layer: an overlay of 0 Å means the atom is directly above an atom in the bottom layer, while an overlay of 1.4 Å means the atom is above the center of a hexagon in the bottom layer. We can thus distinguish local AA and AB stacking, the first indicated by atoms with an overlay of approximately 0 Å (yellow) and the latter by an alternating overlay that approaches 1.4 Å (dark purple) and 0 Å (yellow).

When minimizing the energy, the atoms find their most favourable position. Since a position directly above another atom is the least favourable (see Figure 17), minimization of energy should result in a reduction of area with local AA stacking. Since AB stacking is the most favourable, areas with local AB stacking should be enlarged. For smaller rotation angles (Figures 26 to 29) we indeed see that the areas with local AA stacking are enlarged after relaxation. For relatively large rotation angles, the area of local AA stacking is already (almost) minimized in the rigid configuration before relaxation. For example, Figure 24 shows the overlay for sample (7,1) where the rotation angle is large (13.2°). Prior to relaxation, the local area of AA stacking covers only one atom, which cannot be minimized further. Therefore, the overlay after relaxation is almost identical to the overlay before relaxation. Furthermore we see that the difference between the overlay before and after relaxation is significantly enhanced as the rotation angle gets smaller. The local AA stacked areas are significantly decreased in size, as are the (green) areas with an overlay of 0.6 Å.

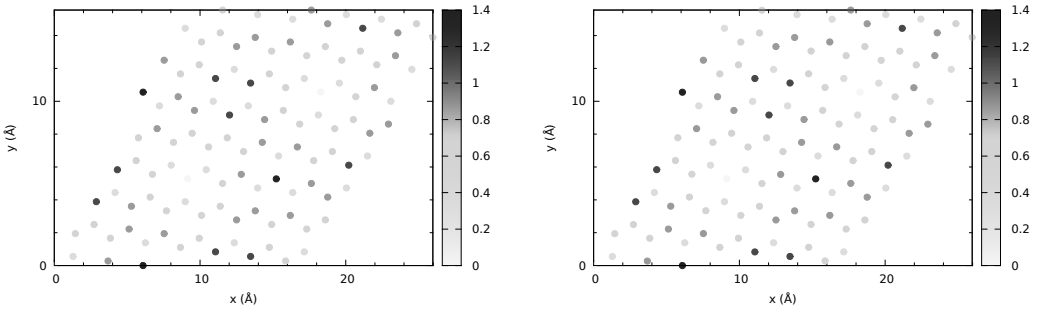

Figure 24: The substrate overlay before (left) and after (right) relaxation for sample (7,1), θ=13.2°, N=114. The substrate overlay does not change significantly due to relaxation.

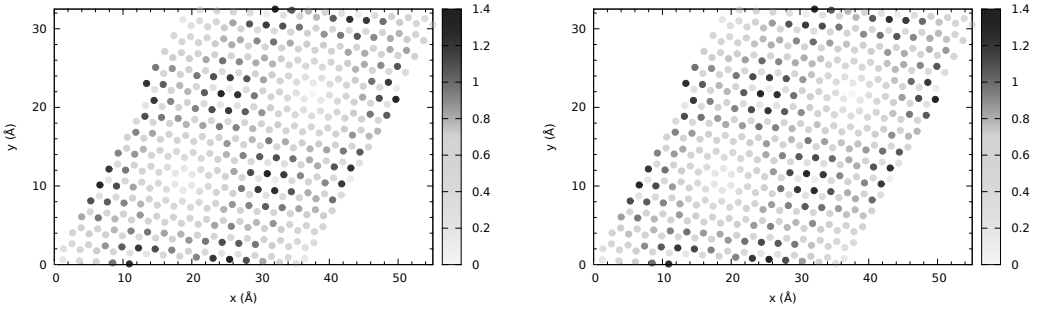

Figure 25: The substrate overlay before (left) and after (right) relaxation for sample (15,1), $\theta = 6.4°$, N= 482. The substrate overlay does not change significantly due to relaxation.

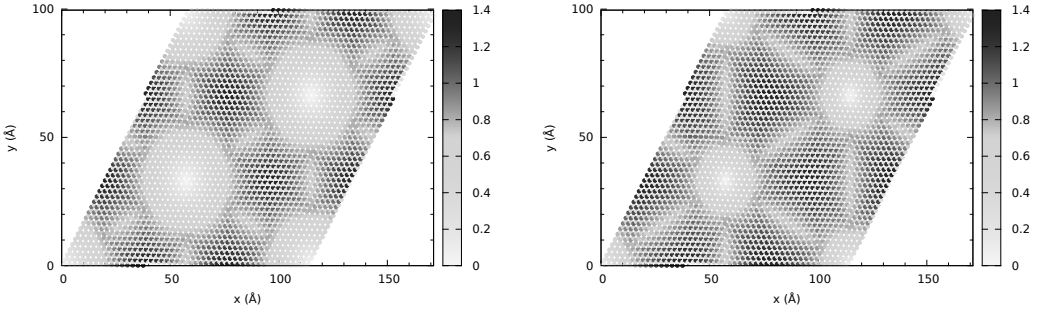

Figure 26: The substrate overlay before (left) and after (right) relaxation for sample (47,1), $\theta = 2.08°$, N= 4514. The substrate overlay after relaxation has visibly smaller areas of AA stacking (yellow). Furthermore, the areas with an overlay of approximately 0.6Å (bright green) are also reduced in size.

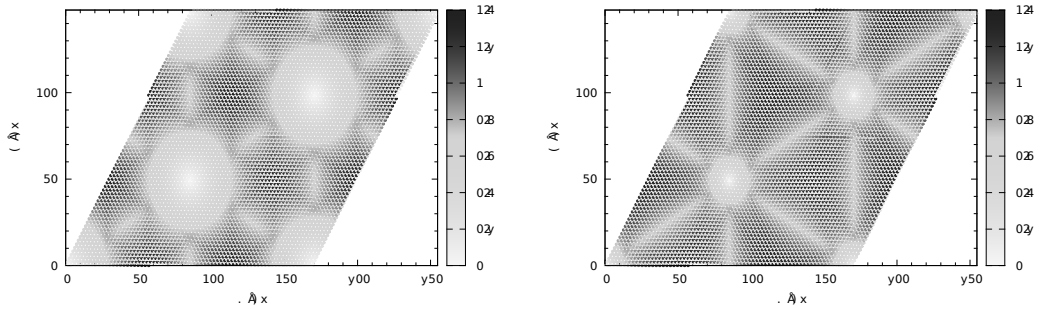

Figure 27: The substrate overlay before (left) and after (right) relaxation for sample (70,1), $\theta = 1.41°$, N= 9942. The substrate overlay after relaxation has significantly smaller areas of AA stacking (yellow). Furthermore, the areas with an overlay of approximately 0.6Å (bright green) are also reduced in size.

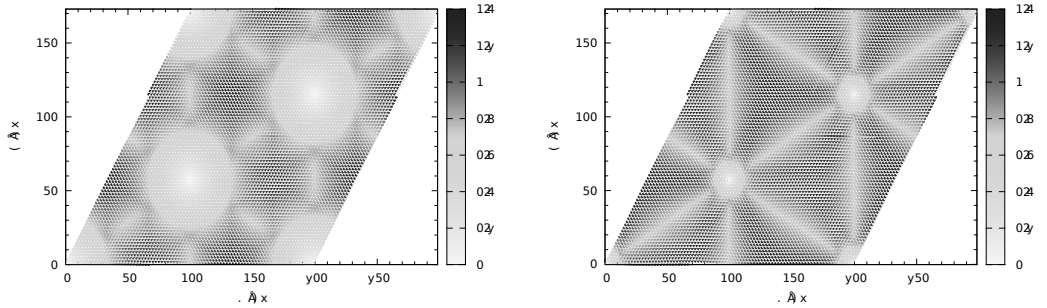

Figure 28: The substrate overlay before (left) and after (right) relaxation for sample (82,1), $\theta = 1.2°$, N= 13614. The substrate overlay after relaxation has significantly smaller areas of AA stacking (yellow). Furthermore, the areas with an overlay of approximately 0.6Å (bright green) are also reduced in size.

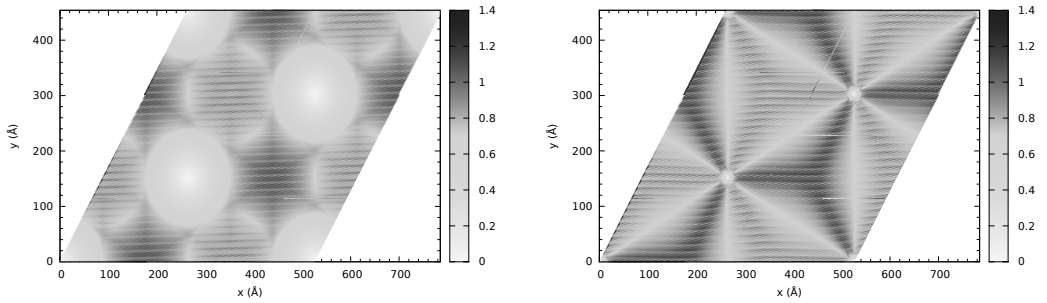

Figure 29: The substrate overlay before (left) and after (right) relaxation for sample (216,1), $\theta = 0.46°$, N= 92746. The substrate overlay after relaxation has much smaller areas of AA stacking (yellow). Furthermore, the areas with an overlay of approximately 0.6Å (bright green) are also reduced in size. (For this sample the colour intensity is slightly less bright than for the other samples. This is an effect of different plot settings due to the extremely large number of atoms in the sample.)

The decrease in AA stacked areas can be seen also in another, much simpler, representation as shown in Figures 30 and 31. We simply plot the top view of two stacked layers of graphene for our sample with $\theta = 1.2°$. Figure 30 shows the sample before relaxation, and Figure 31 shows the sample after relaxation. Indeed, we clearly see the area of AA stacking decrease as a result of minimization of energy. Furthermore, the hexagonal moiré pattern that is nicely framed before relaxation, turns into a hexagonal pattern of the same size with six rays after relaxation.

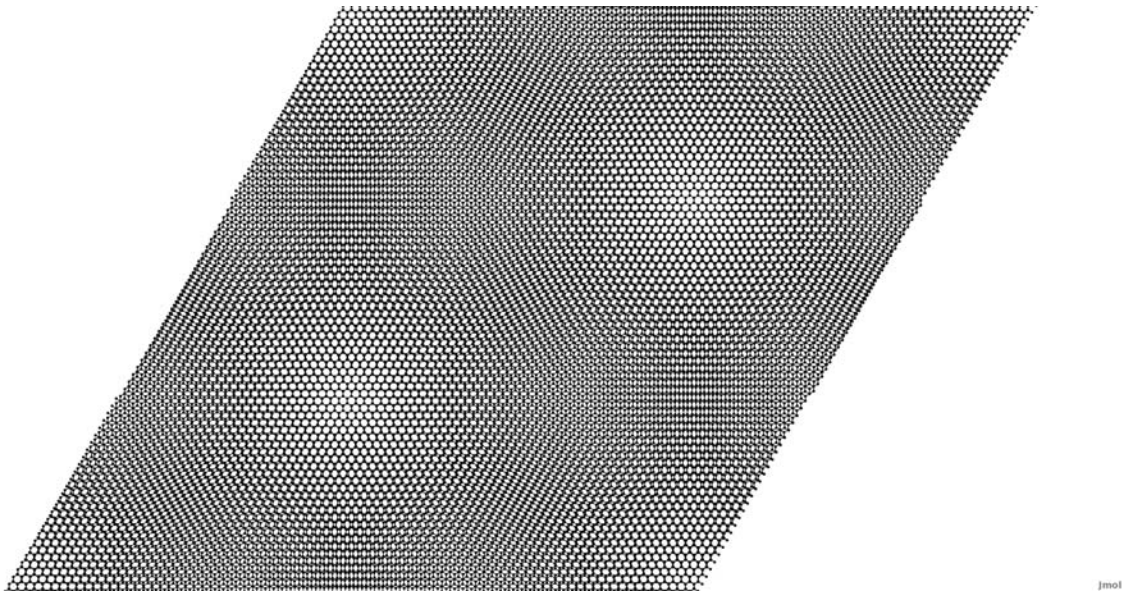

Figure 30: Two layers for sample (82,1), θ=1.2° *before* relaxation.

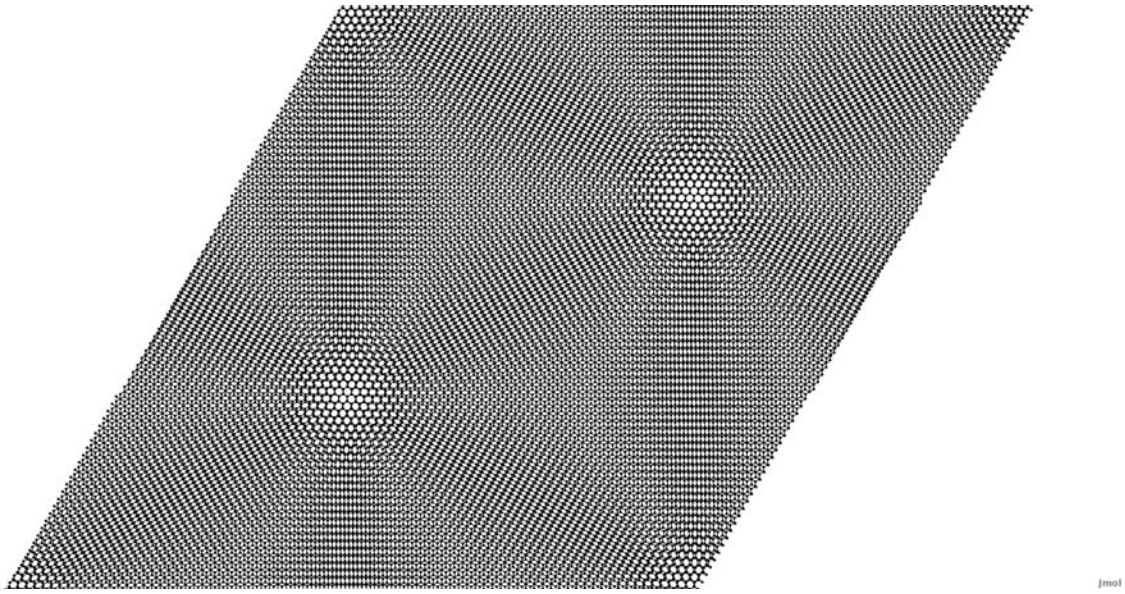

Figure 31: Two layers for sample (82,1), θ=1.2° *after* relaxation.

6.2 Average interatomic distance

Next, we consider the following representation of the system: we calculate the nearest neighbour distance (or interatomic distance) for each atom in the top layer, averaged over its three neighbours after relaxation. The results are shown in Figures 32 to 37. The colour of each atom represents its average interatomic distance, where yellow stands for the equilibrium interatomic distance for ideal graphene, 1.3978 Å. Thus, red areas are stretched while blue areas are compressed compared to the equilibrium state.

Something interesting and unexpected occurs between samples (70,1) and (82,1), as seen in Figures 35 and 36. The pattern within a moiron starts to rotate. In fact, when we look closely we already see a subtle hint of this rotation for sample (70,1). This suggests that there is some transition around critical angle $\theta_c \approx 1.4°$.

When we compare the results below to the plots of the substrate overlay (Figures 24 to 29), we can see how the minimization of AA areas comes about. Where there is local AA stacking prior to minimization, the average bond length after minimization is below the equilibrium bond length. Where there is local AB stacking prior to minimization, the average bond length after minimization is larger than the equilibrium bond length. In other words, graphene is locally compressed to reduce AA areas, while it is stretched to enlarge AB areas.

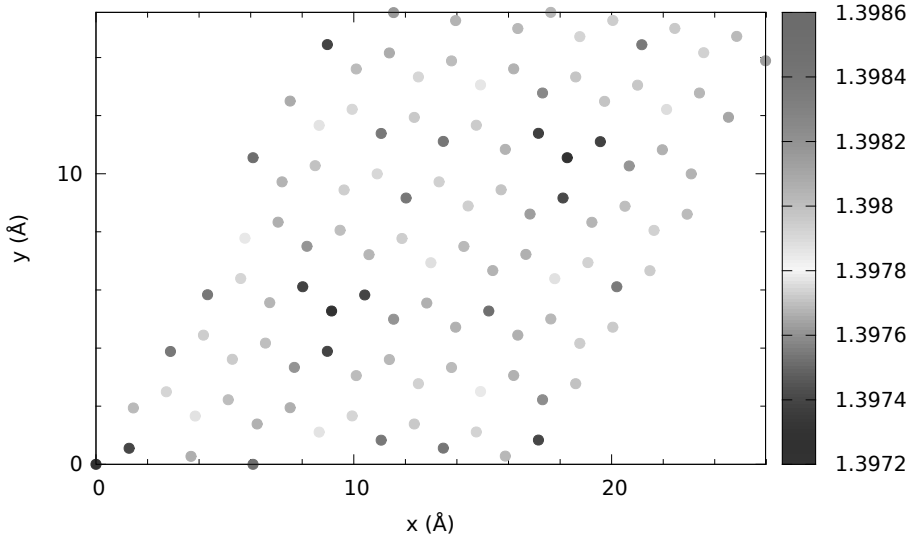

Figure 32: Average interatomic distance for sample (7,1), θ=13.2°, N=114. Yellow is the equilibrium interatomic distance 1.3978 Å, red areas are stretched and blue areas are compressed.

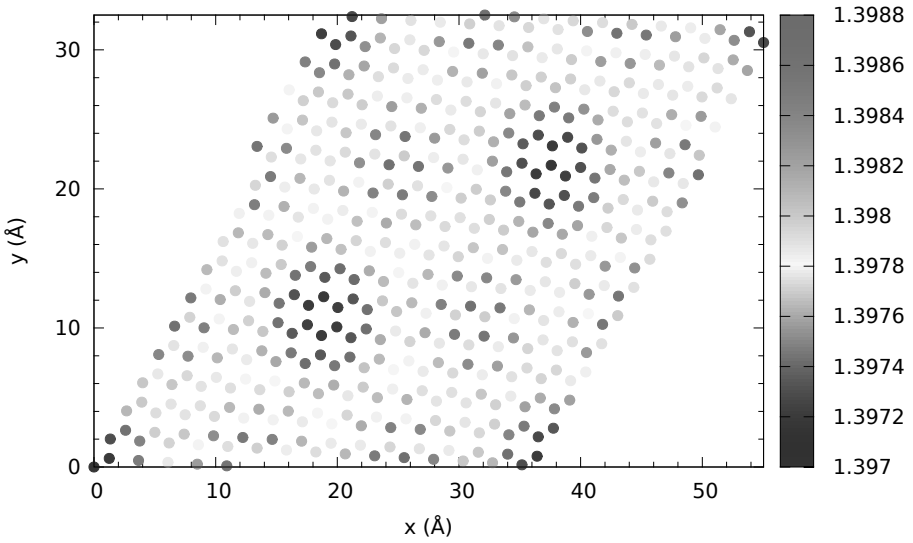

Figure 33: Average interatomic distance for sample (15,1), θ=6.4° , N=482. Yellow is the equilibrium interatomic distance 1.3978 Å, red areas are stretched and blue areas are compressed.

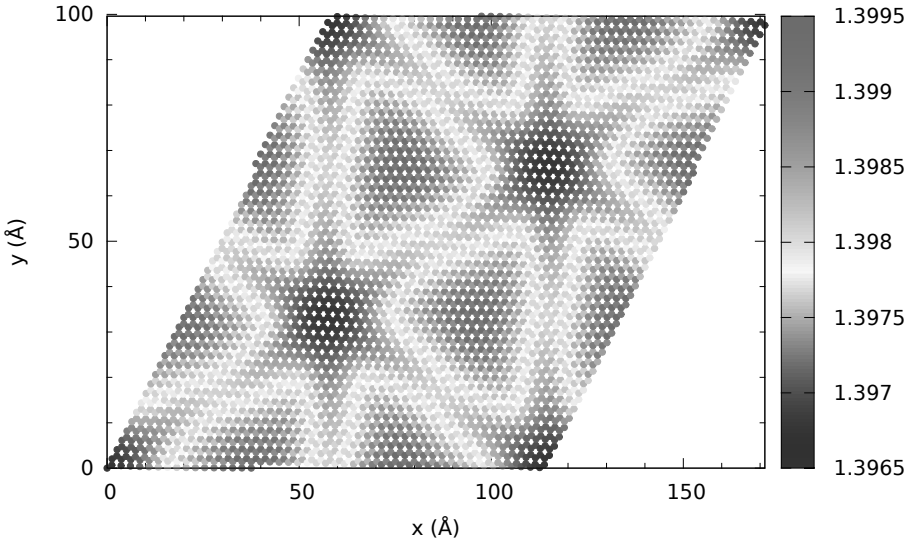

Figure 34: Average interatomic distance for sample (47,1), θ=2.08°, N=4514. Yellow is the equilibrium interatomic distance 1.3978 Å, red areas are stretched and blue areas are compressed. A star-shaped pattern is clearly defined.

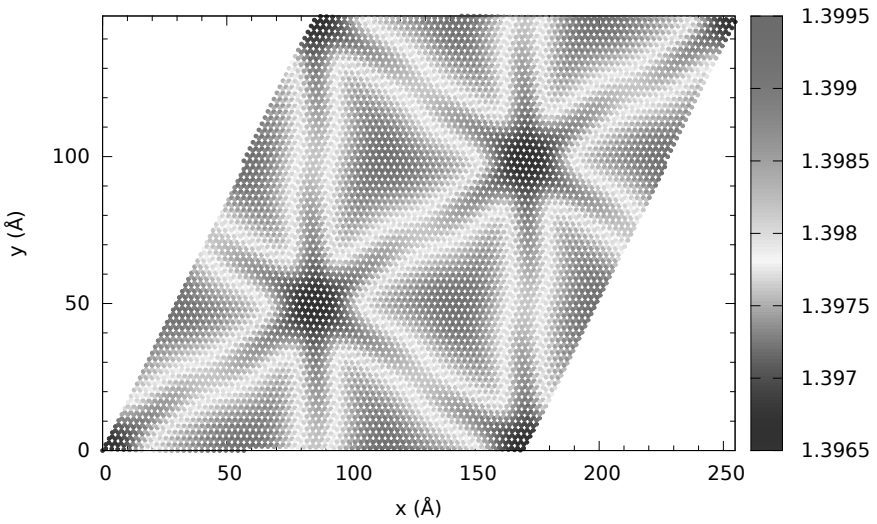

Figure 35: Average interatomic distance for sample (70,1), θ=1.4°, N=9942. Yellow is the equilibrium interatomic distance 1.3978 Å, red areas are stretched and blue areas are compressed. A star-shaped pattern is clearly defined.

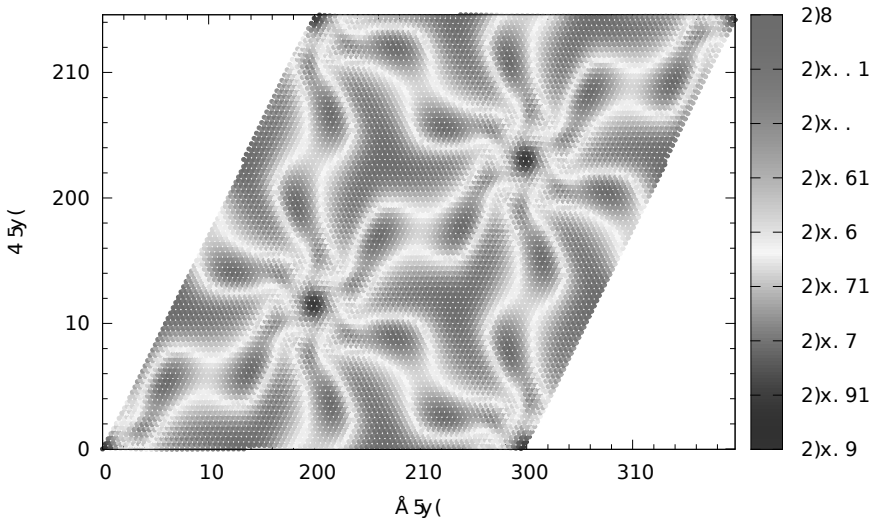

Figure 36: Average interatomic distance for sample (82,1), θ=1.2°, N=13614. Yellow is the equilibrium interatomic distance 1.3978 Å, red areas are stretched and blue areas are compressed. The star-shaped pattern started to rotate, creating some complex pattern.

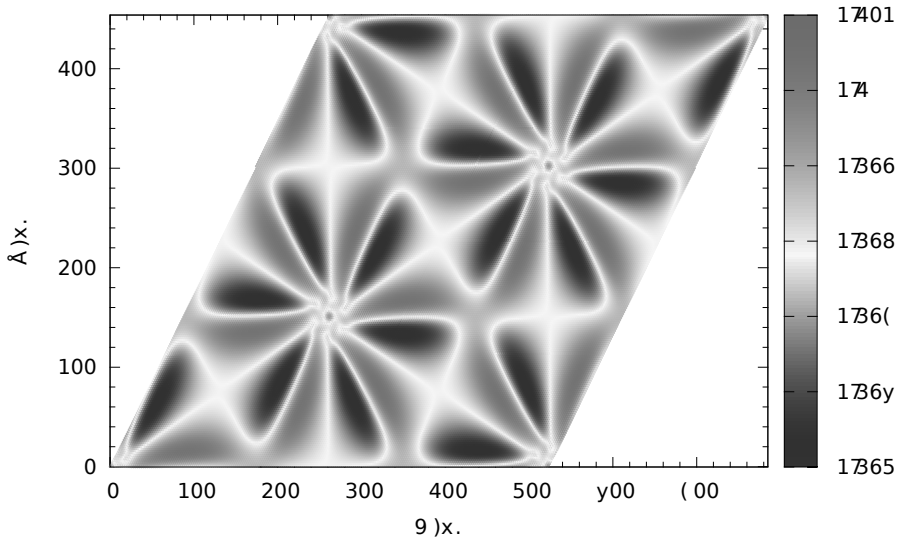

Figure 37: Average interatomic distance for sample (216,1), θ=0.46°, N=93746. Yellow is the equilibrium interatomic distance 1.3978 Å, red areas are stretched and blue areas are compressed. The star-shaped pattern seems to be be rotated, creating some complex well defined pattern.

Let us concentrate on the transition between sample (70,1) and (82,1). To get a more detailed view of what happens between these samples, we plot the average interatomic distance along the bisector (diagonal) of the relaxed layer. An illustration of the bisector for both samples is given in Figure 38. In Figure 39 we plotted the average interatomic distance for both samples across their bisector. We see that sample (70,1) exhibits a sine like behaviour, while sample (82,1) seems to have a double periodicity. Furthermore, Figure 40 shows a histogram of the average interatomic distance for both samples. We see no difference in the shape of the histograms. Thus, we can conclude that the distribution of interatomic distances stays similar, but the location of the interatomic distances within the pattern is changed.

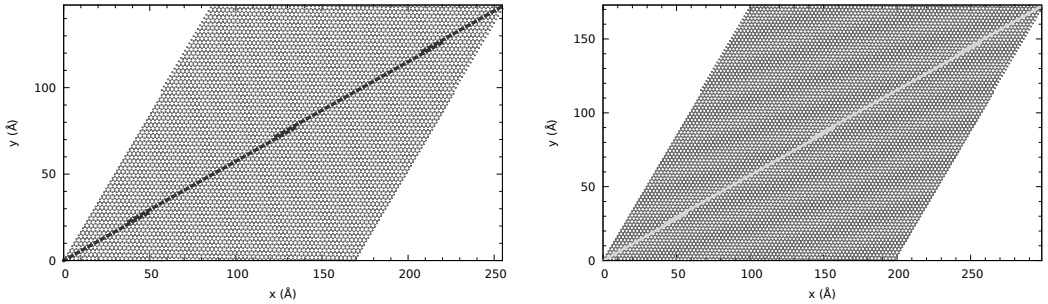

Figure 38: Bisector of samples (70,1), θ=1.4° (left) and (82,1), θ=1.2° (right).

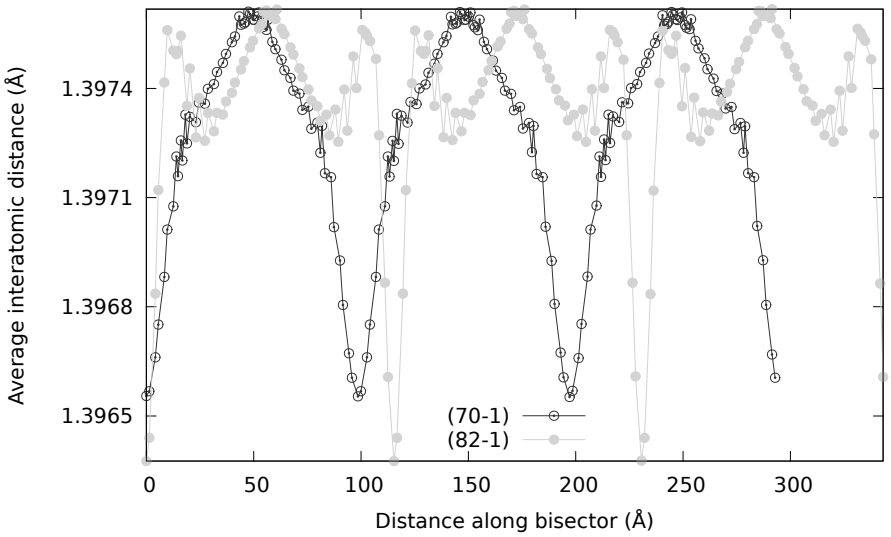

Figure 39: Average interatomic distance for atoms along the angle bisector of the samples (70,1), θ=1.4° and (82,1), θ=1.2°. Sample (70,1) exhibits a sine like behaviour, while sample (82,1) seems to have a double periodicity. When we look closely we already see a subtle hint of this double periodicity for sample (70,1).

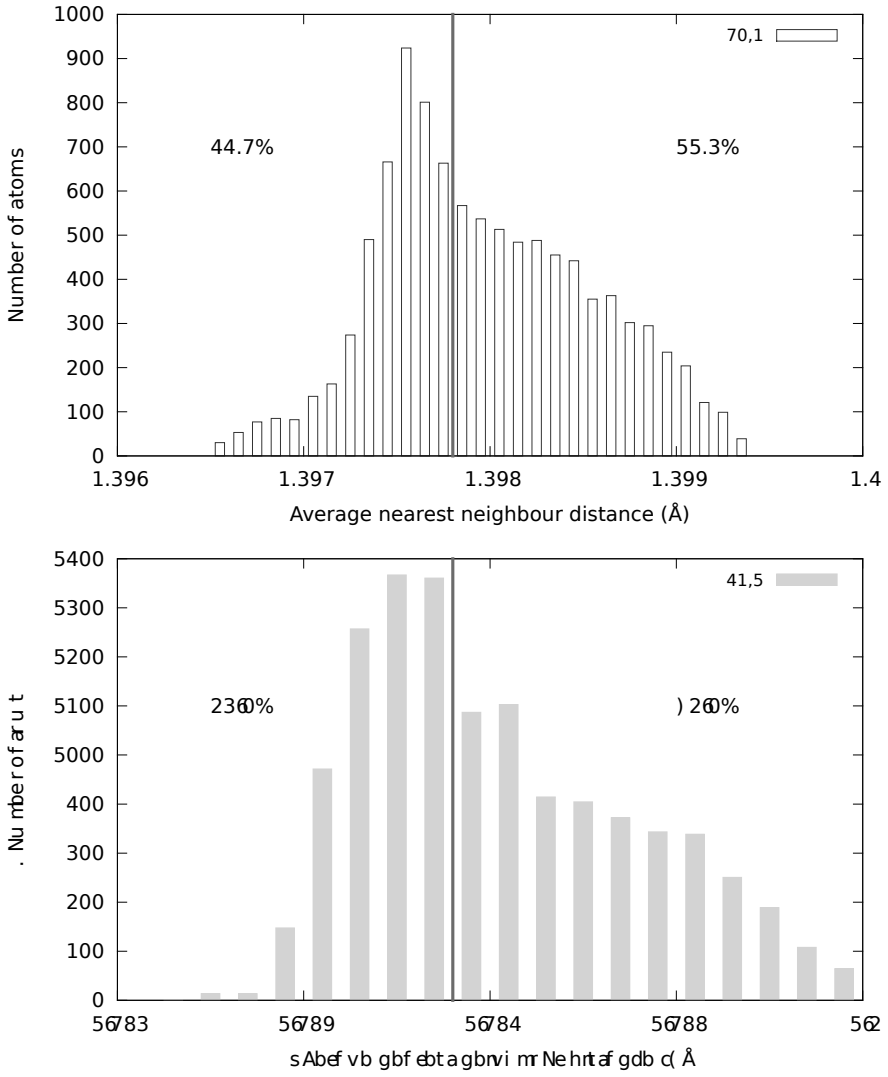

Figure 40: A histogram of the average interatomic distance for samples (70,1) and (82,1). The distribution if interatomic distances is similar for both samples.

6.3 Distortion of hexagons: gauge field

A nice representation of the distortion of the hexagonal lattice in the top layer is gauge field, $\vec{A}$, as defined by Mikhail Katsnelson[9] :

$$A_x = \frac{\sqrt{3}}{2}(t_3 - t_2), \qquad A_y = \frac{1}{2}(t_2 + t_3 - 2t_1),$$

where $t_{1,2,3}$ are the distances between an atom ($\vec{r_0}$) and its nearest neighbours ($\vec{r}_{1,2,3}$) after minimization:

$$t_1 = |\vec{r_0} - \vec{r_1}|, \qquad t_2 = |\vec{r_0} - \vec{r_2}|, \qquad t_3 = |\vec{r_0} - \vec{r_3}|$$

The situation where $\vec{A} = 0$, i.e. $t_1 = t_2 = t_3$ corresponds to an undistorted lattice, for instance ideal graphene. The nearest neighbours are ordered consequently as shown in Figure 41.

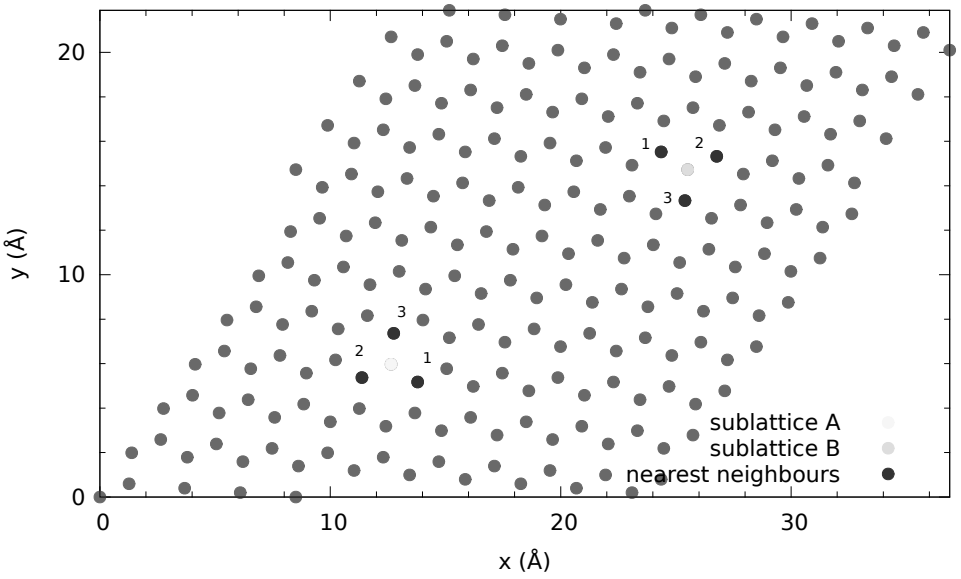

Figure 41: Sublattices A and B and their ordered nearest neighbours

The results for our six selected samples are shown below. Let us start by looking at the results for sample (7,1), $\theta = 13.2°$, N= 114. We see from Figures 42 and 43 that the gauge field goes to zero for atoms that are placed on top of an atom in the bottom layer before relaxation and for atoms that are placed in the middle of a hexagon of the bottom layer. From the point of view of such an atom, there is a special symmetry: its three nearest neighbours are in the same configuration with respect to the bottom layer. Therefore, the three neighbours will exhibit the same behaviour during relaxation and will end up at the same distance from the atom in the

middle. Hence, the gauge field will be zero. If we combine the plots for the gauge field with our results for substrate overlay and average interatomic distance, we see that the local AA stacked areas are compressed uniformly, since the gauge field goes to zero. Thus, for local AA stacked areas, the hexagonal shape of the lattice is preserved. Furthermore, we see similar behaviour in the center of local AB stacked areas: the gauge field goes to zero. This means that the AB stacked areas are uniformly stretched.

Considering a possible transition around θ_c, there is no clear difference between the different samples, although the last three samples in Figure 46, 47 and 48 seem more *wavy* than the samples with a larger rotation angle. Furthermore, we see that the maximal distortion of the lattice gets larger for smaller rotation angles. Finally, we see that for our final sample with a rotation angle of 0.46° the area of small distortion (yellow) is considerably larger than for the other samples. Nevertheless, for this sample our finding is still valid: AA and AB stacked areas are uniformly compressed and stretched respectively.

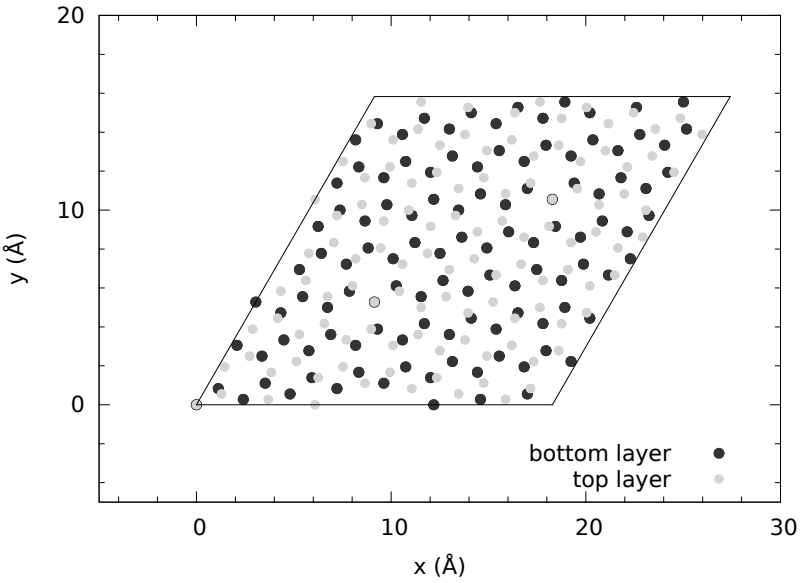

Figure 42: Sample (7,1), $\theta = 13.2°$, N= 114 before relaxation. The blue dots represent the atoms in the bottom layer and the green dots represent the atoms in the top layer. AA stacked atoms are indicated by a green dot with a blue ring around it. In this sample there are three atoms that are perfectly AA stacked, for example the atom in the left bottom corner.

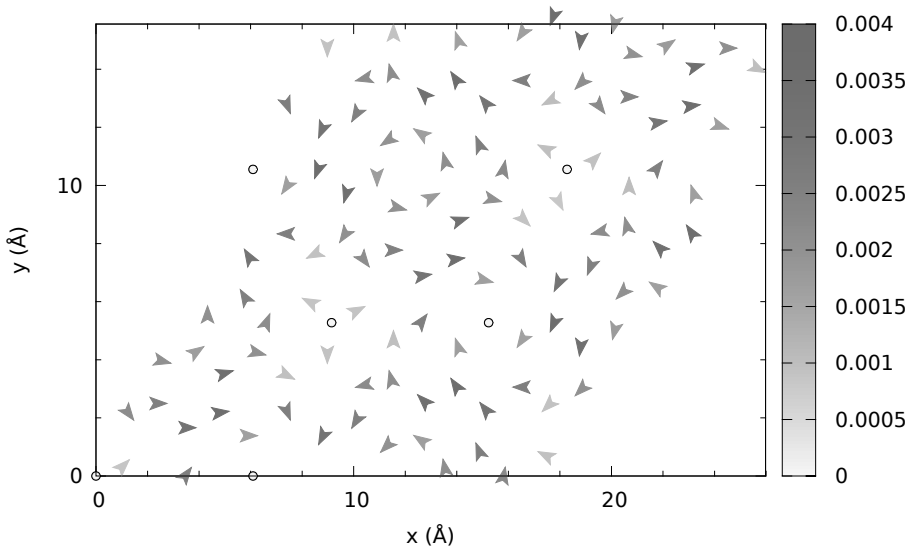

Figure 43: Gauge field for sample (7,1), $\theta = 13.2°$, N= 114. Yellow dots with a black circle represent atoms for which the gauge field is close to zero, namely $|\vec{A}| < 0.0005$

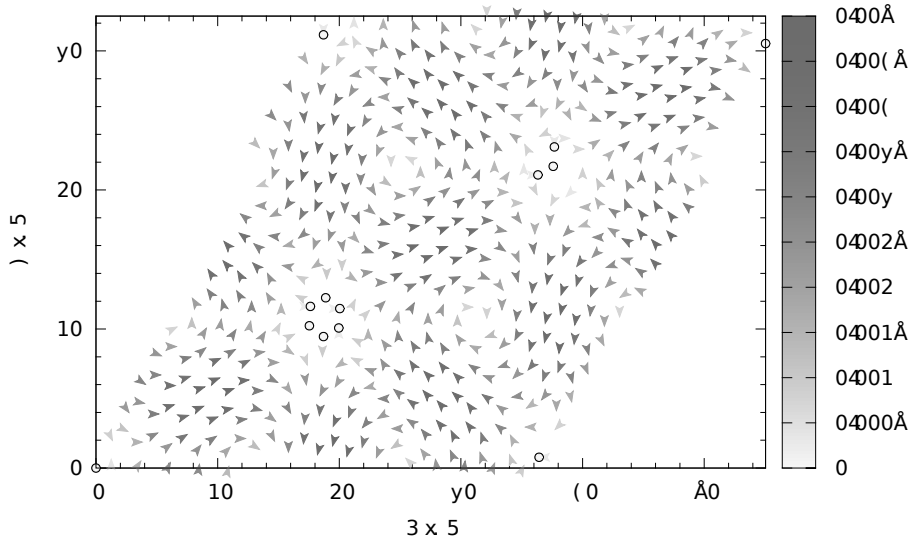

Figure 44: Gauge field for sample (15,1), $\theta = 6.4°$, N= 482. Yellow dots with a black circle represent atoms for which the gauge field is close to zero, namely $|\vec{A}| < 0.0003$.

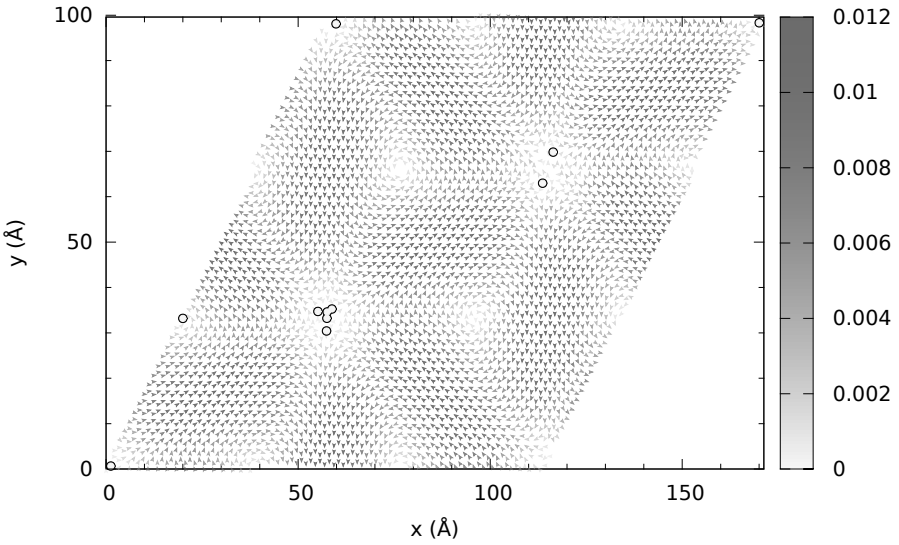

Figure 45: Gauge field for sample (47,1), $\theta = 2.08°$, N= 4514. Yellow dots with a black circle represent atoms for which the gauge field is close to zero, namely $|\vec{A}| < 0.0002$.

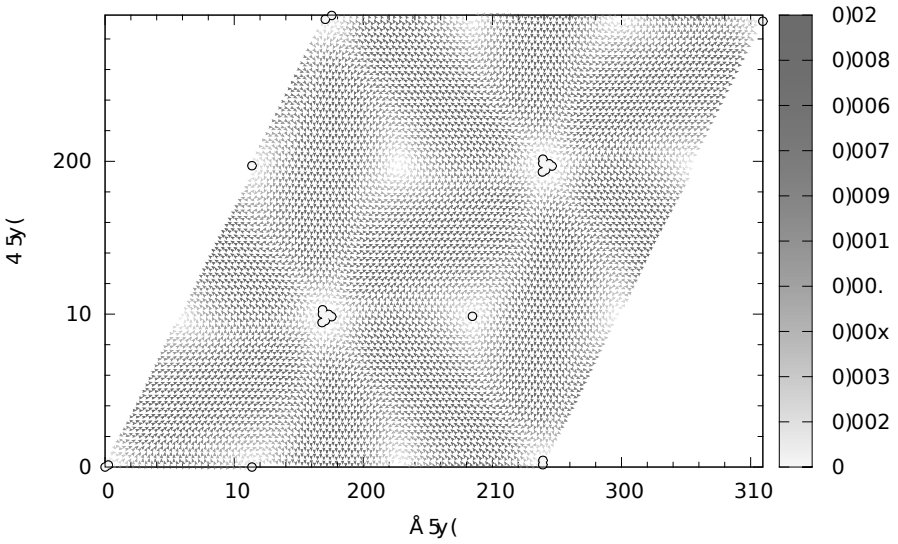

Figure 46: Gauge field for sample (70,1), $\theta = 1.41°$, N= 9942. Yellow dots with a black circle represent atoms for which the gauge field is close to zero, namely $|\vec{A}| < 0.0002$.

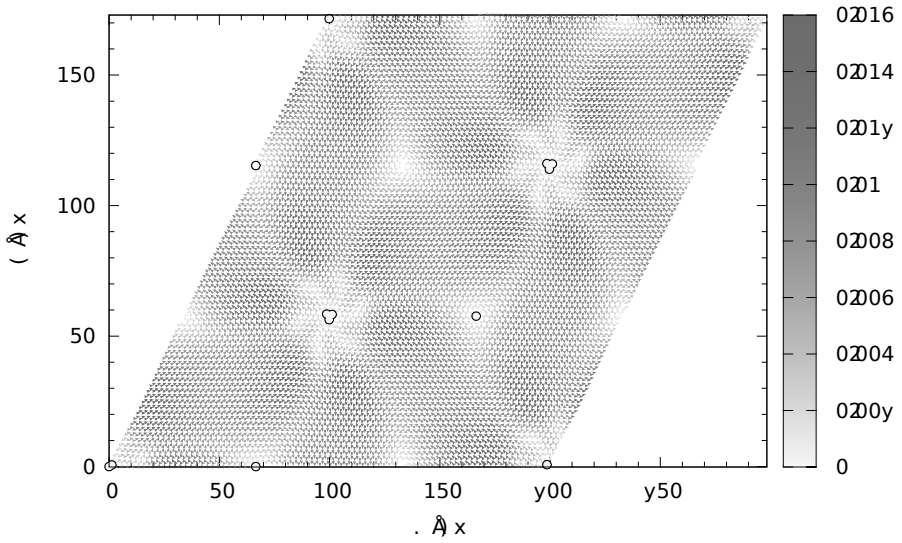

Figure 47: Gauge field for sample (82,1), $\theta = 1.2°$, N= 13614. Yellow dots with a black circle represent atoms for which the gauge field is close to zero, namely $|\vec{A}| < 0.0002$.

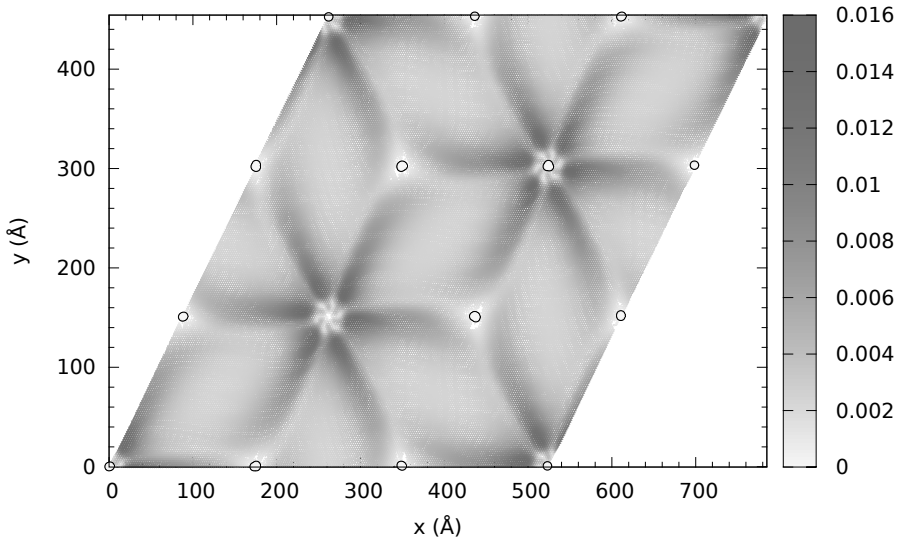

Figure 48: Gauge field for sample (216,1), $\theta = 0.46°$, N= 92746. Yellow dots with a black circle represent atoms for which the gauge field is close to zero, namely $|\vec{A}| < 0.0002$.

6.4 Displacement

The final property of the system we will discuss is the displacement of the atoms in the top layer plane due to minimization. Again, keep in mind that we only allow atomic displacement within the plane, while keeping a fixed interlayer distance. Note that this displacement is not a real physical quantity, since the system prior to relaxation (two stacked layers of *ideal* graphene) is not a real physical system. The displacement shows how the moiré pattern of the minimized sample differs from the rigid moiré pattern. However, this quantity is interesting to consider, as it clearly shows the effect of relaxation on the sample. After discussing our six samples, we will pick one sample and investigate the existence of the Aubry transition.

6.4.1 Vectorfield displacement

We look at the moiré patterns in the total planar displacement for our six samples. The results are shown in Figures 49 to 54. Note that for large samples individual atoms will no longer be visible as arrows in the plot, and they will appear continuously coloured instead of discretely. We see that the atoms in each moiron move in a vortex around the center of the moiron, which is AA stacked. Figure 55 shows the maximal and average displacement for each sample.

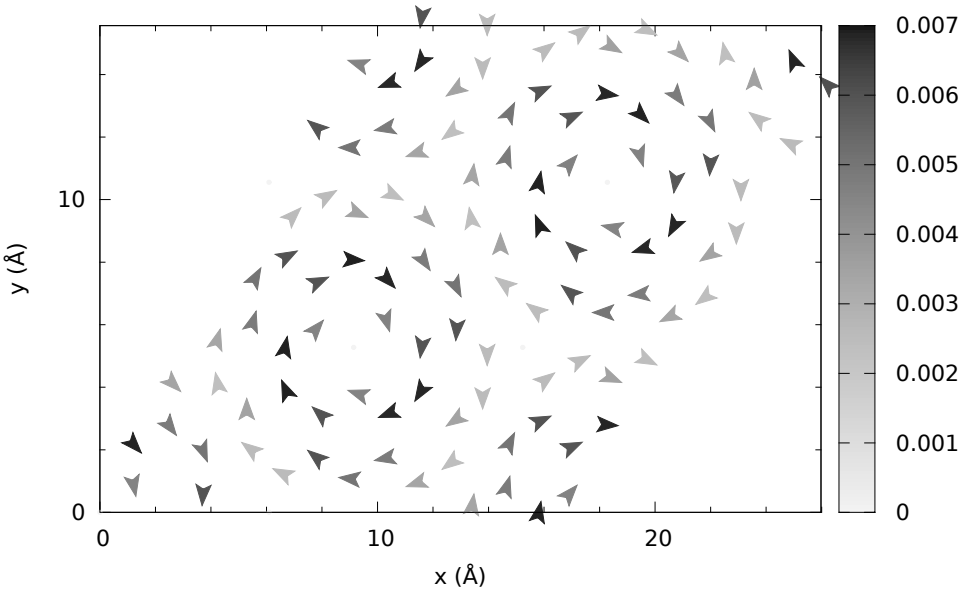

Figure 49: In plane displacement for sample (n,m)=(7,1), θ=13.2°, N=114

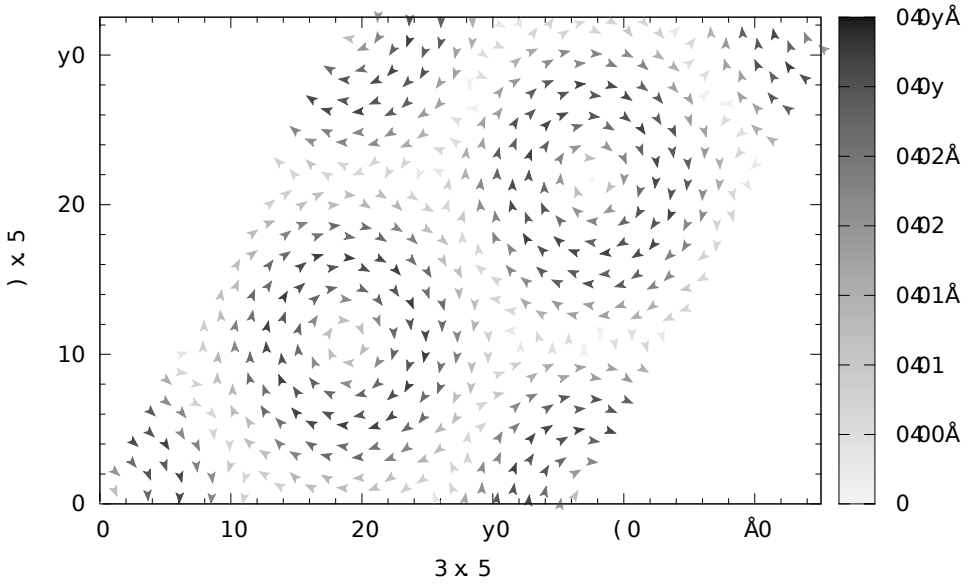

Figure 50: In plane displacement for sample (n,m)=(15,1), θ=6.4°, N=482

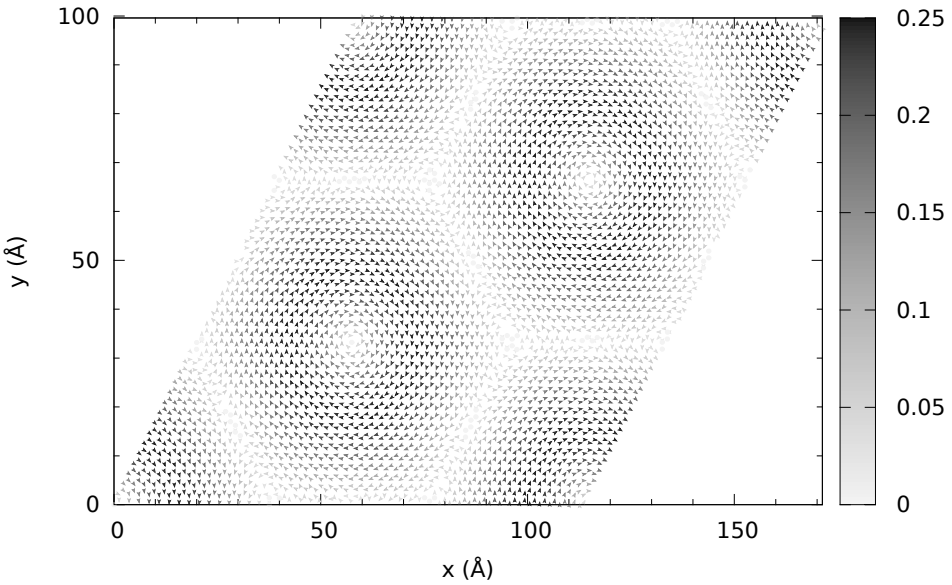

Figure 51: In plane displacement for sample (n,m)=(47,1), θ=2.1°, N=4514

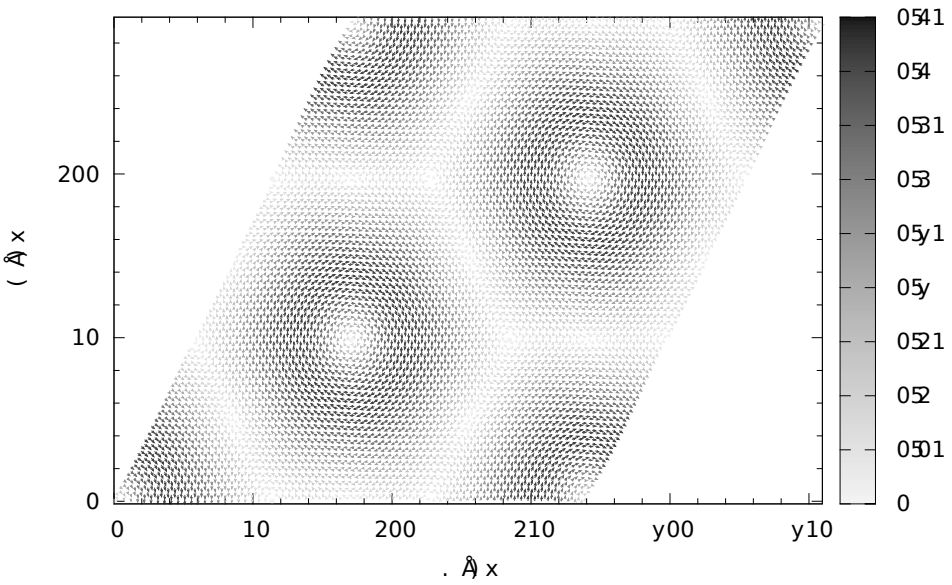

Figure 52: In plane displacement for sample (n,m)=(70,1), θ=1.4°, N=9942

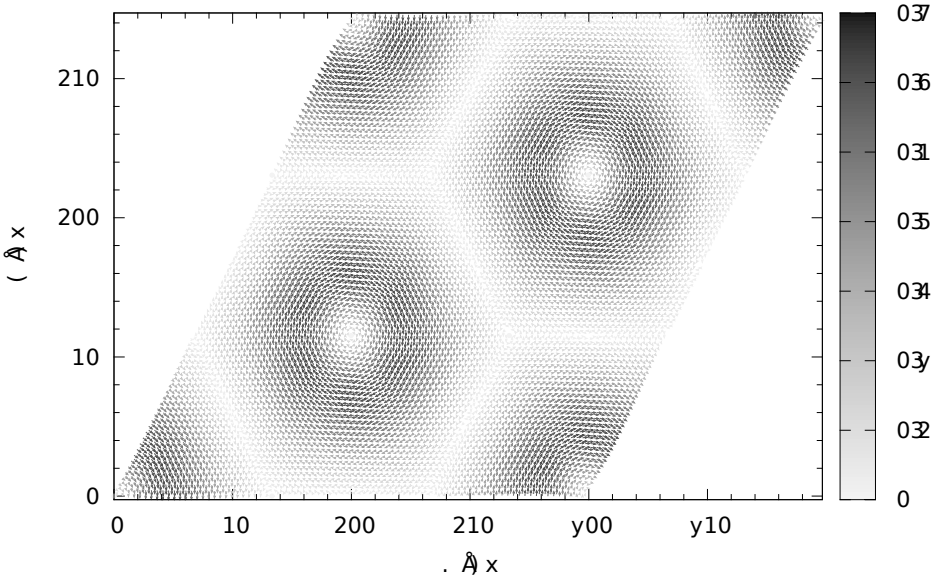

Figure 53: In plane displacement for sample (n,m)=(82,1), θ=1.2°, N=13614

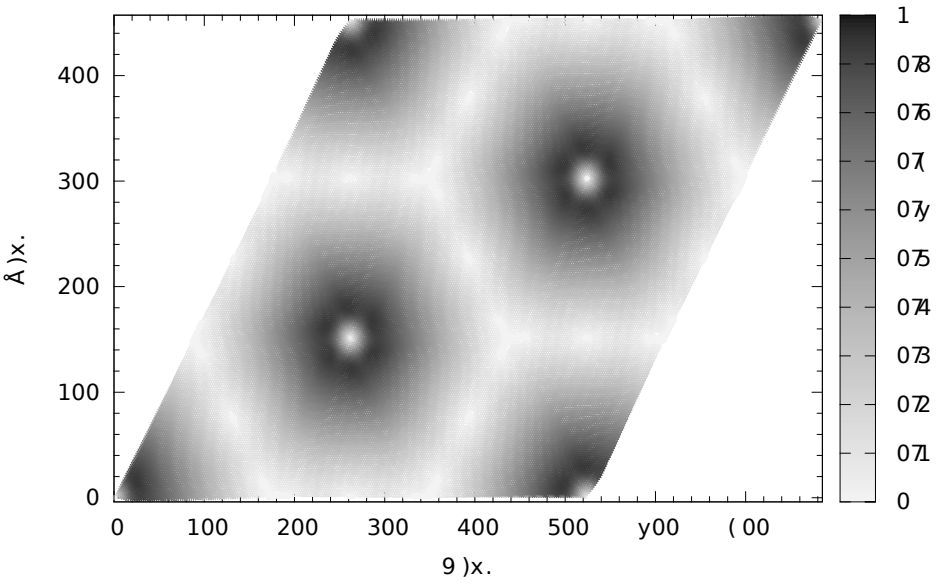

Figure 54: In plane displacement for sample (n,m)=(216,1), θ=0.46°, N=93746

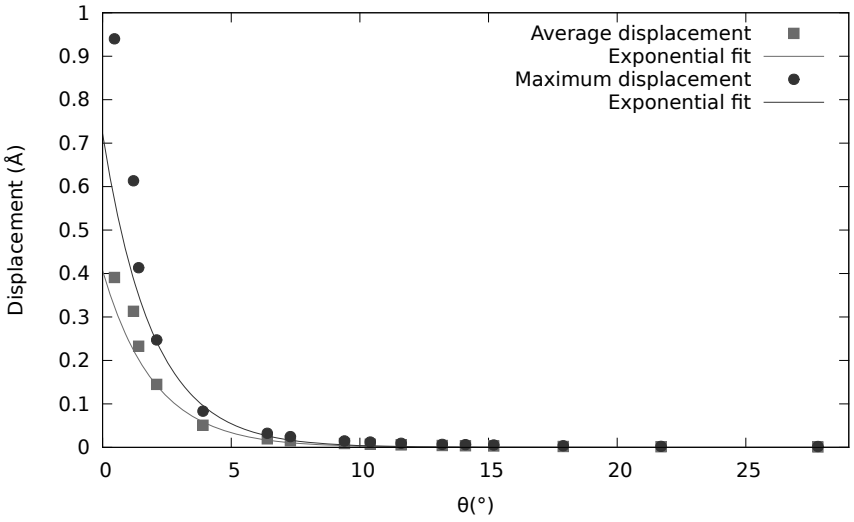

Figure 55: Average and maximal displacement for various samples. Exponential fit for average displacement: $0.406e^{-\theta/2.01}$. Exponential fit for maximal displacement: $0.721e^{-\theta/1.93}$.

In Figures 49 to 54 we see that for small rotation angles, the maximal displacement (dark ring) takes place closer to the center of the moiron than for larger rotation angles. To get a more detailed view of what happens with the displacement when we vary the angle, we plot the displacement along the bisector of the relaxed layer. The results for our six selected samples are shown in Figure 56.

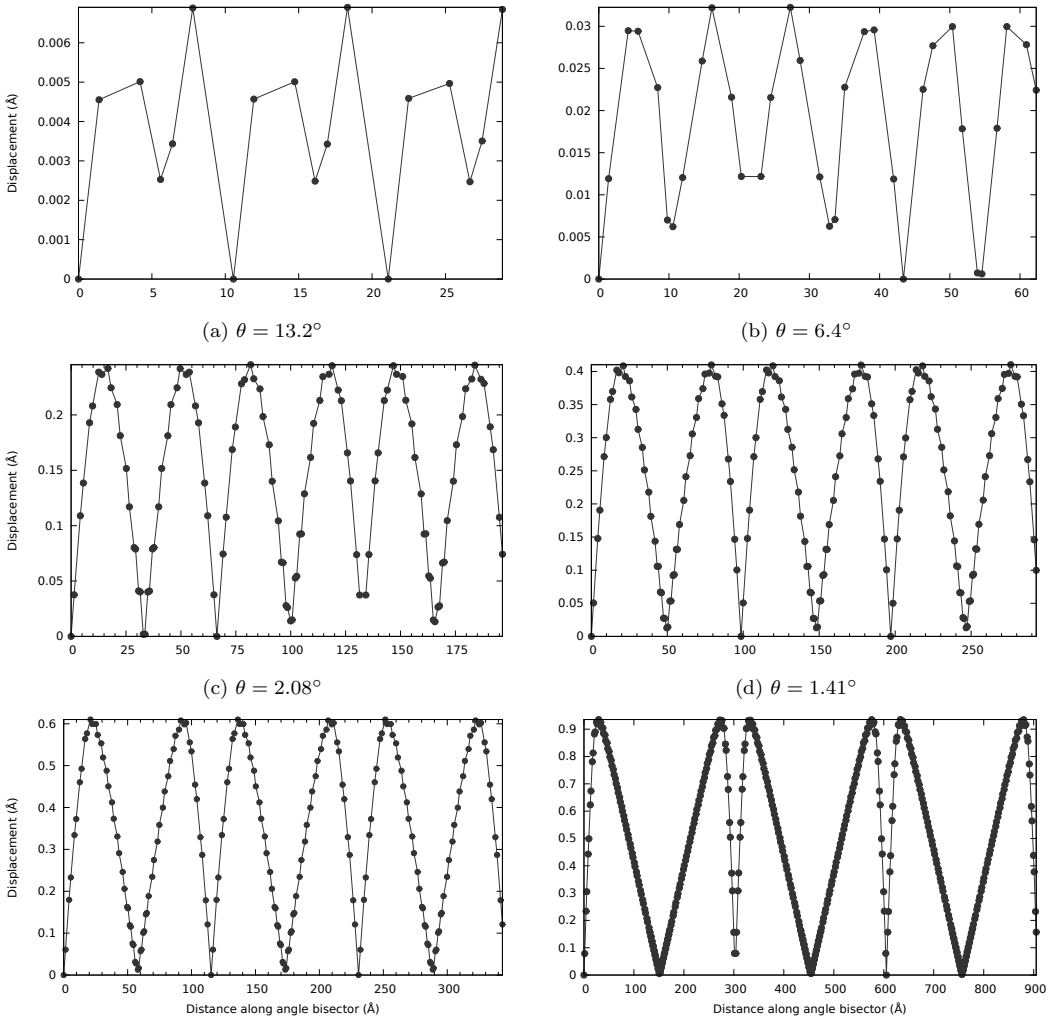

(a) $\theta = 13.2°$ (b) $\theta = 6.4°$

(c) $\theta = 2.08°$ (d) $\theta = 1.41°$

(e) $\theta = 1.2°$ (f) $\theta = 0.46°$

Figure 56: Displacement of the atoms along bisector of the samples (a) (7,1), $\theta = 13.2°$, N= 114; (b) (15,1), $\theta = 6.4°$, N= 482; (c) (47,1), $\theta = 2.08°$, N= 4514; (d) (70,1), $\theta = 1.41°$, N= 9942; (e) (82,1), $\theta = 1.2°$, N= 13614; (f) (216,1), $\theta = 0.46°$, N= 92746.

We see that the moiré pattern is not so well defined for larger angles (Figure56a and b), as predicted by Klaus Hermann.[12] If the angle is large, the pattern is small and there are not many atoms within one moiron. This results in larger differences between the displacement of nearby atoms and therefore a less fluent trend if we plot along the bisector. For smaller angles, Figure 56 shows a clear continuous moiré period. Finally, we see that for very small angles, the displacement becomes discontinuous. This is related to the position of maximal displacement within the moiron. As mentioned before, the ring of maximal displacement gets closer to the center of the moiron for small rotation angles. Let us quantify this phenomenon by considering the following ratio: R=D_{max}/D_{moiron}, where D_{max} is the diameter of the ring of maximal displacement and D_{moiron} the size of the moiron. Figure 57 illustrates how we calculate R for sample (82,1). Table 3 shows the values of R for some of our samples and they are plotted in Figure 58. Indeed we see that R decreases significantly for rotation angles below 1.4°. This supports our previously found evidence for some transition in the average interatomic distance for some critical rotation angle around 1.4°.

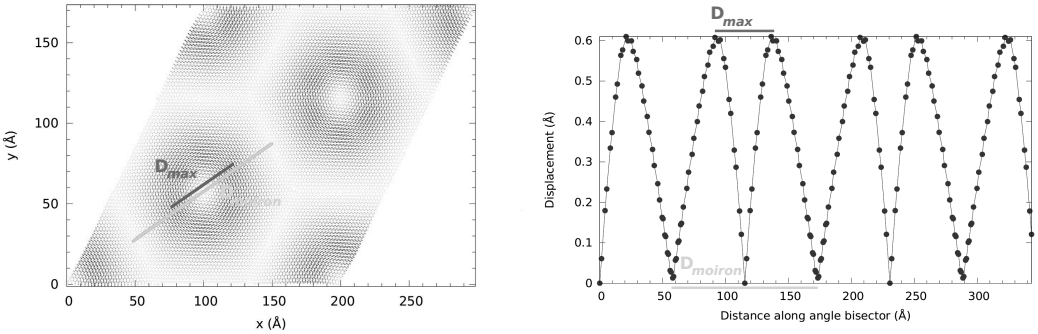

Figure 57: To calculate the diameter of the ring of maximal displacement (D_{max}) we consider the red line and for the size of the moiron (D_{moiron}) we consider the green line. The ratio of the two (R) tells us how close the ring of maximal displacement is to the center of the moiron.

Table 3: Ratio (R) of diameter of ring of maximal displacement to the size of a moiron. N is the number of atoms per layer. Next to the six samples we discussed above, we add more samples to make a clearer trend. For rotation angles larger than approximately 2.9° the pattern is not well defined and no reliable value of R can be calculated.

(n,m)	θ (°)	N	R
(69,2)	2.83	9806	0.48
(36,1)	2.72	2666	0.47
(47,1)	2.08	4514	0.45
(58,1)	1.69	6846	0.42
(70,1)	1.41	9942	0.41
(82,1)	1.2	13614	0.38
(100,1)	0.99	20202	0.34
(216,1)	0.46	92746	0.19
(260,1)	0.38	135722	0.16

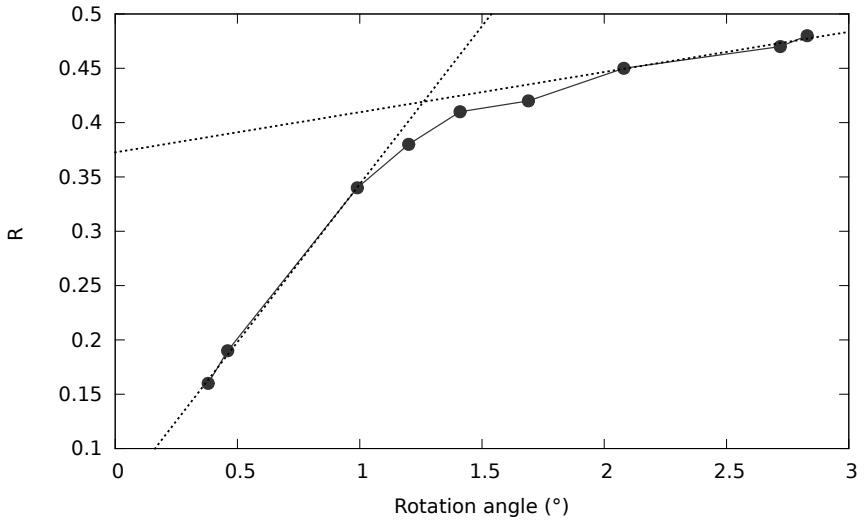

Figure 58: R is the ratio of the diameter of the ring of maximal displacement to the size of the moiron. R decreases significantly for rotation angles below 1.4°. The dashed lines are linear fits for the first and last three datapoints. Their crossing point gives us an estimate of the critical angle.

Let us now compare the plots of atomic displacement (Figures 49 to 54) to the substrate overlay (Figures 24 to 29), and determine the substrate overlay for the atoms with maximal displacement. For large rotation angles the ring of maximal displacement corresponds to atoms with an overlay of approximately 0.6 Å (bright green areas in substrate overlay plots). For small rotation angles the ring of maximal displacement corresponds to atoms with an overlay that approaches 0 Å (yellow areas in substrate overlay plots). So for larger angles, moving the (small number of) local AA stacked atoms is energetically less favourable than moving the atoms with substrate overlay around 0.6 Å. For angles below θ_c, the area of local AA stacking becomes sufficiently large so that it is necessary to start displacing these atoms.

The last representation of the displacement we will discuss is the Lorenz curve (Figure 59). This shows which percentage of the atoms account for which percentage of the displacement. The dashed black line shows the Lorenz curve for the case where all atoms have the same absolute displacement. Note that the Lorenz curve for sample (7,1) (Figure 59a) is less fluent than the others. This is because the sample is much smaller, so there are less atoms to build the distribution. We see no significant change in the Lorenz curve between the samples.

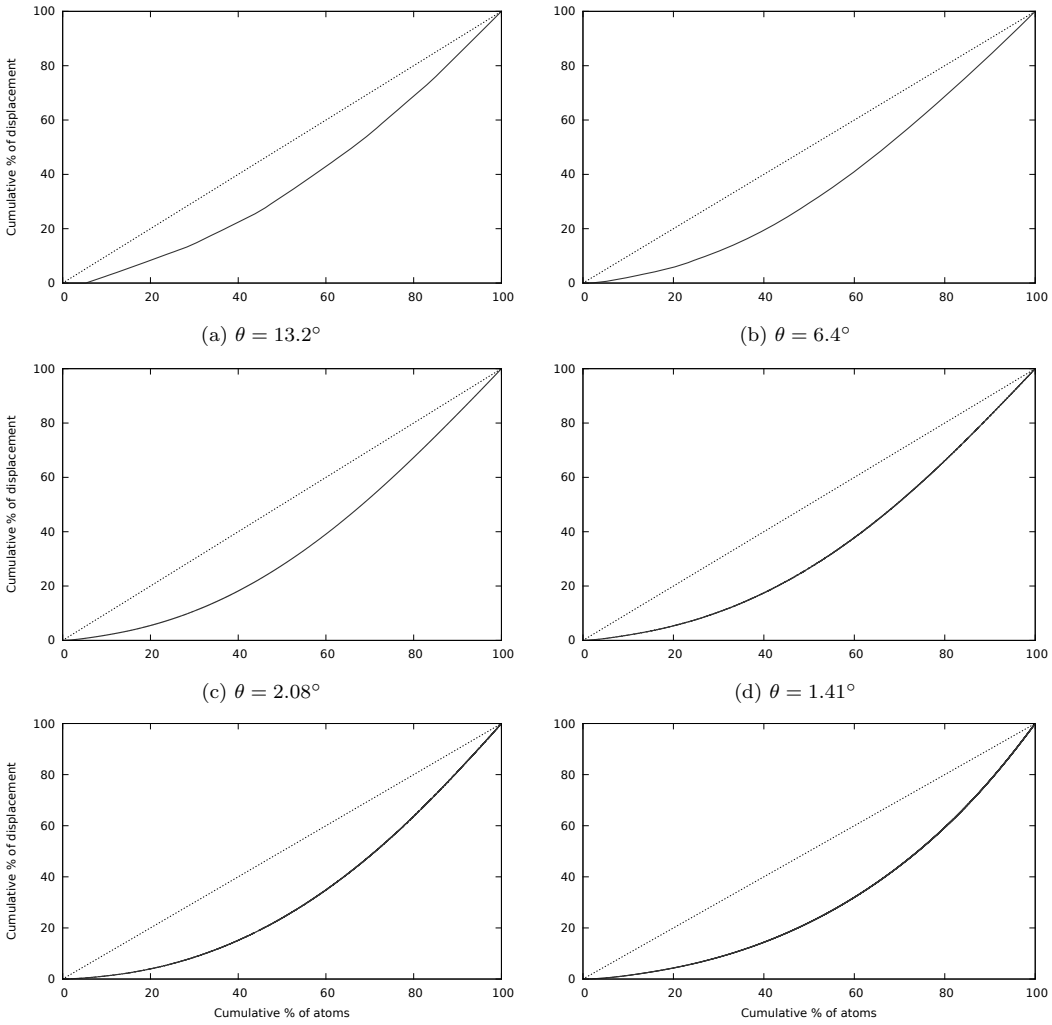

(a) $\theta = 13.2°$ (b) $\theta = 6.4°$

(c) $\theta = 2.08°$ (d) $\theta = 1.41°$

(e) $\theta = 1.2°$ (f) $\theta = 0.46°$

Figure 59: Lorenz curve for the displacement of the atoms in the relaxed top layer for samples (a) (7,1), $\theta = 13.2°$, N= 114; (b) (15,1), $\theta = 6.4°$, N= 482; (c) (47,1), $\theta = 2.08°$, N= 4514; (d) (70,1), $\theta = 1.41°$, N= 9942; (e) (82,1), $\theta = 1.2°$, N= 13614; (f) (216,1), $\theta = 0.46°$, N= 92746.

6.4.2 Aubry transition

Finally we examine the possibility of an Aubry-like transition in our 2-dimensional systems. Since in the Frenkel Kontorova model the key parameter is the interlayer distance, we study the behaviour of the atoms in one specific sample for varying interlayer distance. To be precise, we will consider the atomic displacement for varying interlayer distance for sample: (n,m)=(15,1), θ=6.395°, N=482 atoms per layer, as shown in Figure 60. Figure 61 shows the total displacement of the atoms in the top layer plane due to minimization for a fixed interlayer distance of 3Å. We repeated the sample four times to get a clearer view of the moiré pattern.

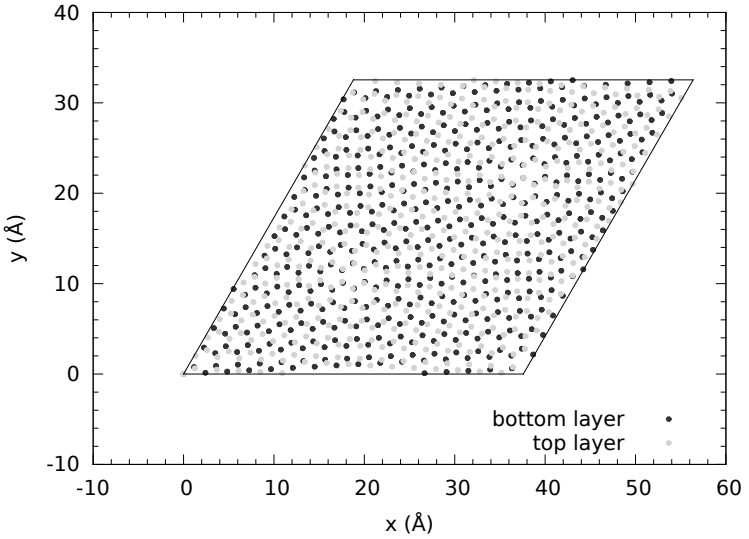

Figure 60: The bottom and top layer for sample (n,m)=(15,1) prior to relaxation show a rigid moiré pattern. The top layer is rotated 6.395° with respect to the bottom layer and each layer contains 482 atoms.

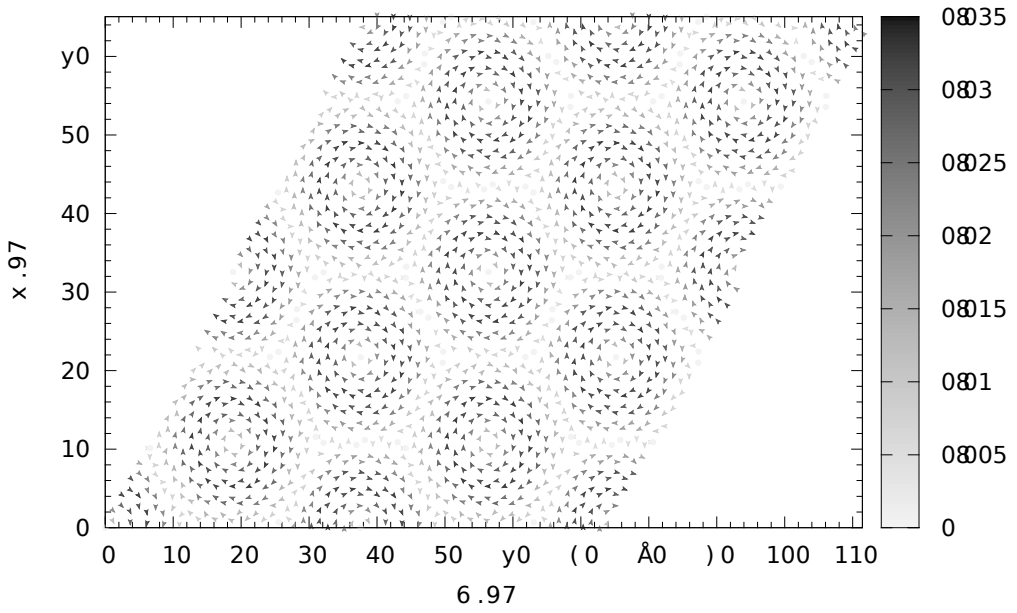

Figure 61: Displacement in the plane after minimization for sample (n,m)=(15,1) with fixed interlayer distance: z = 3 Å. Here we used 4 minimal (15,1) cells to get a clearer view of the moiré pattern; the plot contains 12 moirons. The colour represents the displacement, and the arrows show the direction of the displacement. Atoms that move less than 0.005 Å are displayed as a yellow dot.

Next, we take a closer look at the displacement and study the average and maximum displacements of the atoms in the relaxed layer for varying fixed interlayer distance between 2.7 and 3.45 Å. As discussed in section 3.1, we are searching for discontinuous behaviour indicating a two-dimensional analogue of the Aubry transition, based on the Frenkel-Kontorova model. When varying the interlayer distance, we have to keep in mind that we cannot get too close, because the Kolmogorov Crespi potential is not accurate below approximately 3.1 Å.[22] Furthermore, the REBO potential is made to start making bonds between the layers when the interatomic distance is less than approximately 2.0 Å. Therefore, in addition to varying the interlayer distance we use another way to further increase the effective interlayer potential: we put another rigid layer of graphene, identical to the bottom layer, on top of the layer that we relax, so the relaxed layer is sandwiched (see Figure 62). The relaxed layer is placed exactly in the middle of the two rigid layers. This way, the forces acting on the atoms are twice as big and the amplitude of the potential working on the atoms is twice as high. The results for average and maximal displacements in the relaxed layer due to minimization are shown in Figure 63 and 64 respectively.

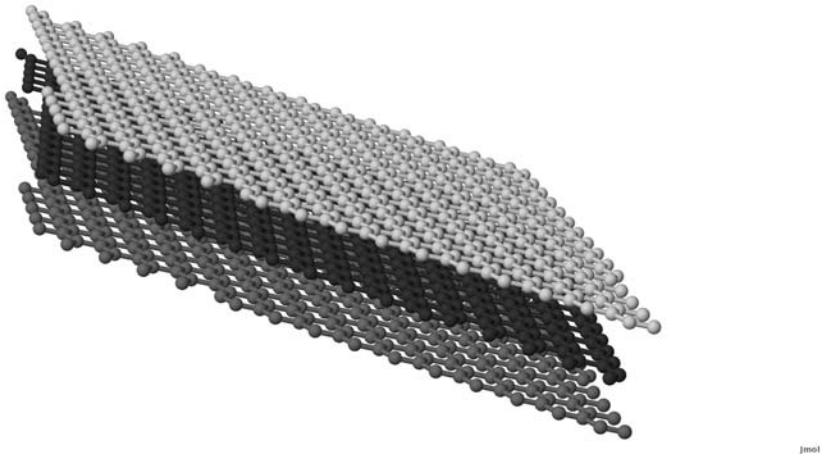

Figure 62: The sandwiched configuration: The relaxed layer (blue) is placed on top of the rigid substrate layer (red) and below a third layer of graphene (green). The green layer is identical to the red layer and they are equally far away from the relaxed layer.

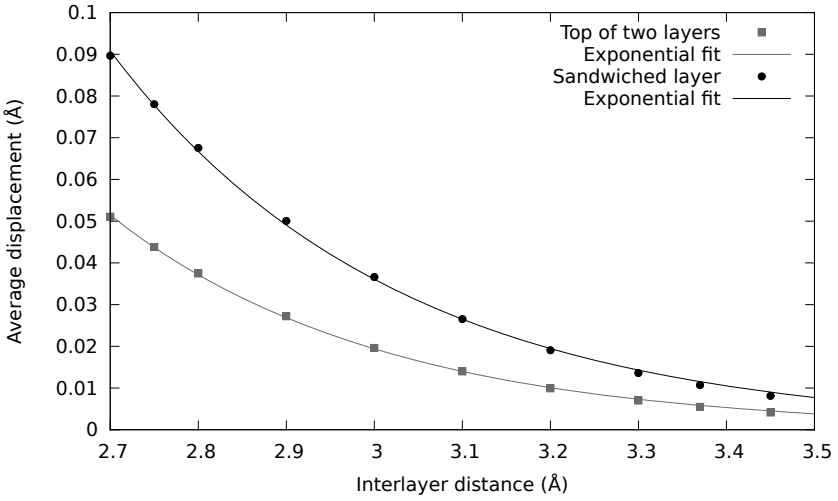

Figure 63: The average displacement of the atoms in the relaxed layer of sample (15,1) for varying interlayer distances. Exponential fit for the two layer configuration: $336.3e^{-z/0.307}$. Exponential fit for the sandwiched layer configuration: $370.6e^{-z/0.325}$. No Aubry transition is detected.

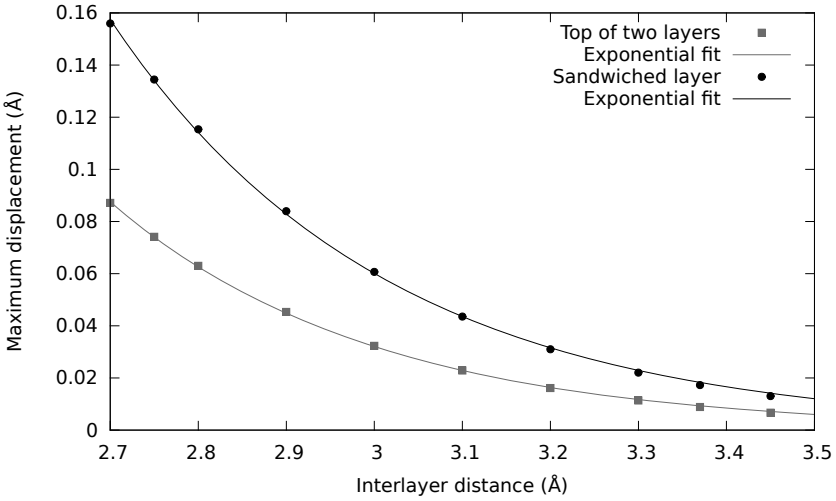

Figure 64: The maximum displacement of the atoms in the relaxed layer of sample (15,1) for varying interlayer distances. Exponential fit for the two layer configuration: $746.0e^{-z/0.298}$. Exponential fit for the sandwiched layer configuration: $922.3e^{-z/0.311}$. No Aubry transition is detected.

Unfortunately, the above results show no sign of discontinuous behaviour. Finally, we try one more configuration that could reveal existence of the Aubry transition: we increase the interatomic distance from 1.3978 to 1.43 Å. This way the springs in the FK model are weaker so the critical amplitude of the potential, W_c, for the transition to occur is lowered. The results for average and maximal displacement are shown below in Figure 65 and 66 respectively. We conclude that we find no evidence of an Aubry transition in the displacements of the atoms due to minimization for rotated graphene on graphene. However, we should keep in mind that the average and maximal displacement may not be the critical quantities in determining the Aubry transition. The fitting parameters of all configurations in this section can be found in Appendix D.

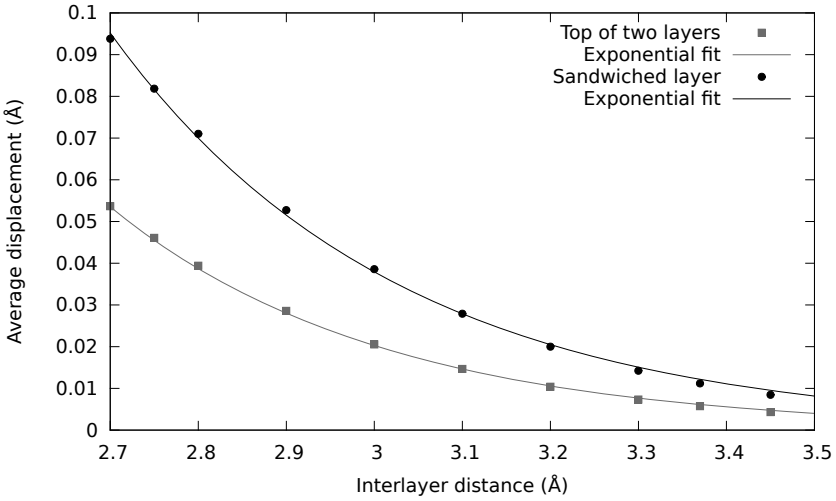

Figure 65: The average displacement of the atoms in the relaxed layer of sample (15,1) for varying interlayer distances. In this case, for all layers the interatomic distance is 1.43Å instead of 1.3978Å. Exponential fit for the two layer configuration: $335.5e^{-z/0.309}$. Exponential fit for the sandwiched layer configuration: $378.8e^{-z/0.326}$. No Aubry transition is detected.

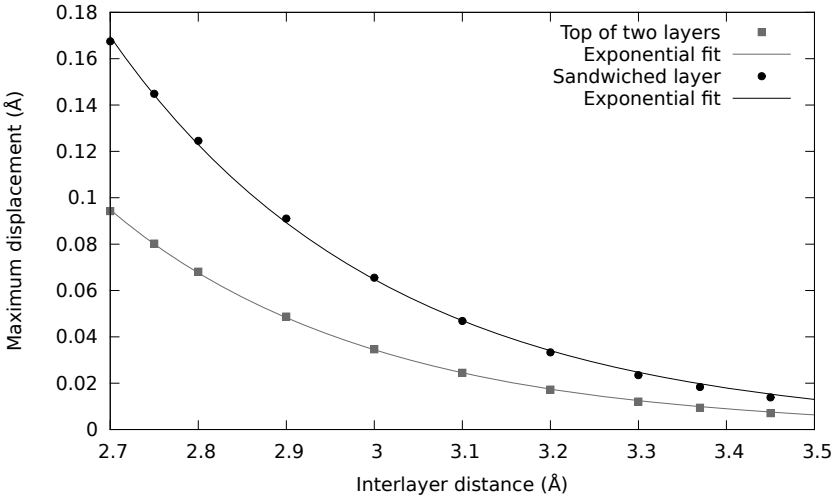

Figure 66: The maximum displacement of the atoms in the relaxed layer of sample (15,1) for varying interlayer distances. In this case, for all layers the interatomic distance is 1.43Å instead of 1.3978ÅĖxponential fit for the two layer configuration: $873.6e^{-z/0.296}$. Exponential fit for the sandwiched layer configuration: $982.4e^{-z/0.311}$. No Aubry transition is detected.

6.5 Comparison between fixed and free interlayer distance

Let us return to the continuous-discontinuous transition we observed around the critical rotation angle θ_c. In our results that showed this transition, the atoms in the top layer were fixed at an interlayer distance of 3 Å. We assumed that keeping the atoms at a fixed interlayer distance would have no qualitative effect on the behaviour of the atoms and that it would only enhance a possible transition. Let us check this by considering only the two samples near the critical rotation angle (samples (70,1), $\theta = 1.41^\circ$ and (82,1), $\theta = 1.2^\circ$) and allowing the atoms to move perpendicular to the plane of the sample as well. First we briefly summarize the results for the case where the interlayer distance is fixed (Figure 67). Second we discuss the results for the case where the atoms are free to move out of the plane as well (Figure 68). In both Figures, the left column represents sample (70,1), $\theta = 1.41^\circ$ and the right column represents sample (82,1), $\theta = 1.2^\circ$.

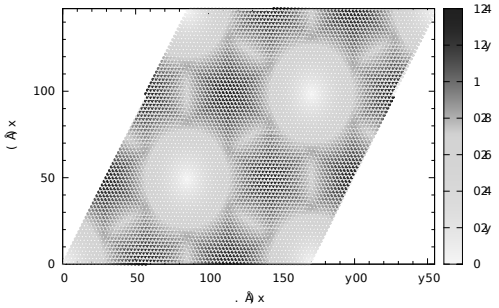

(a) Substrate overlay before relaxation, $\theta = 1.41°$
z *fixed*

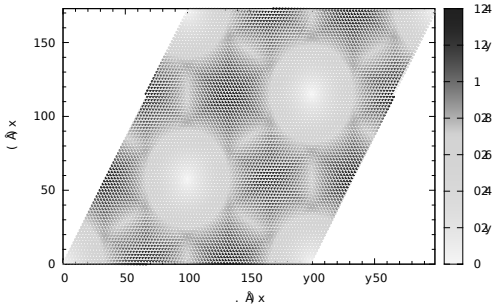

(b) Substrate overlay before relaxation, $\theta = 1.2°$
z *fixed*

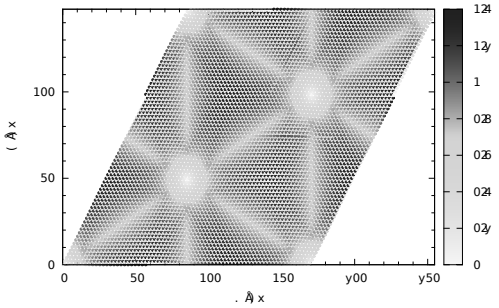

(c) Substrate overlay after relaxation, $\theta = 1.41°$
z *fixed*

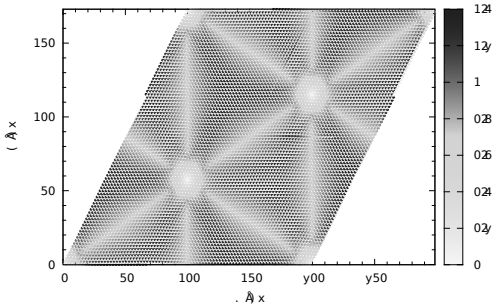

(d) Substrate overlay after relaxation, $\theta = 1.2°$
z *fixed*

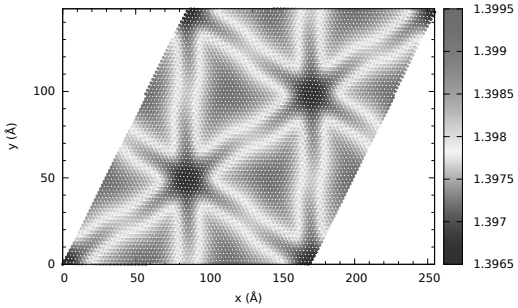

(e) Average interatomic distance, $\theta = 1.41°$
z *fixed*

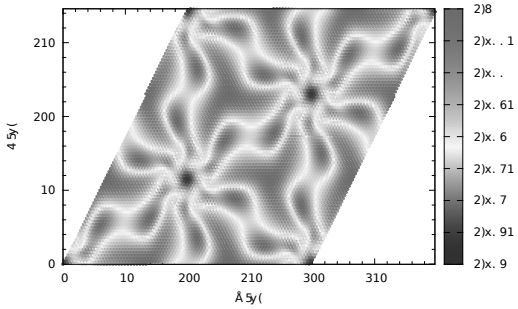

(f) Average interatomic distance, $\theta = 1.2°$
z *fixed*

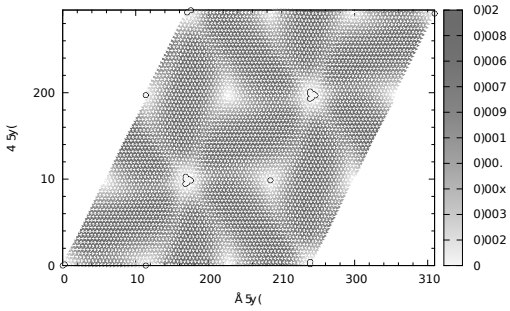

(g) Gauge field, $\theta = 1.41°$
z *fixed*

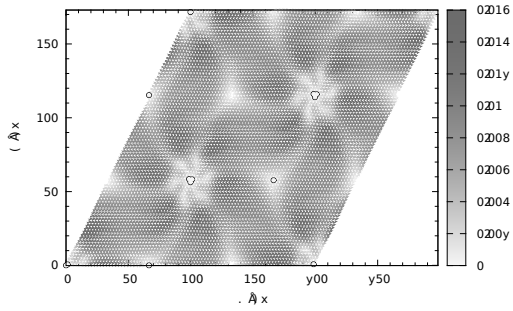

(h) Gauge field, $\theta = 1.2°$
z *fixed*

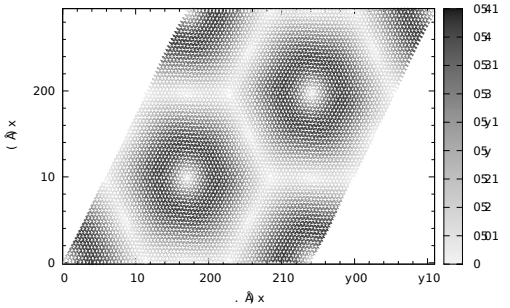

(i) In plane displacement, $\theta = 1.41°$
z *fixed*

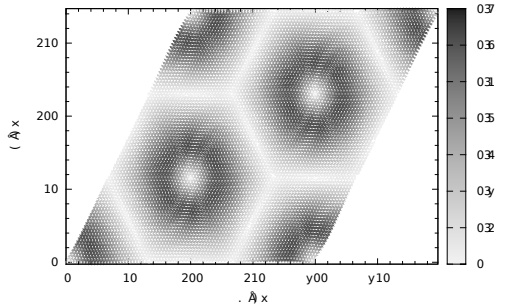

(j) In plane displacement, $\theta = 1.2°$
z *fixed*

Figure 67: The figures in the left column correspond to sample (70,1), $\theta = 1.41°$ where the right column corresponds to sample (82,1), $\theta = 1.2°$ all for a *fixed* interlayer distance of 3Å. Figures (a) and (b) show the substrate overlay *before* minimization of energy and Figures (c) and (d) show the substrate overlay *after* minimization. A yellow area indicates that all atoms are almost directly on top of an atom in the bottom layer, such that we have local AA stacking. An area in which atoms are coloured alternately dark and light indicates local AB stacking. Figures (e) and (f) show the average interatomic distance for each atom, averaged over its three nearest neighbours. The equilibrium interatomic distance for single layer graphene in our potential (1.3978 Å) is yellow. Blue indicates local compression, whereas red indicates local stretching. Figures (g) and (h) show the gauge field as mentioned in section 6.2 as a measure for the deformation of the lattice. Figures (i) and (j) show the total displacement for each atom due to minimization of energy.

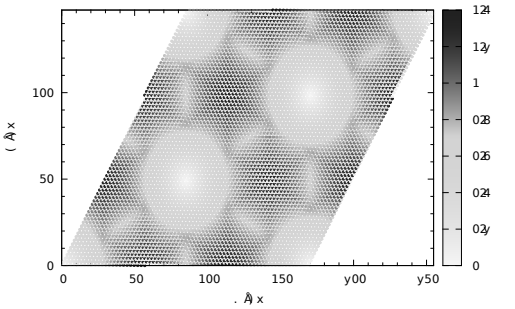

(a) Substrate overlay before relaxation, $\theta = 1.41°$
z *free*

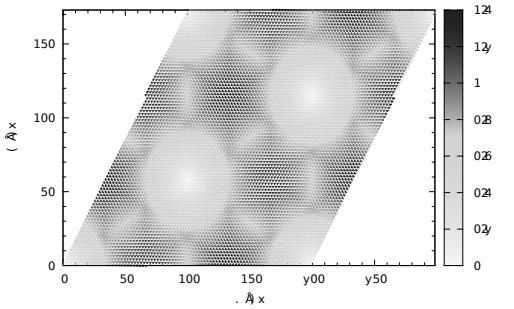

(b) Substrate overlay before relaxation, $\theta = 1.2°$
z *free*

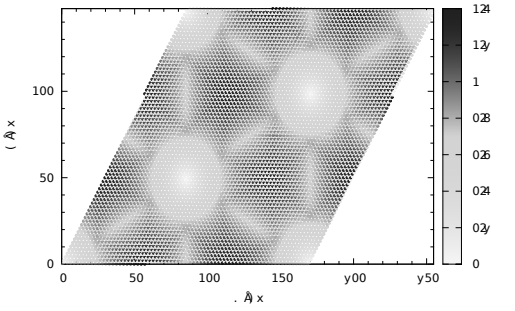

(c) Substrate overlay after relaxation, $\theta = 1.41°$
z *free*

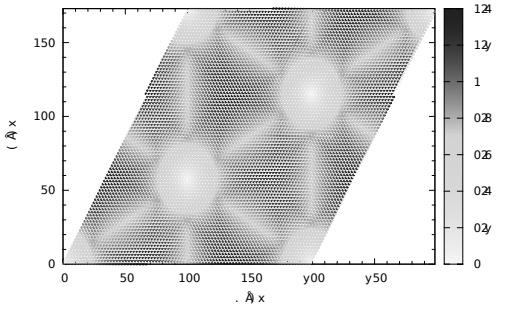

(d) Substrate overlay after relaxation, $\theta = 1.2°$
z *free*

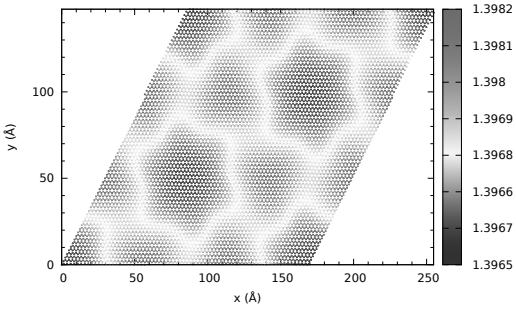

(e) Average interatomic distance, $\theta = 1.41°$
z *free*

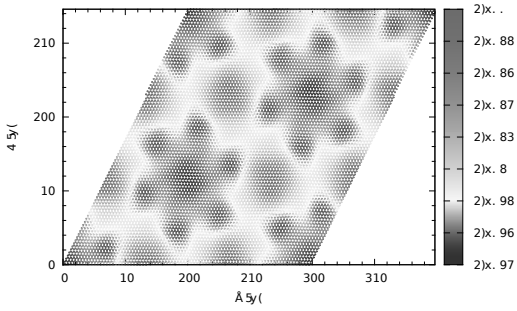

(f) Average interatomic distance, $\theta = 1.2°$
z *free*

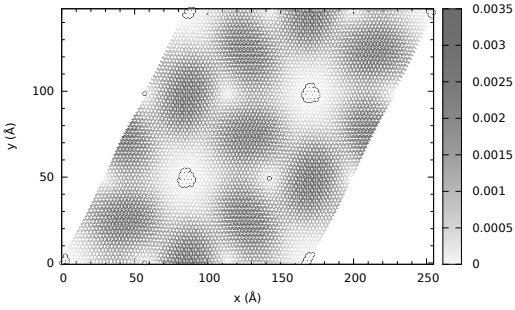

(g) Gauge field, $\theta = 1.41°$
z *free*

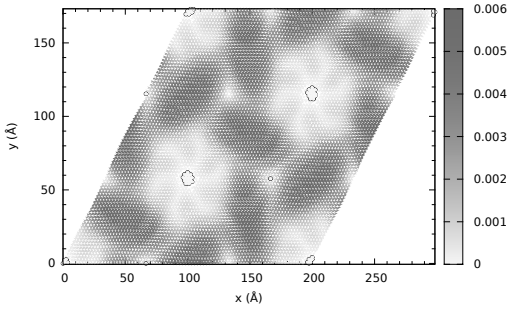

(h) Gauge field, $\theta = 1.2°$
z *free*

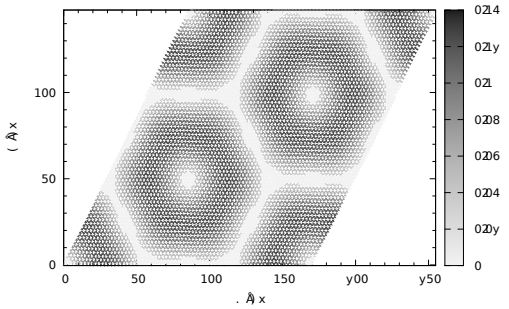

(i) In plane displacement, $\theta = 1.41°$
z *free*

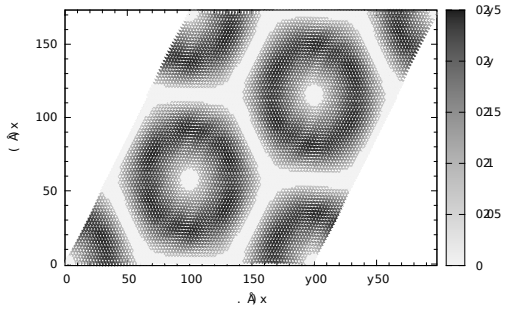

(j) In plane displacement, $\theta = 1.2°$
z *free*

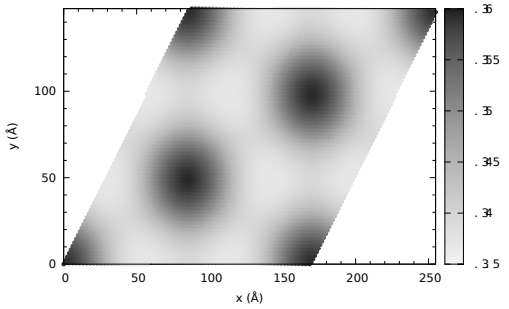

(k) Out of plane displacement, $\theta = 1.41°$
z *free*

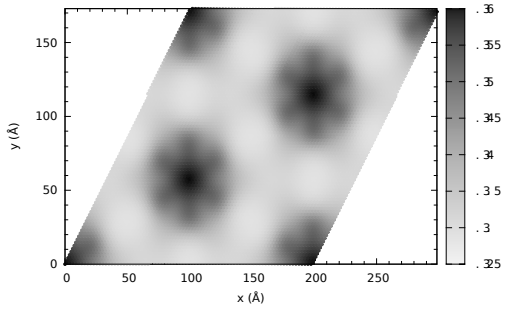

(l) Out of plane displacement, $\theta = 1.2°$
z *free*

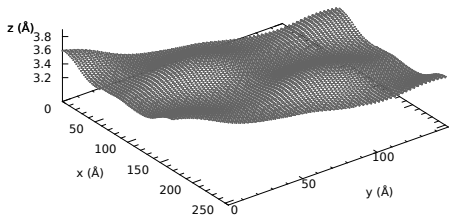

(m) Top layer after relaxation, $\theta = 1.41°$
z *free*

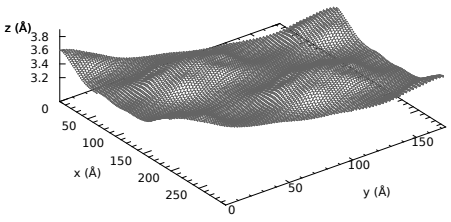

(n) Top layer after relaxation, $\theta = 1.2°$
z *free*

Figure 68: The figures in the left column correspond to sample (70,1) where the right column corresponds to sample (82,1) all for *free* interlayer distance. For Figures (a) to (j) the caption is identical to the caption in Figure 67. Figures (k) and (l) show the distance to the bottom layer for each atom and (m) and (n) contain the same information in a 3-dimensional plot.

First of all, when out of plane displacement is allowed, the differences between the substrate overlay before and after relaxation are hardly visible for both samples. This is as expected, because instead of just finding a better position in the xy-plane, the atoms can now simply move away from the bottom layer to minimize their energy, so only minimal displacement in the plane is necessary. This is why the maximal displacement in the plane is approximately three times smaller when atoms are free to move perpendicular to the plane of the sample (see Figure 67/68 (i) and (j)). Second, from the average interatomic distance (Figures 68(e) and (f)) and the outer plane displacement (Figure 68(k) to (n)) it appears that the transition occurs between the samples (70,1) and (82,1) also when the atoms are free to move out of the plane. Let us plot the average interatomic distance across the bisector of the samples and compare this to the case where the interlayer distance is fixed (see Figure 69). We see that the same kind of continuous-discontinuous transition we found for fixed interlayer distance occurs when we let the atoms move perpendicular to the plane as well. The behaviour of sample (70,1) is now perfectly sinusoidal, whereas the atoms in sample (82,1) show some double periodicity. However, the effect of the transition is more subtle, as we predicted in section 2.4, because the displacements are smaller when the atoms are free to move out of the plane. We conclude that indeed keeping the top layer at a fixed distance from the bottom layer did not qualitatively change the behaviour of the transition we observed.

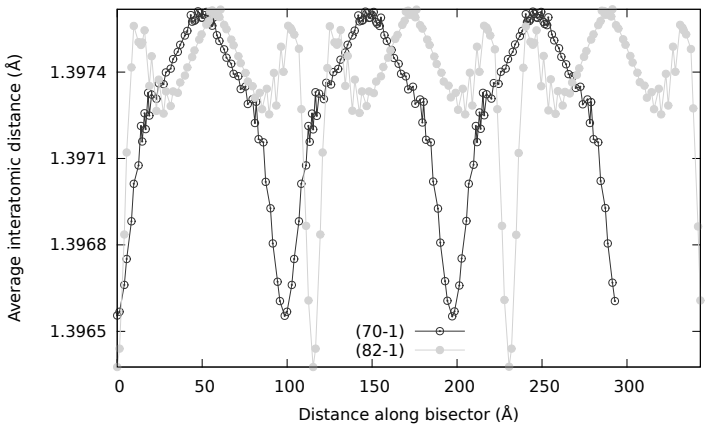

(a) Average interatomic distance for samples (70,1) and (82,1)
z *fixed*

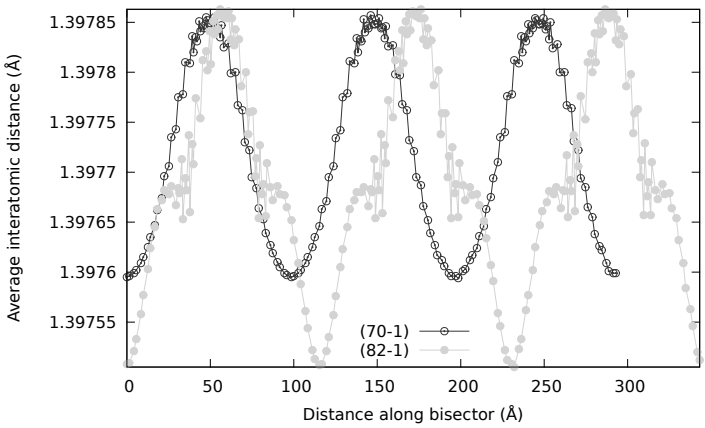

(b) Average interatomic distance for samples (70,1) and (82,1)
z *free*

Figure 69: Average interatomic distance for atoms along the angle bisector of the samples (70,1), $\theta = 1.41°$ and (82,1), $\theta = 1.2°$ for interlayer distance fixed (top) and free (bottom). The continuous-discontinuous transition occurs for both cases: sample (70,1) shows a continuous behaviour, while sample (82,1) seems to have some double periodicity.

7 Results: Graphene on h-BN

In this section we consider the results from the experiments by Woods et al mentioned in section 3.2, where a commensurate-incommensurate transition is suggested for graphene on h-BN. Before we can investigate computationally the transition that was found experimentally, we need to make sure that we have a good model for graphene on h-BN. Therefore, our main focus now is to reproduce the experimental results for unrotated graphene ($\theta = 0$) on h-BN depicted in Figure 15b and d.

We will consider the average interatomic distance to investigate the areas of local compression and stretching and compare these to the experiment. Our aim is now to make the simulations as realistic as possible. Therefore, contrary to previous sections, we will allow the atoms in the top layer to move out of the plane as well. Here we focus on the unrotated case, $\theta = 0$ to build our model. Since there is no empirical potential available for graphene on h-BN, we start introducing the h-BN substrate simply by stretching the bottom layer of graphene, making the lattice constant 1.8% larger than the lattice constant of graphene. This is our first (very naive) estimate to simulate the substrate. We let the top layer of graphene relax under the potential of this substrate and consider the average interatomic distance. The results are shown in Figure 70. For better visibility we plot a repetition of the sample. When we compare Figure 70 to Figure 15b, we see that the compressed and expanded areas in our result are expanded and compressed areas respectively in the experiment. Thus, we need to think of ways to improve our model. The first improvement involves taking into account the difference in interaction between carbon and nitrogen atoms and carbon and boron atoms as discussed by Sachs et al.[23] They found that the interaction between carbon and nitrogen is much stronger than the interaction between carbon and boron. In our first try to model graphene on h-BN (Figure 70), we did not make any distinction between the two sublattices, since we just used expanded graphene. Now, we will include this difference in interaction very roughly and exaggerated: We consider the interaction between carbon and boron to be so small, that we simply delete the sublattice that represents the boron atoms. Hence, we are dealing with a triangular lattice instead of a hexagonal lattice. These results are shown in Figure 71. Indeed, we see that this inverted the distribution of average interatomic distance yielding an expansion of the center of the hexagonal pattern, as in the experiment. However, compared to the experiment, the areas of compression are still too broad. Keeping this in mind, there is another possibility that we need to consider. It is likely that graphene stretches globally to adjust to the h-BN substrate. In our previous set up, this was not allowed, since the number of atoms in the plane is fixed by periodic boundary conditions, and stretching by extreme out of plane displacement is not energetically favourable. Thus, in addition to considering a triangular lattice, we now stretch the top layer of graphene prior to relaxation by increasing the lattice constant of the top layer by 0.9%. This final result is shown in Figure 72. We see that our result now strongly resembles the results from the experiment shown in Figure 15!

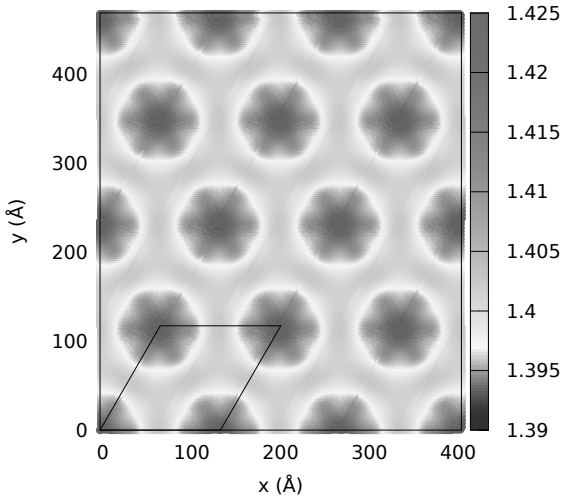

Figure 70: Average interatomic distance for graphene on h-BN, *unrotated* ($\theta = 0$), z free. To simulate the h-BN substrate we simply use a stretched layer of graphene. The colour indicates the average interatomic distance for each atom. Yellow means a value of 1.3978, i.e. the interatomic distance for ideal graphene. The black prism shows the size of one supercell.

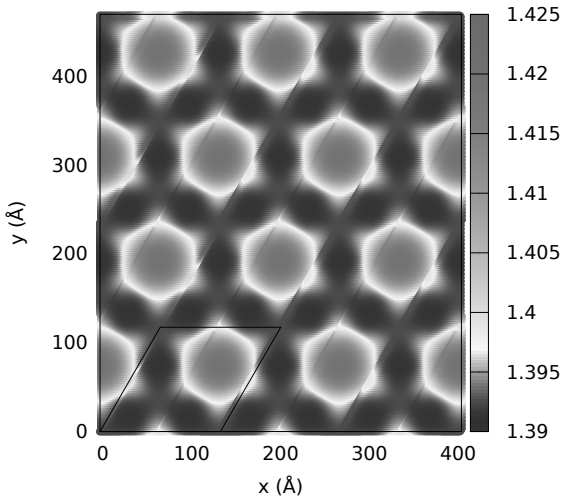

Figure 71: Average interatomic distance for graphene on h-BN, *unrotated* ($\theta = 0$), z free. To simulate the h-BN substrate we use a stretched layer of graphene with only one sublattice present that represents the nitrogen atoms. The colour indicates the average interatomic distance for each atom. Yellow means a value of 1.3978, i.e. the interatomic distance for ideal graphene. The black prism shows the size of one supercell.

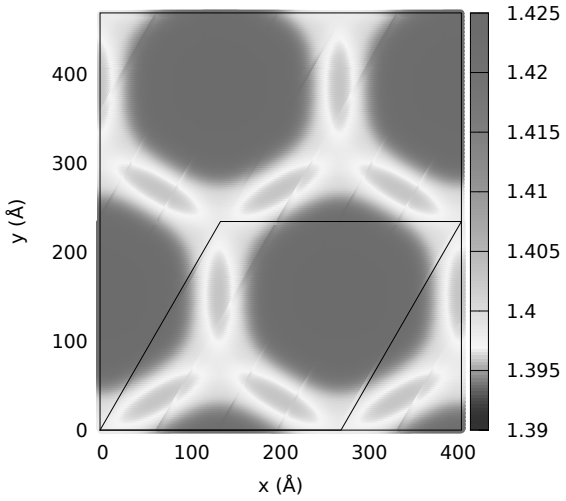

Figure 72: Average interatomic distance for graphene on h-BN, *unrotated* ($\theta = 0$), z free. To simulate the h-BN substrate we use a stretched layer of graphene with only one sublattice present that represents the nitrogen atoms. The top layer of graphene is stretched 0.9% to allow global stretching after relaxation. The colour indicates the average interatomic distance for each atom. Yellow means a value of 1.3978, i.e. the interatomic distance for ideal graphene. The black prism shows the size of one supercell.

Let us look at our final result in the context of the orientation of unrotated graphene on the h-BN lattice before relaxation (see Figure 73). In this Figure the mismatch between the lattice constants is exaggerated to enhance their effect: instead of the actual 1.8% we took the lattice constant of h-BN to be 6.7% larger than the lattice constant of graphene. We can identify three stackings in particular. First of all, the least favourable stacking: AA stacking. This is where the hexagons in the top layer are (almost) directly on top of a hexagon in the bottom layer. The second least favourable stacking is AB′ stacking where carbon atoms are placed on top of the nitrogen atoms and the brown boron atoms in the substrate are visible from above. The optimal stacking is AB stacking where carbon atoms are placed on top of the boron atoms and the green nitrogen atoms in the substrate are visible from above. When we combine Figures 72 and 73 we see that the area with optimal stacking (AB) expands to adjust to the h-BN lattice.

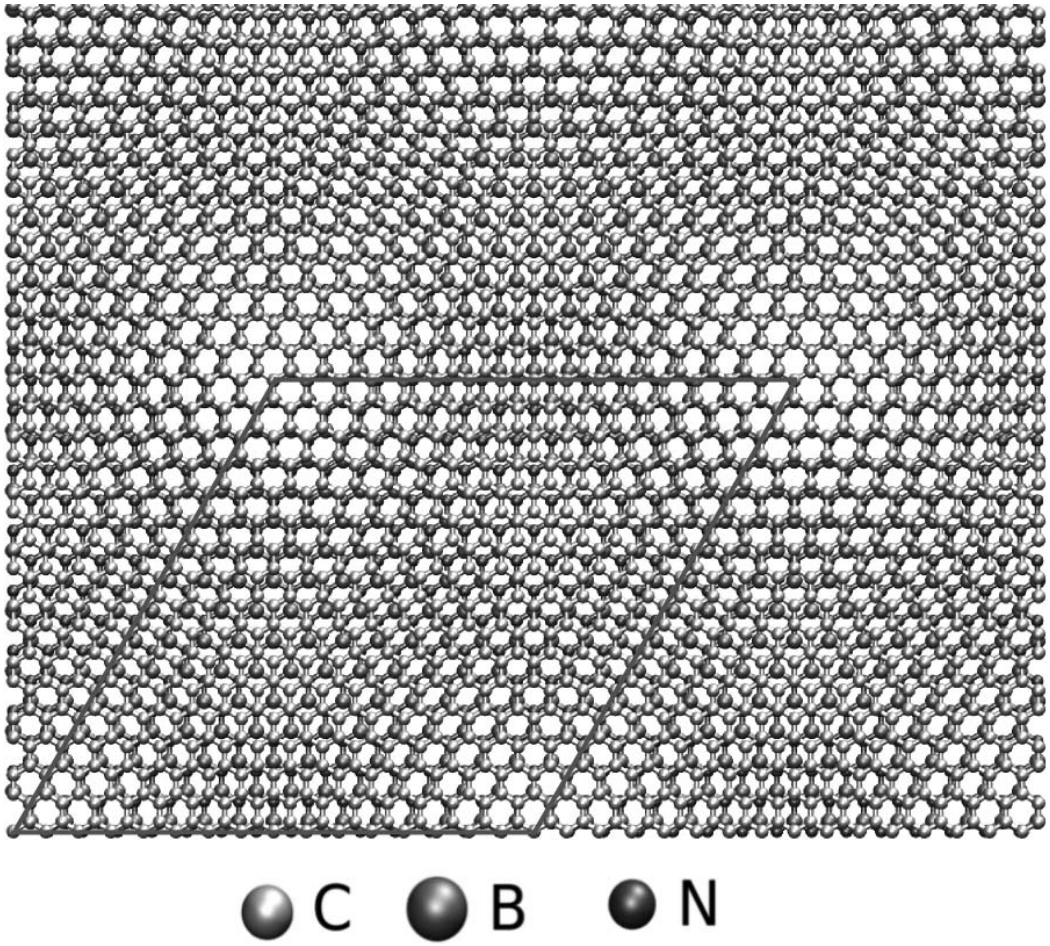

Figure 73: The unrotated graphene lattice on top of h-BN before relaxation. The grey, brown and green atoms represent carbon, boron and nitrogen atoms respectively. We exaggerated the mismatch between the lattice constants and took the lattice constant of h-BN to be 6.7% larger than the one for graphene instead of the actual 1.8%. The red prism shows the size of the supercell. Courtesy of Merel van Wijk

The next step would be to start rotating the layer of graphene with respect to h-BN and investigate the transition found in experiments at some critical rotation angle. Unfortunately, within this project there simply is not enough time. But we have found a simple yet appropriate model for the graphene on h-BN system that can be a starting point for further research where also rotated samples are to be considered.

8 Conclusions

We have studied the equilibrium structure of graphene on graphene and h-BN substrates as a function of the relative angle between the layers. The first important observation from our results is that relaxing the top layer has a great influence on the system. We saw that the atoms in the top layer move to an energetically more favourable location, which results in smaller areas of local AA stacking and larger areas of local AB stacking. Furthermore, by investigating the interatomic distance and the gauge field we found that smaller AA and larger AB areas are achieved through uniform compression and stretching respectively. Finally we considered the displacement of the atoms due to relaxation. We found that the atoms move in a vortex around the center of a moiron, which is AA stacked. The average and maximal displacement of the atoms decay exponentially for increasing rotation angle.

When we compared the behaviour between samples with a different rotation angle, we found an interesting transition that occurs around the critical angle $\theta_c \approx 1.4$. This continuous-discontinuous transition is best seen in the average interatomic distance and the total displacement of atoms in the plane. We found that for angles smaller than θ_c the pattern in the interatomic distance starts to rotate, creating some complex pattern. This rotation we do not yet comprehend. However, we can observe the following: for very small angles the moiré patterns become very big. This gives the atoms more freedom to create more complicated patterns within the periodic boundary conditions of the moiré supercell. It looks as though a second periodicity is added to the pattern. Furthermore, when looking at the total displacement we found that for very large angles the diameter of the ring of maximal displacement is approximately half the size of the moiron. When we decrease the rotation angle, the ring of maximal displacement starts to move towards the center of the moiron. In particular, for angles smaller than θ_c the ring approaches the center of the moiron rapidly. We suggest the following explanation. The center of a moiron is AA stacked. For rotation angles larger than θ_c, this AA stacking *before* relaxation is only a very small area. Most of the displacement then takes place in another part of the moiron, namely the part that has a substrate overlay of about 0.6 Å. For angles smaller than θ_c the AA stacked areas become significantly large, so that during minimization these areas become most important in energy minimization. Hence, for small rotation angles, the ring of maximal displacement approaches the center of the moiron, namely the AA stacked area. To check that our evidence of a transition is not just an effect of keeping the atoms at a fixed distance from the substrate, we considered the samples with $\theta = 1.4°$ and $\theta = 1.2°$ and let the atoms move perpendicular to the plane as well. We found that there is still a similar transition around θ_c when the atoms are free to move within and out of the plane. Thus, we found that keeping the atoms at a fixed distance from the substrate changes the results quantitatively, but not qualitatively.

Although we have found a continuous-discontinuous transition for graphene on graphene, it remains to be established whether this transition is related to the transition observed for graphene on h-BN by Woods et al . The patterns in the interatomic distance do not appear to be equivalent to the experimental results. Note however, that we should be careful comparing our results to the experiments. Their results are based on graphene-on-h-BN systems, while we consider graphene on graphene. It is possible that the difference in lattice parameters between graphene and h-BN is related to the experimentally found transition. Furthermore, the results in Figure 14c and d are shown through the Young's modulus, which is a second derivative of the internal elastic potential energy density with respect to strain. We compared these results to our computational

results for interatomic distance, which would not necessarily demonstrate the same behaviour.

Unfortunately, we did not find a two-dimensional equivalent of the Aubry transition. However, we only considered maximal and average displacement due to minimization of energy. Perhaps these quantities are not critical in determining this transition. To find the possible Aubry transition, other quantities should be considered such as the average interatomic distance as a function of the interlayer distances. Furthermore, samples with other rotation angles should be considered since the orientation of the two layers may affect the behaviour when changing the interlayer distance.

In the final part of this thesis we discussed graphene on h-BN. Our aim was to make an appropriate model for this system that can be used in future research to computationally confirm the experimental results by Woods et al. Our starting point - putting graphene on top of a graphene substrate with a 1.8% larger lattice constant to simulate h-BN - turned out to be too simple. Comparing our results to the experimentally observed patterns, we saw that regions of local stretching or compression in our results correspond to local compression or stretching respectively in the experiment. We needed to make some alterations. First, we took into account the fact that CB interaction is much weaker than CN interaction by completely leaving out the boron atoms. This improved our model enormously, as our results began to resemble the experimental results: Areas of local stretching or compression were now in accordance with the experiment. However, the areas of compression in our results were too large compared with the experiment. The second alteration to our model concerned the possibility that graphene stretches globally to adjust to h-BN. This behaviour was not allowed in our previous setups, because the number of atoms in the plane is fixed. We therefore stretched the top layer of graphene *before* relaxation by 0.9%, which resulted in better proportions between compressed and stretched areas. Global stretching of 0.9% gives good results, but we should keep in mind that this is an estimate. We thus conclude that graphene stretches globally to adjust to the h-BN substrate, and that including the difference in interaction between CN and CB is crucial to simulate graphene on h-BN.

9 Acknowledgements

With this thesis, I conclude my six years in Nijmegen as a physics student. Although I choose not to stay in academia, I can honestly say that the last year of my studies was the year I enjoyed the most. For this I have many people to thank.

First of all, I would like to thank Annalisa for guiding me through this project and most of all for believing in me even when I sometimes did not. Thank you for giving me the opportunity to fully explore the world of research and grow from a student into a beginning researcher. Merel, thank you so much for all your help and patience. I have learned a lot from the way you work, and I could never have imagined that I would improve my computer skills this much. Misha, many thanks to you for your insights and the productive meetings that never finished without a new idea. Thanks to the PhD students in the office for always being ready to help me with any problems and for creating a fun and friendly atmosphere to work in. Furthermore, thanks to everyone at the department for making me feel at home right from the start. I will truly miss the coffee (cake!) breaks, movie nights and dinners.

Many thanks to my parents for always being there for me, no matter what. You are not just my parents, you are also my best friends. Jasper, thanks so much for your big brother advice and being so close to me despite the distance. Finally, I would like to thank my study friends, who have coloured my life here in Nijmegen for the past couple of years: Maria, Rosa, Jan, Maartje, Haiko, Tijs, Gijs and of course my boyfriend Lars.

References

[1] The 2010 Nobel Prize in Physics, *Press Release*.

[2] M. I. Katsnelson and A. Fasolino, Graphene as a prototype crystalline membrane, *Accounts of Chemical Research*, 46(1):97-105, 2013.

[3] A. K. Geim and I. V. Grigorieva, Van der Waals heterostructures, *Nature*, 499:419-425, 2013.

[4] *www.bbc.com/future/story/20130306-bend-and-flex-for-mobile-phones*.

[5] David L. Miller, Kevin D. Kubista, Gregory M. Rutter, Ming Ruan, Structural analysis of multilayer graphene via atomic moiré interferometry, *Physical Review B*, 81:125427, 2010.

[6] M. Dienwiebel, G. S. Verhoeven, N. Pradeep and J. W. M. Frenken, Model calculations of superlubricity of graphite, *Physical Review B*, 70:165418, 2004.

[7] C. R. Dean, A. F. Young, I. Meric, C. Lee, L. Wang, S. Sorgenfrei, K. Watanabe, T. Taniguchi, P. Kim, K. L. Shepard and J. Hone, Boron nitride substrates for high quality graphene electronics, *Nature Nanotechnology*, 5:722-726, 2010.

[8] C. R. Woods, L. Britnell, A. Eckmann, R. S. Ma, J. C. Lu, H. M. Huo, X. Lin, G. L. Yu, Y. Cao, R. V. Gorbachev, A. V. Kretinin, J. Park, L. A. Ponomarenko, M. I. Katsnelson, Yu. N. Gornostyrev, K. Watanabe, T. Taniguchi, C. Casiraghi, H-J. Gao, A. K. Geim and K. S. Novoselov, Commensurate-incommensurate transition for graphene on hexagonal boron nitride, *Nature Physics*, 10:451-456, 2014.

[9] Mikhail I. Katsnelson, Graphene: Carbon in Two Dimensions, ISBN 978-0-521-19540-9, 2012.

[10] D. W. Boukhvalov, M. I. Katsnelson, and A. I. Lichtenstein, Hydrogen on graphene: Electronic structure, total energy, structural distortions and magnetism from first-principles calculations, *Physical Review B*, 77:035427, 2008.

[11] G. Savini, Y. J. Dappe, S. Oberg, J. -C. Charlier, M. I. Katsnelson and A. Fasolino, Bending modes, elastic constants and mechanical stability of graphitic systems, *Elsevier*, 49(1):62-69, 2011.

[12] K. Hermann, Periodic overlayers and moiré patterns: theoretical studies of geometric properties, *Journal of Physics: Condensed Matter*, 24:314210, 2012.

[13] S. R. Sharma, B. Bergersen and B. Joos, Aubry transition in a finite modulated chain, *Physical Review B*, 29(11):6335-6340, 1984

[14] S. Aubry in *Solitons and Condensed Matter*, 1978, edited by A. Bishop and T. Schneider *Solid State Sciences* 8:264.

[15] M. Peyrard and S. Aubry, Critical behaviour at the transition by breaking of analyticity in the discrete frenkel-kontorova model, *Journal of Physics C*, 16:1593, 1983.

[16] Titus Sebastiaan van Erp, Frenkel Kontorova model on quasiperiodic substrate potentials, *Thesis*, 1999.

[17] S. Plimpton, Fast Parallel Algorithms for Short-Range Molecular Dynamics, *Journal of Computational Physics*, 117:1-19, 1995. Website: http://lammps.sandia.gov

[18] Donald W. Brenner, Olga A. Shenderova, Judith A. Harrison, Steven J. Stuart, Boris Ni and Susan B. Sinnott, A second-generation reactive empirical bond order (REBO) potential energy expression for hydrocarbons, *Journal of Physics: Condensed Matter*, 14:783, 2002.

[19] Aleksey N. Kolmogorov and Vincent H. Crespi, Smoothest bearings: interlayer sliding in multiwalled carbon nanotubes, *Physical Review Letters*, 85(22):4727, 2000.

[20] Steven J. Stuart, Alan B. Tutein, and Judith A. Harrison, A reactive potential for hydrocarbons with intermolecular interactions, *The Journal of Chemical Physics*, 112(14):6472, 2000.

[21] Erik Bitzek, Pekka Koskinen, Franz Gahler, Michael Moseler, and Peter Gumbsch, Structural Relaxation Made Simple, *Physical Review Letters*, 97:170201, 2006.

[22] M. Reguzzoni, A. Fasolino, E. Molinari, and M. C. Righi1, Potential energy surface for graphene on graphene: Ab initio derivation, analytical description, and microscopic interpretation, *Physical Review B*, 86:245434, 2012.

[23] B. Sachs, T.O. Wehling, M.I. Katsnelson and A.I. Lichtenstein, Adhesion and electronic structure of graphene on hexagonal boron nitride substrates, *Physical Review B*, 84:195414, 2011.

A Minimal number of atoms in layer with corresponding angle

Table 4: The values of N_{min} and their corresponding angle θ from Figure 9 and Equations 8 and 13

n	m	θ (°)	N_{min}
15	1	6.395879	482
14	1	6.835962	422
13	1	7.340993	366
12	1	7.926470	314
11	1	8.613238	266
10	1	9.430008	222
9	1	10.417438	182
8	1	11.635051	146
7	1	13.173551	114
13	2	14.105354	398
6	1	15.178179	86
11	2	16.426421	294
5	1	17.896551	62
14	3	19.030676	494
9	2	19.652860	206
13	3	20.316660	434
4	1	21.786789	42
11	3	23.483062	326
7	2	24.432698	134
10	3	25.461056	278
13	4	26.007824	474
3	1	27.795772	26
11	4	29.841724	362
8	3	30.590689	194
5	2	32.204228	78
12	5	33.254348	458
7	3	33.992176	158
9	4	34.960340	266
11	5	35.567302	402
2	1	38.213211	14
11	6	40.725193	446
9	5	41.266002	302
7	4	42.103449	186
5	3	43.573579	98
8	5	44.821821	258
11	7	45.377779	494
3	2	46.826449	38
10	7	48.364949	438
7	5	49.007267	218
4	3	50.569992	74
9	7	51.744379	386
5	4	52.659007	122
6	5	53.991017	182
7	6	54.774152	254
8	7	55.591545	338
9	8	56.109762	434

B Example input file LAMMPS

```
# Set essential simulation values and periodic boundary conditions
clear
units metal
dimension 3
boundary p p s
atom_style atomic
timestep 0.001
neighbor 2.0 nsq


# Choose n and m to define the supercell and set the interlayer distance
variable n equal 15
variable m equal 1
variable z equal (3.0)/(1.3978)
variable 2z equal (2*$z)
variable interlayer equal 1.3978*$z
print "Interlayer distance is $interlayer "


# Calculate the rotation angle and the number of atoms per layer
variable angle equal acos((2*$n*$n+2*$n*$m-$m*$m)/(2*($n*$n+$n*$m+$m*$m)))
variable degr equal (180*$angle/PI)
print "The commensurate angle is $degr"
variable atomslayer equal (2*($n*$n+$n*$m+$m*$m))
print "The number of atoms per layer is N= $atomslayer"


# Calculate the size of the prism-shaped supercell
variable prismx equal 1.3978*sqrt(3)*sqrt($n*$n+$n*$m+$m*$m)
variable prismy equal cos(PI/6)*$prismx
variable prismxy equal sin(PI/6)*$prismx


# You may choose to multiply the dimensions of the supercell by some integer:
variable celx equal 1*$prismx
variable cely equal 1*$prismy
variable celxy equal 1*$prismxy


# We distinguish three different regions
# region1 is the region of the bottom layer
# region2 is the region of the top layer
# region3 is the total region of simulation
region region1 prism -0.01 $celx-0.01 -0.01 $cely-0.01 0 3.00 $celxy 0 0
region region2 prism -0.01 $celx-0.01 -0.01 $cely-0.01 3.00 6.5 $celxy 0 0
region region3 prism -0.01 $celx-0.01 -0.01 $cely-0.01 0 6.5 $celxy 0 0
```

```
# Create the box for the simulation
create_box 2 region3


# Define the variables needed for the graphene lattice in the bottom layer
variable theta equal acos((2*$n*$n+2*$n*$m-$m*$m)/(2*($n*$n+$n*$m+$m*$m)))
variable alpha equal (0.5)*$theta
variable s equal sin($alpha)
variable c equal cos($alpha)
variable a1x equal sqrt(3)*$c
variable a1y equal sqrt(3)*$s
variable a2x equal (0.5)*sqrt(3)*$c-(1.5)*$s
variable a2y equal (0.5)*sqrt(3)*$s+(1.5)*$c


# Create the bottom layer which we keep fixed
# Vectors a1 and a2 are rotated by alpha=theta/2 with respect to the prism region
# The base atoms are in terms of vectors a1, a2 and a3
lattice custom 1.3978 a1 $a1x $a1y 0 a2 $a2x $a2y 0 a3 0 0 100.0 &
basis 0 0 0 basis 0.333333333333 0.3333333333 0
create_atoms 1 region region3
mass 1 12.01


# Give the bottom layer a group-ID
# Fix the bottom layer by using the setforce command
group layer1 region region1
fix freeze layer1 setforce 0.0 0.0 0.0


#Define the variables needed for the graphene lattice in the top layer
variable beta equal (-1)*$alpha
variable s equal sin($beta)
variable c equal cos($beta)
variable b1x equal sqrt(3)*$c
variable b1y equal sqrt(3)*$s
variable b2x equal (0.5)*sqrt(3)*$c-(1.5)*$s
variable b2y equal (0.5)*sqrt(3)*$s+(1.5)*$c


# Create the top layer
# Vectors b1 and b2 are rotated by beta=-theta/2 with respect to the prism region
# The angle between the two layers is therefore theta
lattice custom 1.3978 a1 $b1x $b1y 0 a2 $b2x $b2y 0 a3 0 0 $2z &
basis 0 0 0.5 basis 0.333333333333 0.3333333333 0.5
create_atoms 2 region region3
mass 2 12.01
```

```
# Give the top layer a group-ID
# Let the top layer relax in desired directions using the setforce command
group layer2 region region2
fix relax layer2 setforce NULL NULL 0.0


# Choose the appropriate potential
pair_style hybrid airebo 3.0 0 0 TKC 14.0 3.34
pair_coeff * * airebo /scratch/lammps-23Sep13/potentials/CH.airebo C C
pair_coeff 1 2* TKC 10.238


# Delete atoms that are created twice
delete_atoms overlap 0.1 all all


# Compute and print desired thermodynamic information
thermo 10
thermo_style custom step etotal fmax fnorm
thermo_modify norm yes


# Choose settings output
dump 1 all xyz 100000 dump.xyz
dump_modify 1 element C C


# Choose settings for energy minimization
min_style fire
minimize 0.0 3.12e-4 1000000 10000000
```

C Selected samples

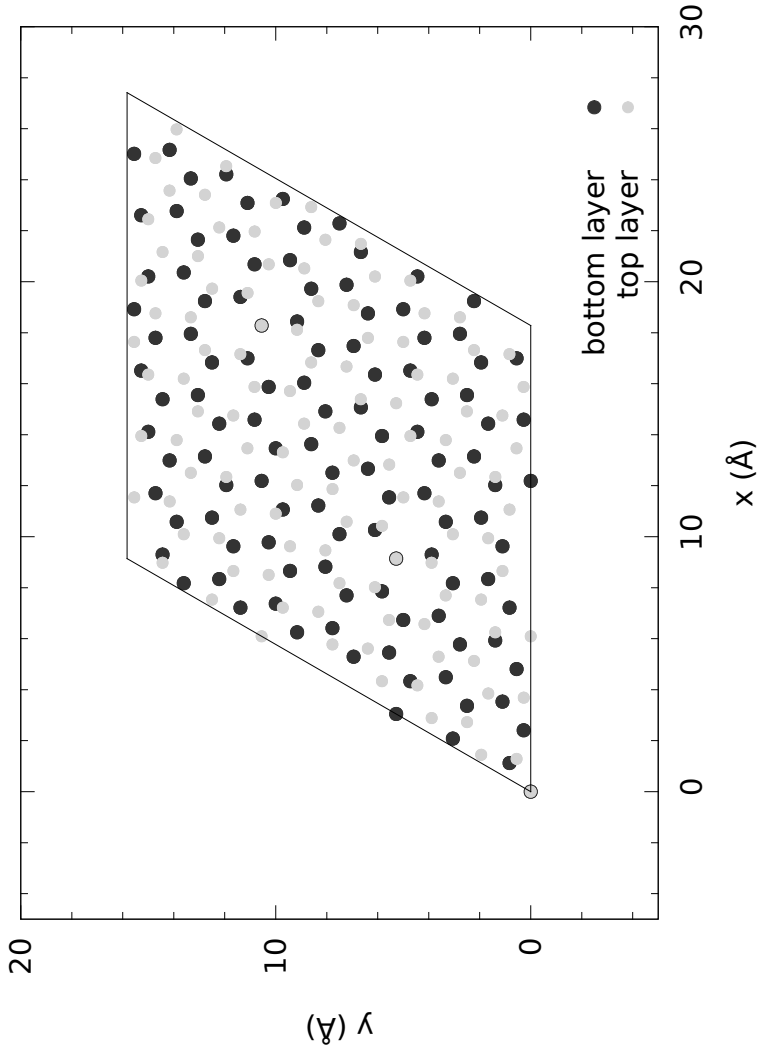

Figure 74: The bottom and top layer for sample (n,m)=(7,1) prior to relaxation. The top layer is rotated 13.2° with respect to the bottom layer and each layer contains 114 atoms.

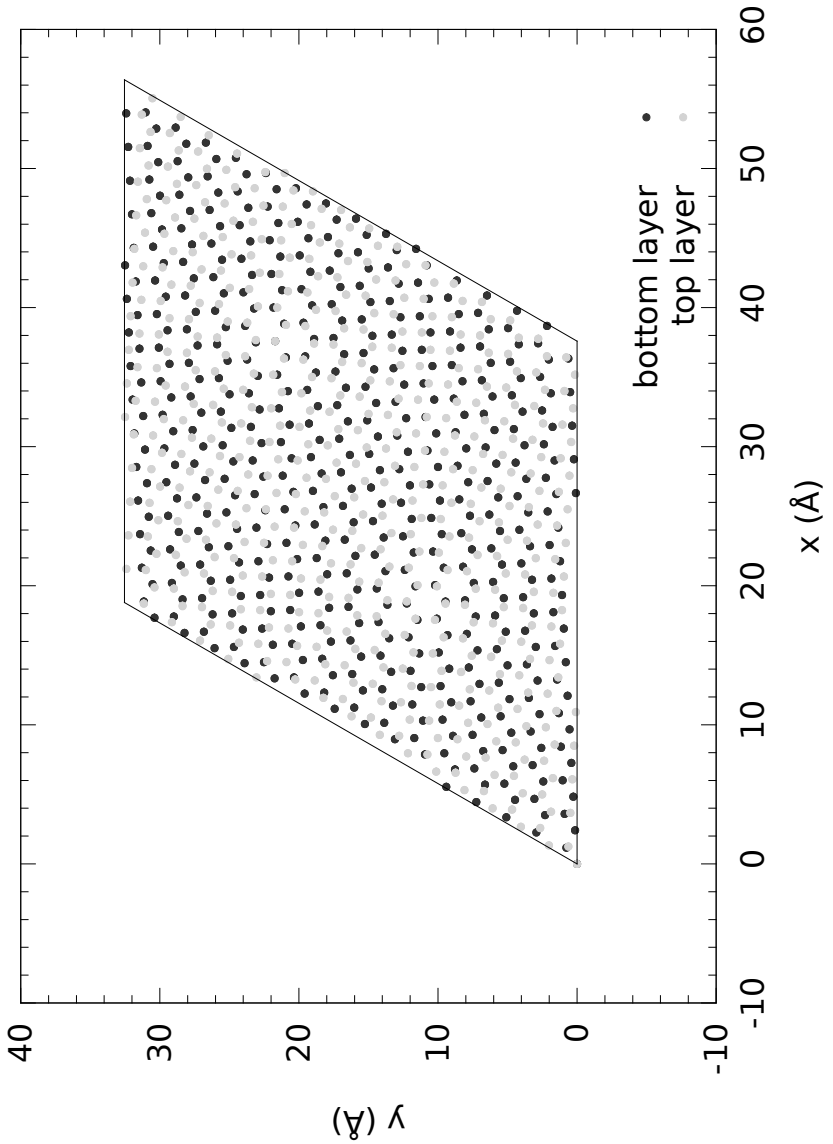

Figure 75: The bottom and top layer for sample (n,m)=(15,1) prior to relaxation. The top layer is rotated 6.395° with respect to the bottom layer and each layer contains 482 atoms.

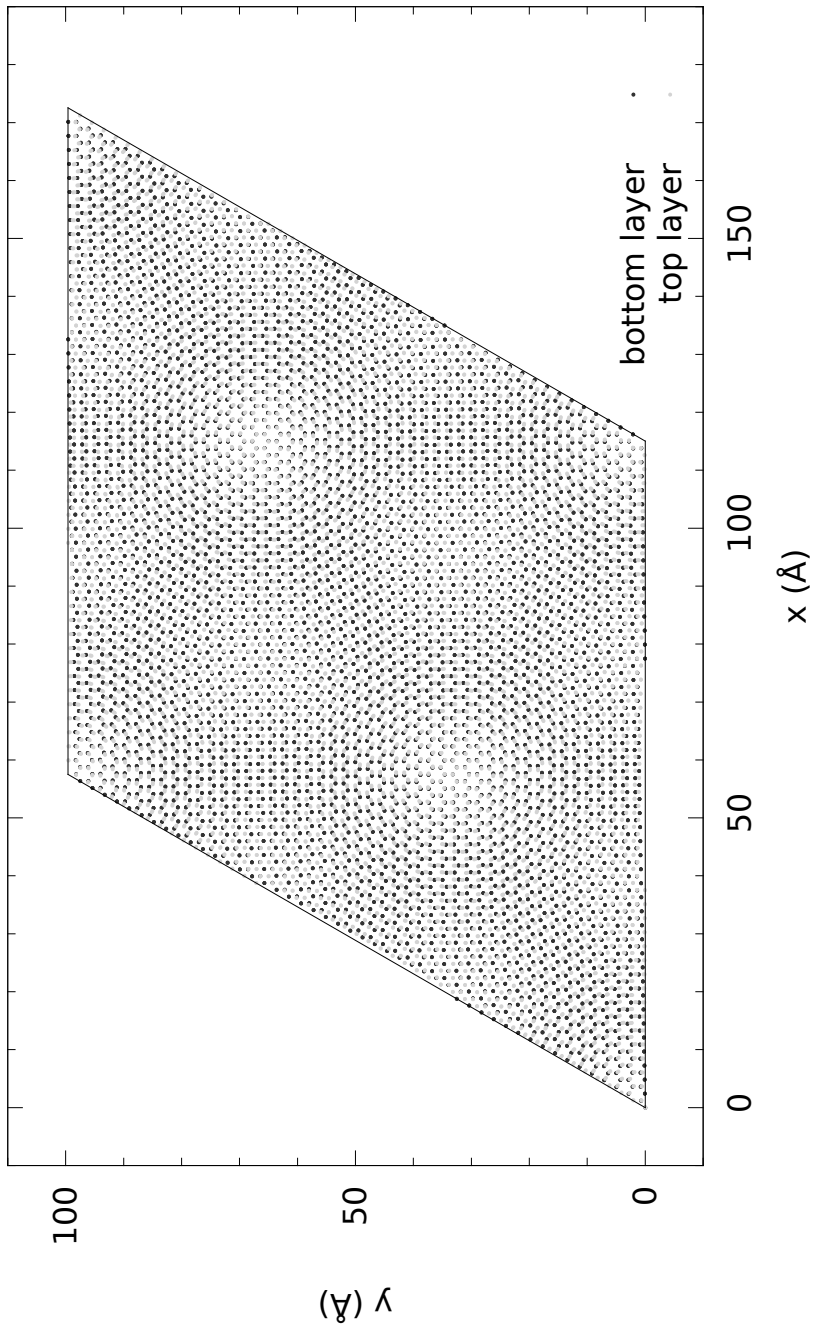

Figure 76: The bottom and top layer for sample (n,m)=(47,1) prior to relaxation. The top layer is rotated 2.08° with respect to the bottom layer and each layer contains 4514 atoms.

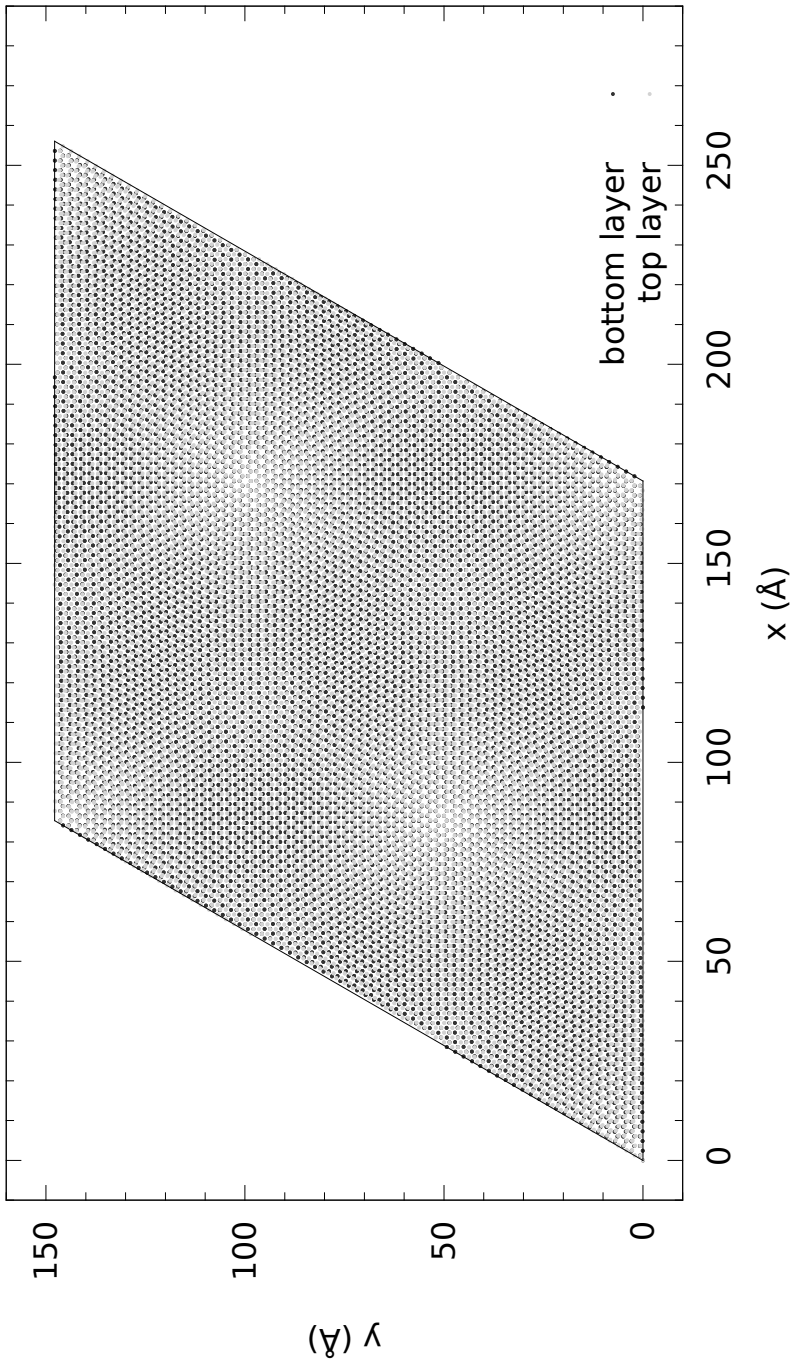

Figure 77: The bottom and top layer for sample (n,m)=(70,1) prior to relaxation. The top layer is rotated 1.41° with respect to the bottom layer and each layer contains 9942 atoms.

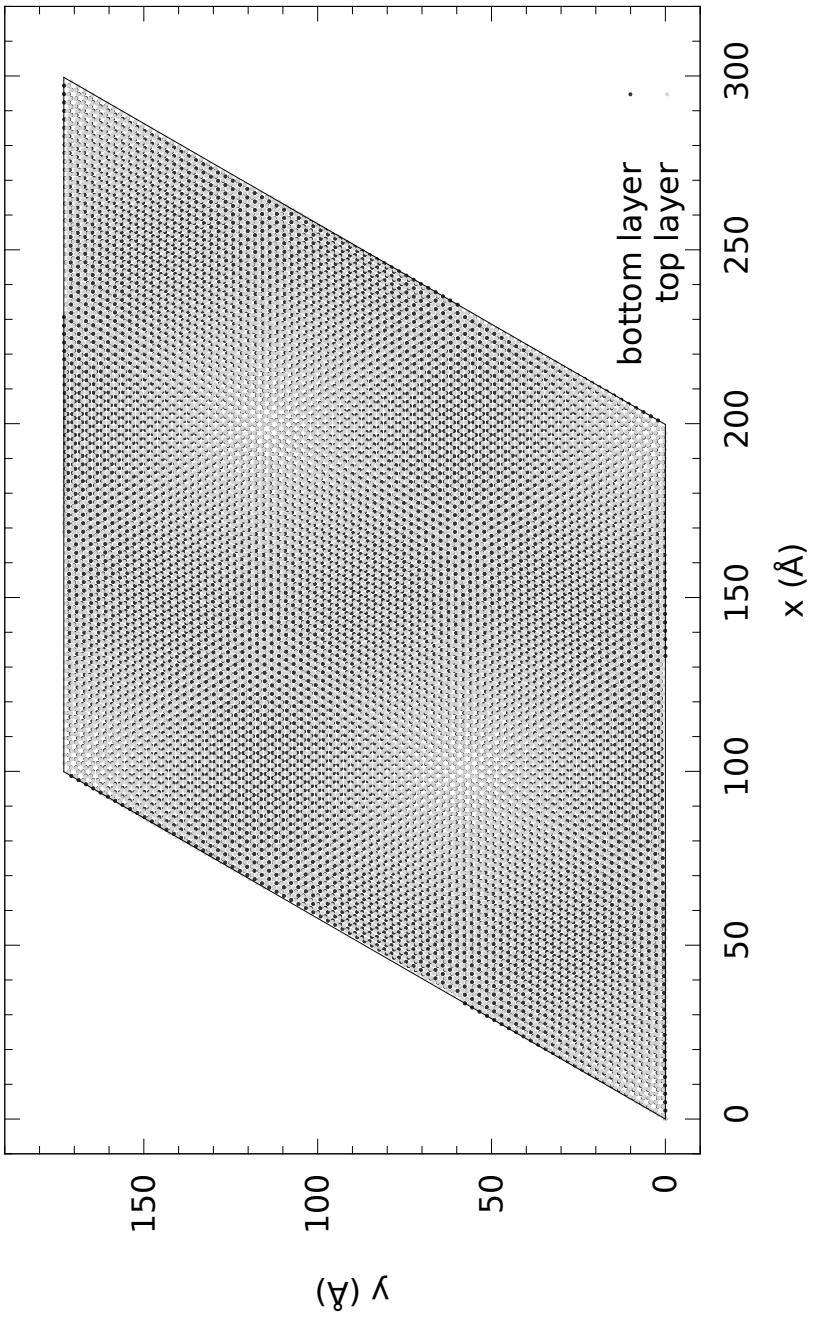

Figure 78: The bottom and top layer for sample (n,m)=(82,1) prior to relaxation. The top layer is rotated 1.2° with respect to the bottom layer and each layer contains 13614 atoms.

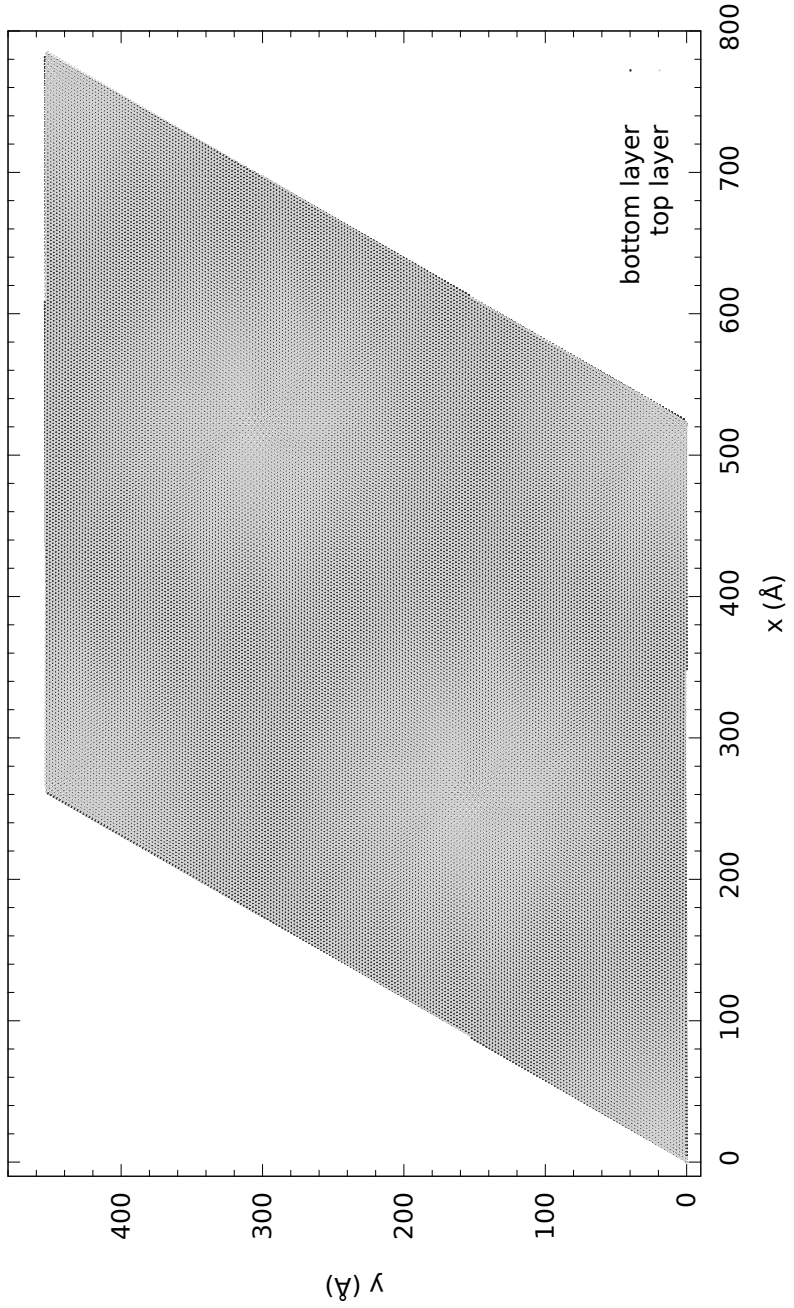

Figure 79: The bottom and top layer for sample (n,m)=(216,1) prior to relaxation. The top layer is rotated 0.46° with respect to the bottom layer and each layer contains 92746 atoms.

D Fitting parameters average and maximal displacement sample (15,1)

Table 5: Values of the exponential fitting parameters ($A^{-z/b}$) for average and maximal displacement of sample (15,1).

	Interatomic distance 1.3978Å		Interatomic distance 1.43 Å	
	A (Å)	b (Å)	A (Å)	b (Å)
r_{avg} 2 layers	336.3 ± 26.9	0.307 ± 0.003	335.5 ± 37.2	0.309 ± 0.004
r_{avg} sandwich	370.6 ± 41.8	0.325 ± 0.004	378.8 ± 48.4	0.326 ± 0.005
r_{max} 2 layers	746.0 ± 43.6	0.298 ± 0.002	873.6 ± 55.4	0.296 ± 0.002
r_{max} sandwich	922.3 ± 79.4	0.311 ± 0.003	982.4 ± 108.2	0.311 ± 0.004